SEPARATION PROCESS PRINCIPLES

Second Edition

J. D. SEADER / ERNEST J. HENLEY

Chapter 17

Crystallization, Desublimation, and Evaporation

Crystallization is a solid–fluid separation operation in which crystalline particles are formed from a homogeneous fluid phase. Ideally, the crystals are a pure chemical, obtained in a high yield with a desirable shape and a reasonably uniform and desirable size. Crystallization is one of the oldest known separation operations, with the recovery of sodium chloride as salt crystals from water by evaporation dating back to antiquity. Even today, the most common applications are the crystallization from aqueous solution of various inorganic salts, a short list of which is given in Table 17.1. All these cases are referred to as *solution crystallization* because the inorganic salt is clearly the solute, which is crystallized, and water is the solvent, which remains in the liquid phase. The phase diagram for systems suitable for solution crystallization is a solubility curve, such as shown in Figure 17.1a and described earlier in Chapter 4.

For the formation of organic crystals, organic solvents such as acetic acid, ethyl acetate, methanol, ethanol, acetone, ethyl ether, chlorinated hydrocarbons, benzene, and petroleum fractions may be preferred choices, but they must be used with great care when they are toxic or flammable with a low flash point and a wide range of explosive limits.

For either aqueous or organic solutions, crystallization is effected by cooling the solution, evaporating the solvent, or a combination of the two. In some cases, a mixture of two or more solvents may be best, examples of which include water with the lower alcohols, and normal paraffins with chlorinated solvents. Also, the addition of a second solvent is sometimes used to reduce the solubility of the solute. When water is the additional solvent, the process is called *watering-out;* when an organic solvent is added to an aqueous salt solution, the process is called *salting-out.* For both of these cases of solvent addition, fast crystallization called *precipitation* can occur, resulting in large numbers of very small crystals. Precipitation also occurs when one product of two reacting solutions is a solid with low solubility. For example, when aqueous solutions of silver nitrate and sodium chloride are mixed together, insoluble silver chloride is precipitated leaving an aqueous solution of mainly soluble sodium nitrate.

When both components of a homogeneous, binary solution have melting (freezing) points not far removed from each other, the solution is referred to as a *melt.* If, as in Figure 17.1b, the phase diagram for the melt exhibits a eutectic point, it is possible to obtain, in one step called *melt crystallization,* pure crystals of one component or the other, depending on whether the composition of the melt is to the left or right of the eutectic composition. If, however, solid solutions form, as shown in Figure 17.1c, a process of repeated melting and freezing steps, called *fractional melt crystallization,* is required to obtain nearly pure crystalline products. A higher degree of purity can be achieved by a technique called *zone melting* or *refining.* Examples of binary organic systems that form eutectics include metaxylene-paraxylene and benzene-naphthalene. Binary systems of naphthalene-beta naphthol and naphthalene-β naphthylamine, which form solid solutions, are not as common.

Crystallization can also occur from a vapor mixture by a process more properly called *desublimation.* A number of pure compounds, including phthalic anhydride and benzoic acid, are produced in this manner. When two or more compounds tend to desublime, a fractional desublimation process can be employed to obtain near-pure products.

Crystallization of a compound from a dilute, aqueous solution is often preceded by *evaporation* in one or more vessels, called *effects,* to concentrate the solution, and followed by partial separation and washing of the crystals from the resulting slurry, called the *magma,* by centrifugation or filtration. The process is completed by drying the crystals to a specified moisture content.

17.0 INSTRUCTIONAL OBJECTIVES

After completing this chapter, you should be able to:

- Describe different types of crystallization.
- Explain how crystals grow.
- Explain how crystal-size distribution can be measured, tabulated, and plotted.

- Explain the importance of supersaturation in crystallization.
- Differentiate between primary and secondary nucleation of crystals.
- Use mass-transfer theory to determine rate of crystal growth.
- Describe major types of batch and continuous solution-crystallization equipment.
- Apply the MSMPR model to design of a continuous, vacuum, evaporating crystallizer of the draft-tube baffled (DTB) type.
- Understand precipitation.
- Describe equipment for melt crystallization.
- Apply mass-transfer theory to a falling-film melt crystallizer.
- Apply the ideal zone-melting model.
- Differentiate between crystallization and desublimation.
- Describe evaporation equipment.
- Derive and apply the ideal evaporator model.
- Design multiple-effect evaporation systems.

Industrial Example

Consider the crystallization of $MgSO_4 \cdot 7H_2O$ (Epsom salt) from an aqueous solution. The solid–liquid phase diagram for the $MgSO_4 \cdot H_2O$ system at 1 atm is shown in Figure 17.2. Depending on the temperature, four different hydrated forms of $MgSO_4$ are possible: $MgSO_4 \cdot H_2O$, $MgSO_4 \cdot 6H_2O$, $MgSO_4 \cdot 7H_2O$, and $MgSO_4 \cdot 12H_2O$. Furthermore, a eutectic of the latter hydrate with ice is possible. To obtain the usually desired heptahydrate, crystallization must occur in the temperature range from 36°F to 118°F (Point *b* to Point *c*). Within this range, the solubility of $MgSO_4$ (anhydrous or hydrate-free basis) increases almost linearly from about 21 to 33 wt%.

A representative commercial process for producing 4,205 lb/hr (dry basis) of $MgSO_4 \cdot 7H_2O$ crystals from a 10 wt% aqueous solution at 1 atm and 70°F is shown in Figure 17.3. This solution is first concentrated in a double-effect evaporation system with forward feed and then mixed with recycled mother liquors from the hydroclone and centrifuge. The combined feed of 14,326 lb/h containing 31.0 wt% $MgSO_4$ at 120°F and 1 atm enters an evaporative, vacuum crystallizer constructed of 316 stainless steel and shown in more detail in Figure 17.4.

The crystallizer utilizes internal circulation of 6,000 gpm of magma up through a draft tube equipped with a 3-Hp marine-propeller agitator to obtain near-perfect mixing of

Table 17.1 Some Inorganic Salts Recovered from Aqueous Solutions

Chemical Name	Formula	Common Name	Crystal System
Ammonium chloride	NH_4Cl	sal-ammoniac	cubic
Ammonium sulfate	$(NH_4)_2SO_4$	mascagnite	orthorhombic
Barium chloride	$BaCl_2 \cdot 2H_2O$		monoclinic
Calcium carbonate	$CaCO_3$	calcite	rhombohedral
Copper sulfate	$CuSO_4 \cdot 5H_2O$	blue vitriol	triclinic
Magnesium sulfate	$MgSO_4 \cdot 7H_2O$	Epsom salt	orthorhombic
Magnesium chloride	$MgCl_2 \cdot 6H_2O$	bischofite	monoclinic
Nickel sulfate	$NiSO_4 \cdot 6H_2O$	single nickel salt	tetragonal
Potassium chloride	KCl	muriate of potash	cubic
Potassium nitrate	KNO_3	nitre	hexagonal
Potassium sulfate	K_2SO_4	arcanite	orthorhombic
Silver nitrate	$AgNO_3$	lunar caustic	orthorhombic
Sodium chlorate	$NaClO_3$		cubic
Sodium chloride	$NaCl$	salt, halite	cubic
Sodium nitrate	$NaNO_3$	chile salt petre	rhombohedral
Sodium sulfate	$Na_2SO_4 \cdot 10H_2O$	glauber's salt	monoclinic
Sodium thiosulfate	$Na_2S_2O_3 \cdot 5H_2O$	hypo	monoclinic
Zinc sulfate	$ZnSO_4 \cdot 7H_2O$	white vitriol	orthorhombic

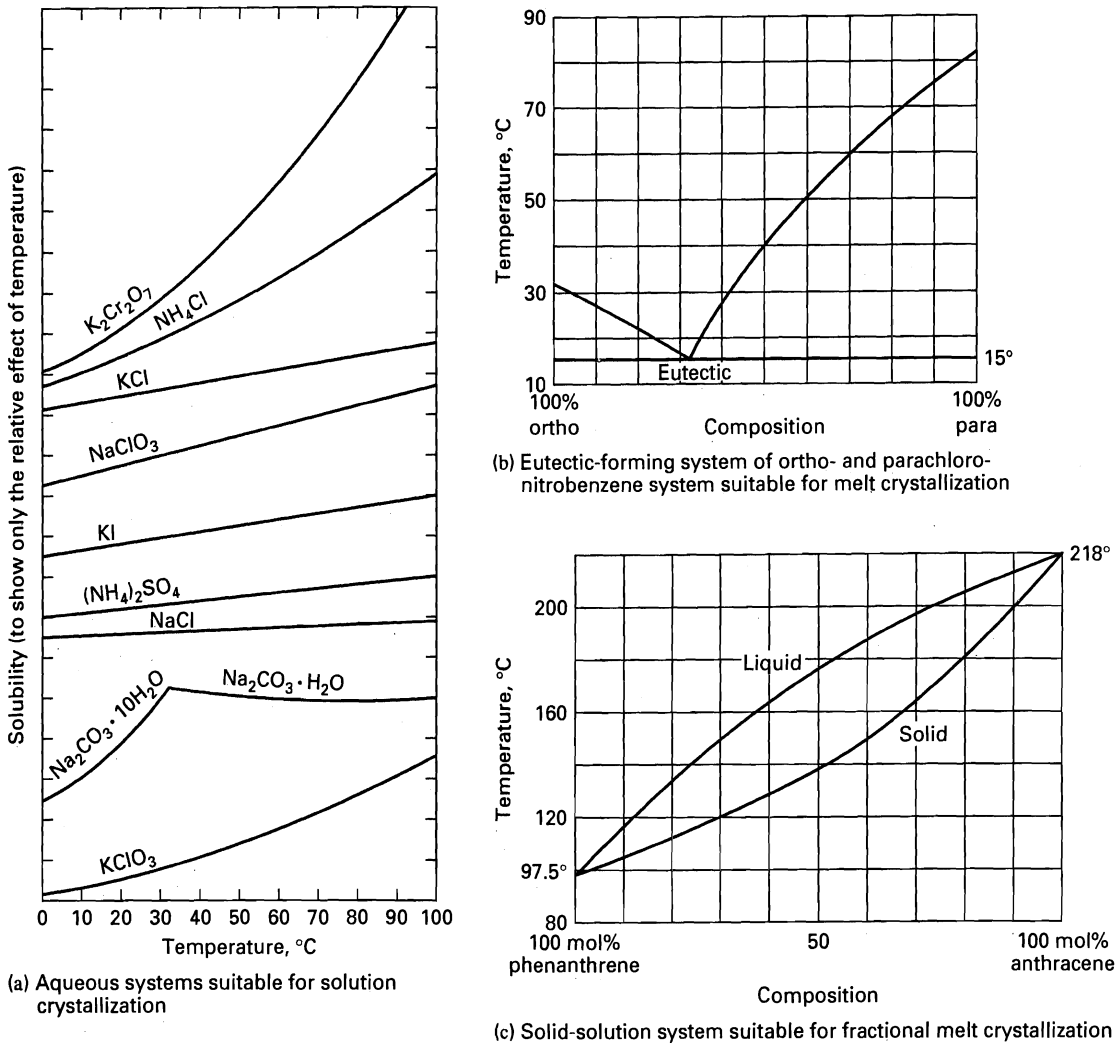

Figure 17.1 Different types of solubility curves.

[From *Handbook of Separation Techniques for Chemical Engineers,* 2nd ed., P.A. Schweitzer, Editor-in-chief, McGraw-Hill, New York (1988) with permission.]

the magma. Mother liquor, which is separated from crystals during upward flow outside of the skirt baffle, is circulated externally at the rate of 625 gpm, by a 10-Hp stainless-steel pump, through a 300-ft^2 stainless-steel, plate-and-frame heat exchanger, where 2,052,000 Btu/hr of heat is transferred to the solution from 2,185 lb/h of condensing 20 psig steam to provide supersaturation and energy to evaporate 2,311 lb/h of water in the crystallizer.

The vapor leaving the top of the crystallizer is condensed by direct contact with cooling water in a barometric condenser, attached to which are ejectors to pull a vacuum of 0.867 psia in the vapor space of the crystallizer. The product magma, at a temperature of 105°F, consists of 7,810 lb/h of mother liquor saturated with 30.6 wt% $MgSO_4$ and 4,205 lb/h of crystals. This corresponds to a magma containing 35% crystals by weight or 30.2% crystals by volume, based on a crystal density of 1.68 g/cm^3 and a mother liquor density of 1.35 g/cm^3. The boiling-point elevation of the saturated mother liquor at 105°F is 8°F. Thus, the vapor leaving the crystallizer is superheated by the same 8°F. The magma residence time in the crystallizer is 4 hours, which is sufficient to produce the following crystal-size distribution:

35 wt% on 20 mesh U.S. screen
80 wt% on 40 mesh U.S. screen
99 wt% on 100 mesh U.S. screen

The crystallizer for the representative process is 30 ft high with a vapor-space diameter of 5-1/2 ft and a magma-space diameter of 10 ft. The magma is thickened to 50 wt% crystals in a hydroclone, from which the mother-liquor overflow is recycled to the crystallizer and the underflow slurry is sent to a continuous centrifuge, where the slurry is further thickened to 65 wt% crystals and washed. Filtrate mother liquor from the centrifuge is also recycled to the crystallizer. The centrifuge cake is fed to a continuous direct-heat rotary dryer to reduce the moisture content of the crystals to 1.5 wt%.

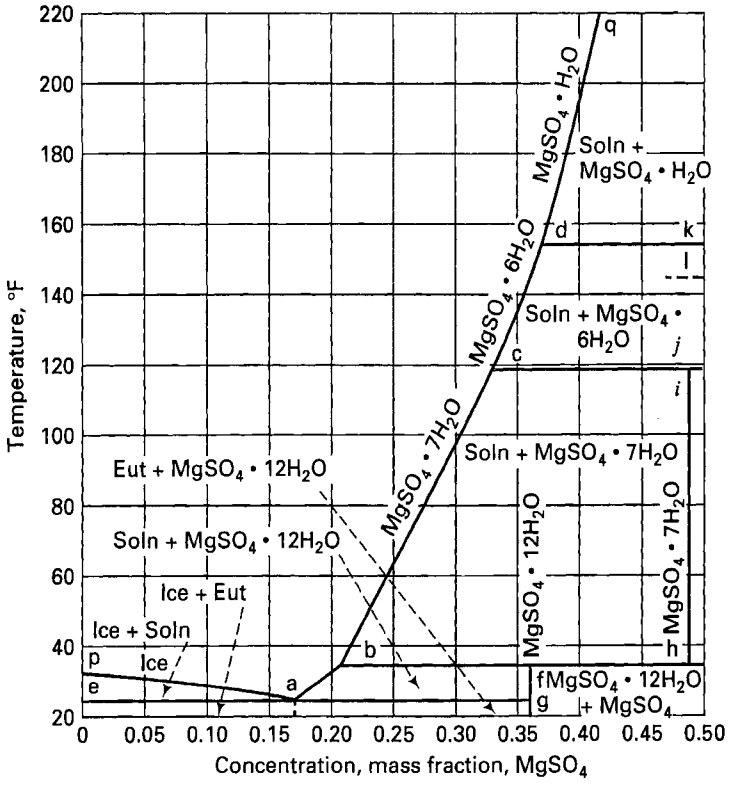

Figure 17.2 Solid–liquid phase diagram for the $MgSO_4$-nH_2O system at 1 atm.
[From W.L. McCabe, J.C. Smith, and P. Harriott, *Unit Operations of Chemical Engineering*, 5th ed., McGraw-Hill, New York (1993) with permission.]

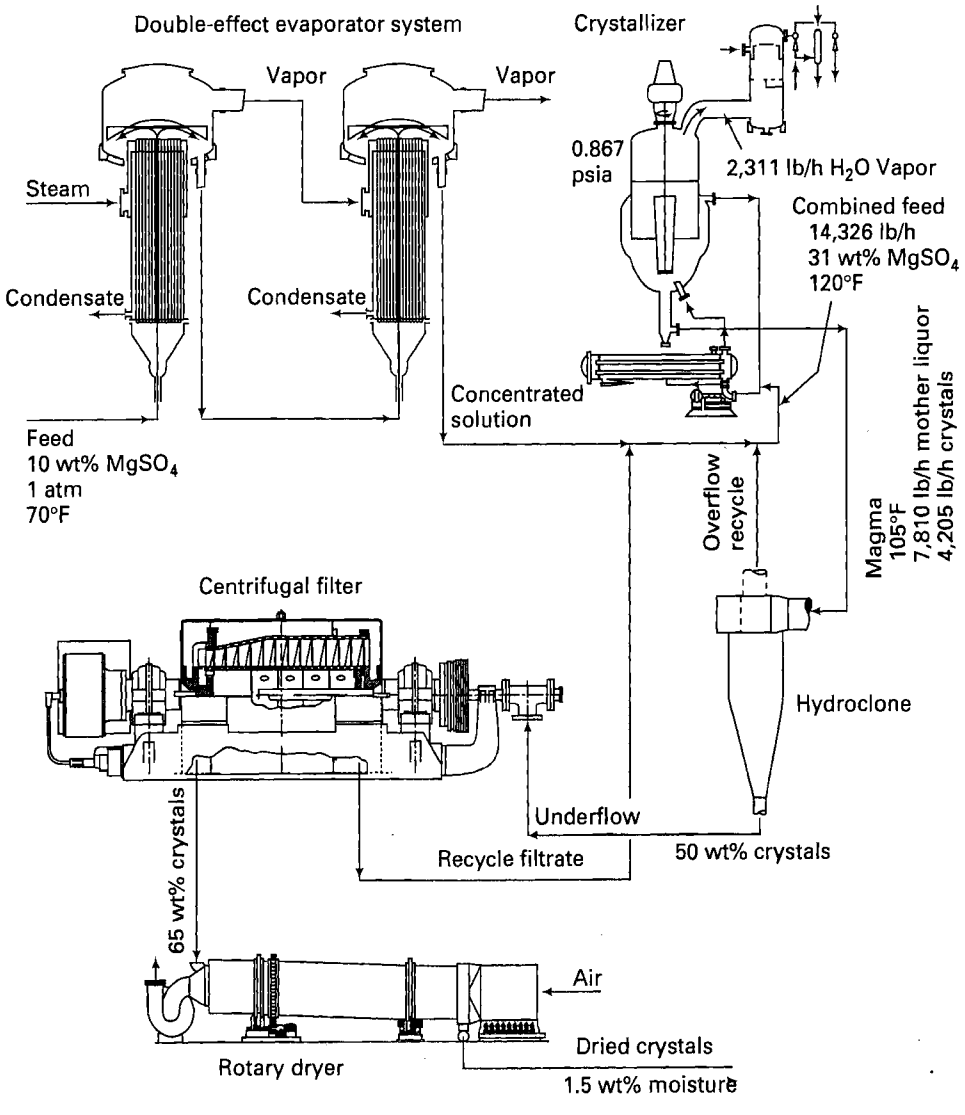

Figure 17.3 Process for production of $MgSO_4 \cdot 7H_2O$.

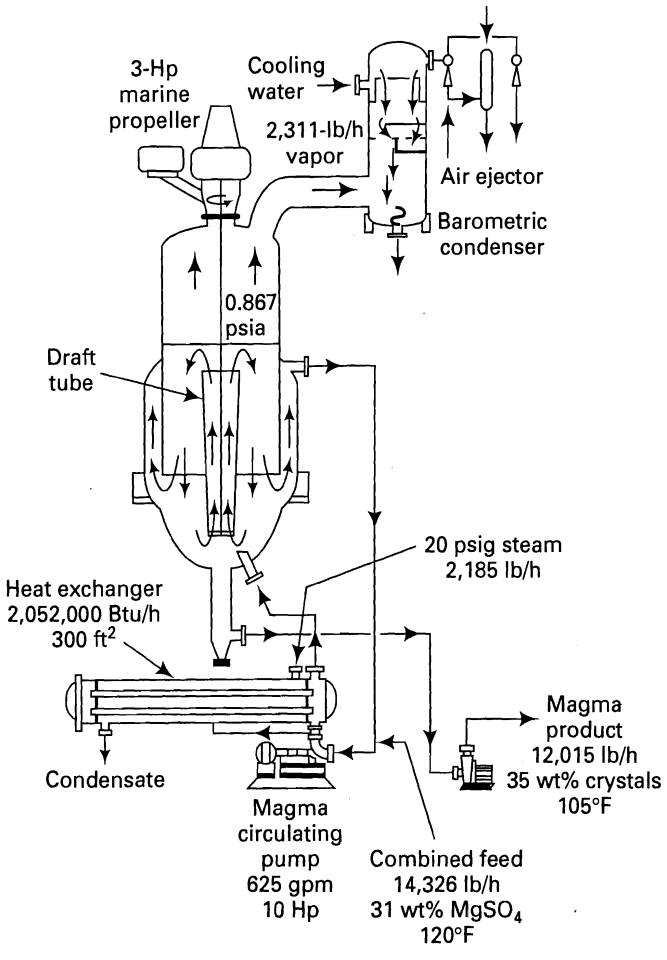

Figure 17.4 Crystallizer for production of $MgSO_4 \cdot 7H_2O$ crystals.

17.1 CRYSTAL GEOMETRY

In a solid, the motion of molecules, atoms, or ions is restricted largely to oscillations about fixed positions. If the solid is amorphous, these positions are not arranged in a regular or lattice pattern; if the solid is crystalline, they are. Amorphous solids are isotropic, such that physical properties are independent of the direction of measurement; crystalline solids are anisotropic, unless the crystals are cubic in structure.

When crystals grow, unhindered by other surfaces such as container walls and other crystals, they form polyhedrons with flat sides and sharp corners. Crystals are never spherical in shape. Although two crystals of a given chemical may appear quite different in size and shape, they always have something in common, known as the Law of Constant Interfacial Angles, proposed by Hauy in 1784. This law states that the angles between corresponding faces of all crystals of a given substance are constant, even though the crystals vary in size and in the development of the various faces (called the *crystal habit*). The interfacial angles and lattice dimensions can be measured accurately by x-ray crystallography.

As discussed by Mullin [1], early investigators found that crystals consist of many units, each shaped like the larger crystal. This led to the concept of a space lattice as a regular arrangement of points (molecules, atoms, or ions) such that if a line is drawn between any two points and then extended in both directions, the line will pass through other lattice points with an identical spacing. In 1848, Bravais showed that only the 14 space lattices shown in Figure 17.5 are possible. Based on the symmetry of the three mutually perpendicular axes with respect to their relative lengths (a, b, c) and the angles (α, β, γ) between the axes, the 14 lattices can be classified into the seven crystal systems listed in Table 17.2. For example, the cubic (regular) system includes the simple cubic lattice, the body-centered cubic lattice, and the face-centered lattice. Examples of the seven crystal systems are included in Table 17.1. The five sodium salts included in that table form three of the seven crystal systems.

Actual crystals of a given substance and a given crystal system can exhibit markedly different appearances when the faces grow at different rates, particularly when these rates vary markedly from stunted growth in one direction, so as to give plates, or by exaggerated growth in another direction, to give needles. For example, potassium sulfate, which belongs to the orthorhombic-crystal system, can take on any of the shapes (crystal habits) shown in Figure 17.6, including plates, needles, and prisms. When product crystals of a particular crystal habit are desired, experimental research may be required to find the necessary processing conditions. Modifications of crystal habit are most often accomplished by deliberate addition of impurities to the solution.

Crystal-Size Distributions

Typical magmas from a crystallizer contain a distribution of crystal sizes and shapes. It is highly desirable to characterize a batch of crystals (or particles in general) by an average crystal size and a crystal-size distribution. This is often accomplished by defining a characteristic crystal dimension. However, as shown in Figure 17.6, some crystal shapes might require two characteristic dimensions, while one might suffice for others. One solution to this problem, which is particularly applicable to the correlation of transport rates involving particles, is to relate the irregular-shaped particle to a sphere by the sphericity, ψ, defined as

$$\psi = \frac{\text{surface area of a sphere with the same volume as the particle}}{\text{surface area of the particle}} \tag{17-1}$$

For a sphere, $\psi = 1$, while for all other particles, $\psi < 1$. For a spherical particle of diameter, D_p, the surface area, s_p, to volume, v_p, ratio is

$$(s_p/v_p)_{\text{sphere}} = (\pi D_p^2)/(\pi D_p^3/6) = 6/D_p$$

Therefore, (17-1) becomes

$$\psi = \frac{6}{D_p}\left(\frac{v_p}{s_p}\right)_{\text{particle}} \tag{17-2}$$

Table 17.2 The Seven Crystal Systems

Crystal System	Space Lattices	Length of Axes	Angles between Axes
Cubic (regular)	Simple cubic Body-centered cubic Face-centered cubic	$a = b = c$	$\alpha = \beta = \gamma = 90°$
Tetragonal	Square prism Body-centered square prism	$a = b < c$	$\alpha = \beta = \gamma = 90°$
Orthorhombic	Simple orthorhombic Body-centered orthorhombic Base-centered orthorhombic Face-centered orthorhombic	$a \neq b \neq c$	$\alpha = \beta = \gamma = 90°$
Monoclinic	Simple monoclinic Base-centered monoclinic	$a \neq b \neq c$	$\alpha = \beta = 90°$ $\gamma \neq 90°$
Rhombohedral (trigonal)	Rhombohedral	$a = b = c$	$\alpha = \beta = \gamma \neq 90°$
Hexagonal	Hexagonal	$a = b \neq c$	$\alpha = \beta = 90°$ $\gamma \neq 120°$
Triclinic	Triclinic	$a \neq b \neq c$	$\alpha \neq \beta \neq \gamma \neq 90°$

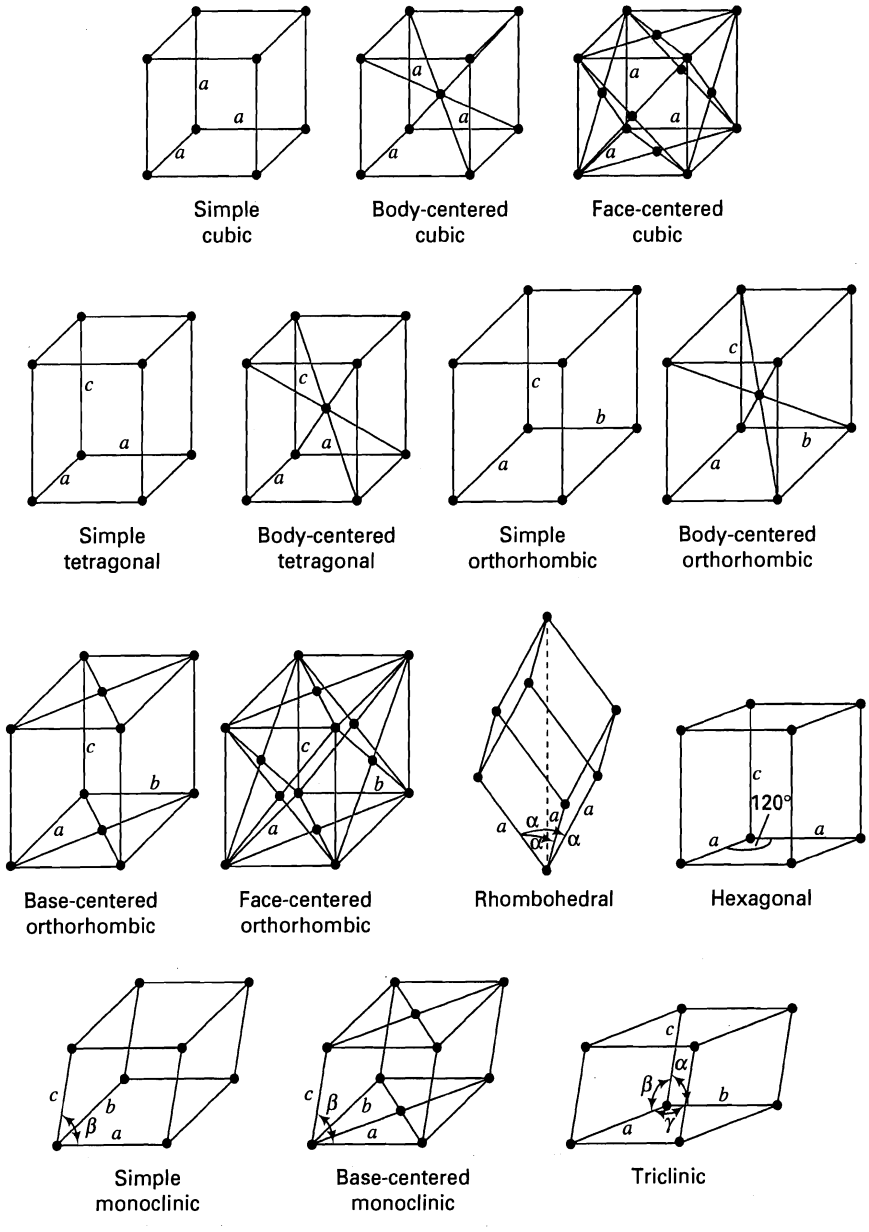

Figure 17.5 The 14 space lattices of Bravais.

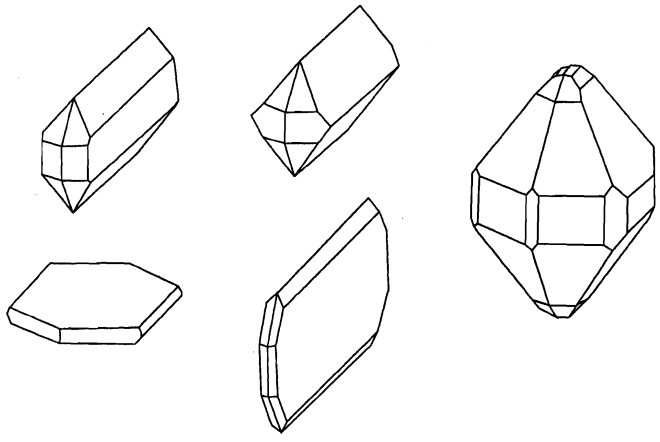

Figure 17.6 Some crystal habits of orthorhombic, potassium-sulfate crystals.

EXAMPLE 17.1

Estimate the sphericity of a cube of dimension a on each side.

SOLUTION

$$v_{\text{cube}} = a^3$$

$$s_{\text{cube}} = 6a^2$$

From (17-2),

$$\psi = \frac{6}{D_p}\left(\frac{a^3}{6a^2}\right) = \frac{a}{D_p}$$

Because the volumes of the sphere and the cube must be equal,

$$\pi D_p^3/6 = a^3$$

Solving,

$$D_p = 1.241\,a$$

Then,

$$\psi = a/(1.241\,a) = 0.806$$

The most common methods for measuring particle size are listed in Table 17.3 together with their useful particle-size ranges. Because of the irregular shapes of crystals, it should not be surprising that the different methods can give results that may differ by as much as 50%. Crystal-size distributions are most often determined with U.S. (or British) standard wire-mesh screens [ASTM Ell (1989)] derived from the earlier Tyler standard screens. The U.S. standard is based on a 1-mm (1000-μm)-square *aperture-opening* screen called Mesh No. 18 because there are 18 apertures per inch. The standard Mesh numbers are listed in Table 17.4, where each successively smaller aperture differs from the preceding aperture by a factor of approximately $(2)^{1/4}$. Mechanical shaking is applied to conduct the sieving operation, using a stack of ordered screens.

Table 17.3 Methods of Measuring Particle Size

Method	Size Range, Microns
Woven-wire screen	32–5600
Coulter electrical sensor	1–200
Gravity sedimentation	1–50
Optical microscopy	0.5–150
Laser-light scattering	0.04–2000
Centrifugal sedimentation	0.01–5
Electron microscopy	0.001–5

Table 17.4 U.S. Standard Screens ASTM EII

Mesh Number	Opening of Square Aperture		
	in.	mm	μm
3-1/2	0.220	5.60	5600
4	0.187	4.75	4750
5	0.157	4.00	4000
6	0.132	3.35	3350
7	0.110	2.80	2800
8	0.0929	2.36	2360
10	0.0787	2.00	2000
12	0.0669	1.70	1700
14	0.0551	1.40	1400
16	0.0465	1.18	1180
18	0.0394	1.000	1000
20	0.0335	0.850	850
25	0.0280	0.710	710
30	0.0236	0.600	600
35	0.0197	0.500	500
40	0.0167	0.425	425
45	0.0140	0.355	355
50	0.0118	0.300	300
60	0.00984	0.250	250
70	0.00835	0.212	212
80	0.00709	0.180	180
100	0.00591	0.150	150
120	0.00492	0.125	125
140	0.00417	0.106	106
170	0.00354	0.090	90
200	0.00295	0.075	75
230	0.00248	0.063	63
270	0.00209	0.053	53
325	0.00177	0.045	45
400	0.00150	0.038	38
450	0.00126	0.032	32

When wire-mesh screens are used to determine crystal-size distribution, the crystal size is taken to correspond to the screen aperture through which the crystal just passes. However, because of the irregularity of particle shape, this should be considered as a nominal value only. This is particularly true for plates and needles, as illustrated in Figure 17.7.

Particle-size-distribution data, called a *screen analysis,* are presented in the form of a table, from which differential and cumulative plots can be made, usually on a mass-fraction

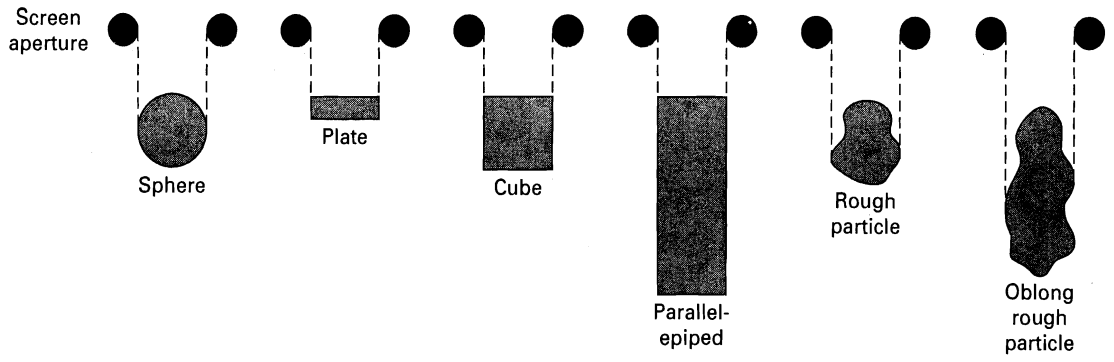

Figure 17.7 Different particle shapes that just pass through the same screen.

basis. Consider the following laboratory screen-analysis data presented by Graber and Taboada [2] for crystals of $Na_2SO_4 \cdot 10H_2O$ (Glauber's salt) grown at about 18°C during an average residence time of 37.2 min in a well-mixed, laboratory, cooling crystallizer. The smallest screen used was 140 mesh, with particles passing through that screen being retained on a pan.

Mesh Number	Aperture, D_p, mm	Mass Retained on Screen, Grams	% Mass Retained
14	1.400	0.00	0.00
16	1.180	9.12	1.86
18	1.000	32.12	6.54
20	0.850	39.82	8.11
30	0.600	235.42	47.95
40	0.425	89.14	18.15
50	0.300	54.42	11.08
70	0.212	22.02	4.48
100	0.150	7.22	1.47
140	0.106	1.22	0.25
Pan	—	0.50	0.11
		491.00	100.00

Differential Screen Analysis

A *differential screen analysis* is made by determining the arithmetic-average aperture for each mass fraction that passes through one screen but not the next screen. Thus, from the above table, a mass fraction of 0.0186 passes through a screen of 1.400-mm aperture, but does not pass through a screen of 1.180-mm aperture. The average of these two apertures is 1.290 mm, which is taken to be the nominal particle size for that mass fraction. The following differential analysis is computed in this manner, where the designation $-14 + 16$ refers to those particles passing through a 14-mesh screen and retained on a 16-mesh screen.

Mesh Range	$\bar{D}_p$, Average Particle Size, mm	Mass Fraction, x_i
$-14 + 16$	1.290	0.0186
$-16 + 18$	1.090	0.0654
$-18 + 20$	0.925	0.0811
$-20 + 30$	0.725	0.4795
$-30 + 40$	0.513	0.1815
$-40 + 50$	0.363	0.1108
$-50 + 70$	0.256	0.0448
$-70 + 100$	0.181	0.0147
$-100 + 140$	0.128	0.0025
$-140 + (170)$	0.098	0.0011
		1.0000

A plot of the differential screen analysis is shown in Figure 17.8 both as (a) an x-y plot and as (b) a histogram. If a wide range of screen aperture is covered, it is best to use a log scale for that variable.

Cumulative Screen Analysis

Screen analysis data can also be plotted as cumulative-weight-percent oversize or (which is more common) undersize as a function of screen aperture. For the above data of Graber and Taboada [2], the two types of *cumulative screen analysis* are as follows:

Aperture, D_p, mm	Cumulative wt% Undersize	Cumulative wt% Oversize
1.400	100.00	0.00
1.180	98.14	1.86
1.000	91.60	8.40
0.850	83.49	16.51
0.600	35.54	64.46
0.425	17.39	82.61
0.300	6.31	93.69
0.212	1.83	98.17
0.150	0.36	99.64
0.106	0.11	99.89

Because 0.11 wt% passed through a 0.106-mm aperture but was retained on a pan with no indication of just how small these retained particles were, the cumulative wt% undersize and oversize cannot be taken to 0 and 100%, respectively.

The above cumulative screen analyses are plotted in Figure 17.8c. The two curves, which are mirror images of each other, cross at a median size where 50 wt% is larger in size and 50 wt% is smaller. As with differential plots, a log scale is preferred if a large range of screen aperture is covered. A log scale for the cumulative wt% may also be preferred if an appreciable fraction of the data points lie below 10%.

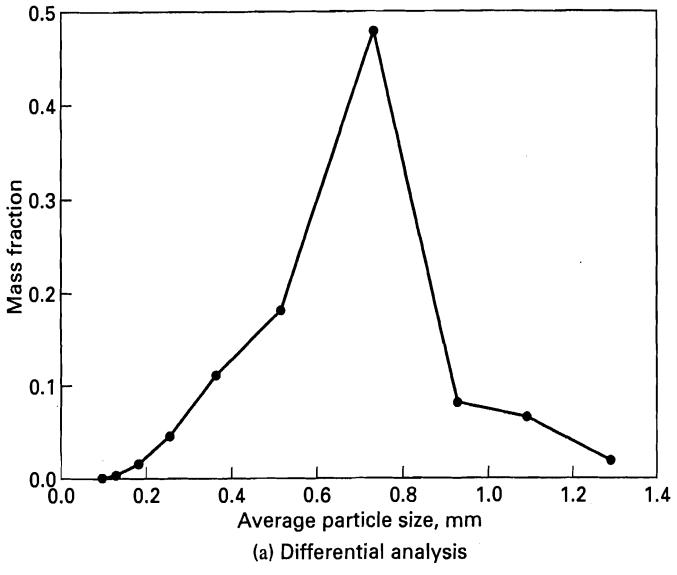

(a) Differential analysis

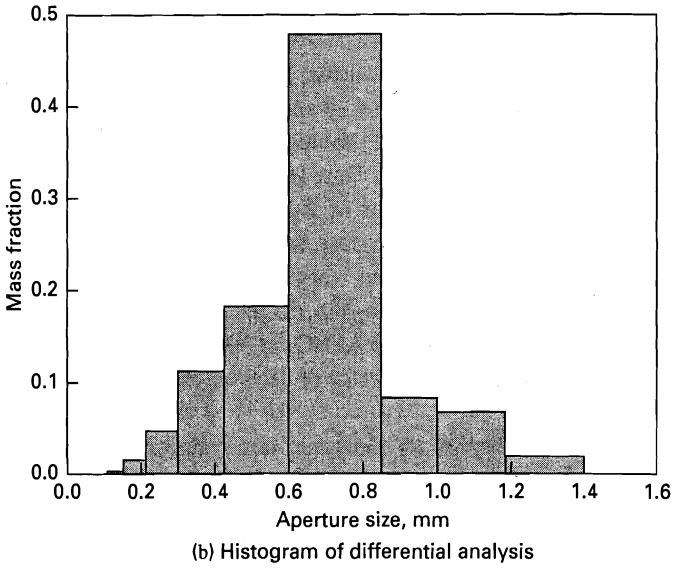

(b) Histogram of differential analysis

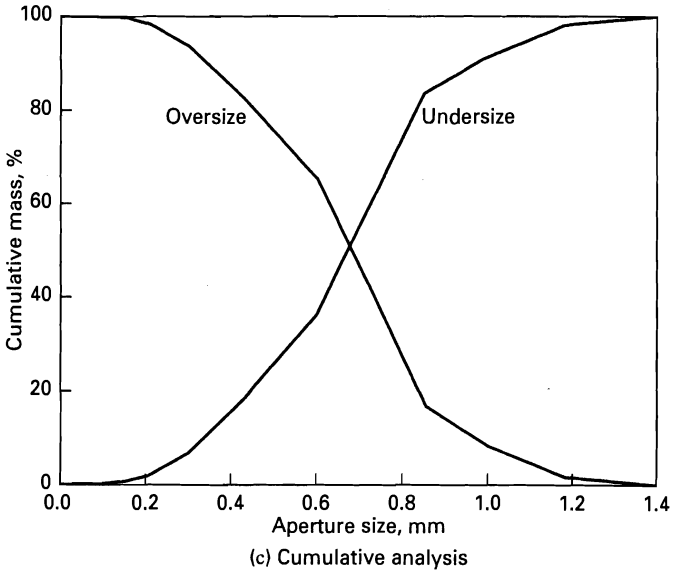

(c) Cumulative analysis

Figure 17.8 Screen analyses for data of Graber and Taboada [2].

A number of different mean particle sizes that are derived from screen analysis are used in practice, depending upon the application. Of these, the most useful are: (1) surface-mean diameter, (2) mass-mean diameter, (3) arithmetic-mean diameter, and (4) volume-mean diameter.

Surface-Mean Diameter

The specific surface area (area/mass) of a particle of spherical or other shape is defined by

$$A_w = s_p/m_p = s_p/v_p\rho_p \tag{17-3}$$

Combining (17-2) and (17-3)

$$A_w = 6/\psi\rho_p D_p \tag{17-4}$$

For n mass fractions, x_i, each of average aperture $\bar{D}_{p_i}$, from a screen analysis, the overall specific surface area is given by

$$A_w = \sum_{i=1}^{n} \frac{6x_i}{\psi\rho_p \bar{D}_{p_i}} = \frac{6}{\psi\rho_p} \sum \frac{x_i}{\bar{D}_{p_i}} \tag{17-5}$$

The surface-mean diameter is defined by

$$A_w = \frac{6}{\psi\rho_p \bar{D}_S} \tag{17-6}$$

Combining (17-5) and (17-6),

$$\bar{D}_S = \frac{1}{\sum_{i=1}^{n} \frac{x_i}{\bar{D}_{p_i}}} \tag{17-7}$$

which can be used to determine $\bar{D}_S$ from a screen analysis. This mean diameter is sometimes referred to as the Sauter mean diameter and as the volume-surface-mean diameter. It is often used for skin friction, heat-transfer, and mass-transfer calculations involving particles.

Mass-Mean Diameter

The mass-mean diameter is defined by

$$\bar{D}_W = \sum_{i=1}^{n} x_i \bar{D}_{p_i} \tag{17-8}$$

Arithmetic-Mean Diameter

The arithmetic-mean diameter is defined in terms of the number of particles, N_i, in each size range:

$$\bar{D}_N = \frac{\sum_{i=1}^{n} N_i \bar{D}_{p_i}}{\sum N_i} \tag{17-9}$$

The number of particles is related to the mass fraction of particles by

$$x_i = \frac{\text{mass of particles of average size } \bar{D}_{p_i}}{\text{total mass}} = \frac{N_i f_v \left(\bar{D}_{p_i}\right)^3 \rho_p}{M_t} \tag{17-10}$$

where

f_v = volume shape factor defined by $v_p = f_v \bar{D}_{p_i}^3$

M_t = total mass (17-11)

For spherical particles, $f_v = \pi/6$.

If (17-10) is solved for N_i, substituted into (17-9), and simplified, we obtain

$$\bar{D}_N = \frac{\sum_{i=1}^{n} \left(\frac{x_i}{\bar{D}_{p_i}^2} \right)}{\sum_{i=1}^{n} \left(\frac{x_i}{\bar{D}_{p_i}^3} \right)} \tag{17-12}$$

Volume-Mean Diameter

The volume-mean diameter, $\bar{D}_V$, is defined by

$$(f_v \bar{D}_V^3) \sum_{i=1}^{n} N_i = \sum_{i=1}^{n} (f_v \bar{D}_{p_i}^3) N_i \tag{17-13}$$

Solving (17-13) for $\bar{D}_V$ for a constant value of f_v gives

$$\bar{D}_V = \left(\frac{\sum_{i=1}^{n} N_i \bar{D}_{p_i}^3}{\sum_{i=1}^{n} N_i} \right) \tag{17-14}$$

The corresponding relation in terms of x_i rather than N_i is obtained by combining (17-14) with (17-10), giving

$$\bar{D}_V = \left(\frac{1}{\sum \frac{x_i}{\bar{D}_{p_i}^3}} \right)^{1/3} \tag{17-15}$$

EXAMPLE 17.2

Using the screen analysis data of Graber and Taboada given above, compute all four mean diameters.

SOLUTION

Since the data are given in weight (mass) fractions, use (17-7), (17-8), (17-12), and (17-15).

$\bar{D}_p$, mm	x	$x/\bar{D}_p$	$x\bar{D}_p$	$x/\bar{D}_p^2$	$x/\bar{D}_p^3$
1.290	0.0186	0.0144	0.0240	0.0112	0.0087
1.090	0.0654	0.0600	0.0713	0.0550	0.0505
0.925	0.0811	0.0877	0.0750	0.0948	0.1025
0.725	0.4795	0.6614	0.3476	0.9122	1.2583
0.513	0.1815	0.3538	0.0931	0.6897	1.3444
0.363	0.1108	0.3052	0.0402	0.8409	2.3164
0.256	0.0448	0.1750	0.0115	0.6836	2.6703
0.181	0.0147	0.0812	0.0027	0.4487	2.4790
0.128	0.0025	0.0195	0.0003	0.1526	1.1921
0.098	0.0011	0.0112	0.0001	0.1145	1.1687
	1.0000	1.7695	0.6658	4.0032	12.5909

From (17-7),

$$\bar{D}_S = \frac{1}{1.7695} = 0.565\,\text{mm}$$

From (17-8),

$$\bar{D}_W = 0.666\,\text{mm}$$

From (17-12),

$$\bar{D}_N = \frac{4.0032}{12.5909} = 0.318\,\text{mm}$$

From (17-15),

$$\bar{D}_V = \left(\frac{1}{12.5909} \right)^{1/3} = 0.430\,\text{mm}$$

Thus, the mean diameters vary significantly.

17.2 THERMODYNAMIC CONSIDERATIONS

Solubility and Material Balances

Important thermodynamic properties for crystallization operations include melting point, heat of fusion, solubility, heat of crystallization, heat of solution, heat of transition, and supersaturation. For binary systems of water and soluble inorganic and organic chemicals, Mullin [1] presents extensive tables of solubility, as a function of temperature, and heat of solution at infinite dilution and room temperature (approximately 18–25°C). Data in water are listed in Table 17.5 for the inorganic salts of Table 17.1, where solubility data are given on a hydrate-free basis.

Solubilities are seen to vary widely from as low as 4.8 g/100 g of water for Na_2SO_4 (as the decahydrate) at 0°C to 952 g/100 g of water for $AgNO_3$ at 100°C. For KNO_3, the solubility increases by a factor of 18.6 for the same temperature increase.

The solubility of an inorganic compound can be even much lower than that shown for Na_2SO_4. Such compounds are generally considered to be just slightly or sparingly soluble or almost insoluble. The solubility of such compounds is usually expressed as a solubility product, K_c, in terms of ion concentrations. Data for several compounds are given in Table 17.6. For example, consider $Al(OH)_3$, which is sparingly soluble with a solubility product of $K_c = 1.1 \times 10^{-15}$ at 18°C and dissolves according to the equation

$$Al(OH)_{3_{(s)}} \Leftrightarrow Al^{3+}_{(aq)} + 3OH^-_{(aq)}$$

By the law of mass action, the equilibrium constant, called the solubility product for dissolution, is given by

$$K_c = \frac{(c_{Al^{3+}})(c_{OH^-})^3}{a_{Al(OH)_3}} = (c_{Al^{3+}})(c_{OH^-})^3 = 1.1 \times 10^{-15}$$

where the activity of $Al(OH)_3$ solid is taken as 1.0. Since, by stoichiometry,

$$(c_{OH^-}) = 3(c_{Al^{3+}}) \quad \text{and} \quad K_c = (c_{Al^{3+}})^4(3)^3 = 1.1 \times 10^{-15}$$

then,

$$(c_{Al^{3+}}) = c_{\text{dissolved } Al(OH)_3} = 8 \times 10^{-5}\,\text{gmoles/L}$$

which is a very small concentration.

Table 17.5 Solubility and Heat of Solution at Infinite Dilution of Some Inorganic Compounds in Water (A Positive Heat of Solution Is Endothermic)

Compound	Heat of Solution of Stable Hydrate (at Room Temperature) kcal/mole Compound	Solubility (Hydrate-free Basis) g/100 g H_2O at T, °C								Stable Hydrate at Room Temperature
		0	10	20	30	40	60	80	100	
NH_4Cl	+3.8	29.7	33.4	37.2	41.4	45.8	55.2	65.6	77.3	0
$(NH_4)_2SO_4$	+1.5	71.0	73.0	75.4	78.0	81.0	88.0	95.3	103.3	0
$BaCl_2$	+4.5	31.6	33.2	35.7	38.2	40.7	46.4	52.4	58.3	2
$CuSO_4$	+2.86	14.3	17.4	20.7	25.0	28.5	40.0	55.0	75.4	5
$MgSO_4$	+3.18	22.3	27.8	33.5	39.6	44.8	55.3	56.0	50.0	7
$MgCl_2$	−3.1	52.8	53.5	54.5	56.0	57.5	61.0	66.0	73.0	6
$NiSO_4$	+4.2	26	32	37	43	47	55	63	—	7
KCl	+4.4	27.6	31.0	34.0	37.0	40.0	45.5	51.1	56.7	0
KNO_3	+8.6	13.3	20.9	31.6	45.8	63.9	110	169	247	0
K_2SO_4	+6.3	7.4	9.3	11.1	13.1	14.9	18.3	21.4	24.2	0
$AgNO_3$	+5.4	122	170	222	300	376	525	669	952	0
$NaClO_3$	+5.4	80	89	101	113	126	155	189	233	0
NaCl	+0.93	35.6	35.7	35.8	36.1	36.4	37.1	38.1	39.8	0
$NaNO_3$	+5.0	72	78	85	92	98	—	133	163	0
Na_2SO_4	+18.7	4.8	9.0	19.4	40.8	48.8	45.3	43.7	42.5	10
$Na_2S_2O_3$	+11.4	52	61	70	84	103	207	250	266	5
Na_3PO_4	+15.0	1.5	4	11	20	31	55	81	108	12

Table 17.6 Concentration Solubility Products of Some Sparingly Soluble Inorganic Compounds

Compound	T, °C	K_c
Ag_2CO_3	25	6.15×10^{-12}
AgCl	25	1.56×10^{-10}
$Al(OH)_3$	15	4×10^{-13}
$Al(OH)_3$	18	1.1×10^{-15}
$BaSO_4$	18	0.87×10^{-10}
$CaCO_3$	15	0.99×10^{-8}
$CaSO_4$	10	1.95×10^{-4}
$CuSO_4$	16–18	2×10^{-47}
$Fe(OH)_3$	18	1.1×10^{-36}
$MgCO_3$	12	2.6×10^{-5}
ZnS	18	1.2×10^{-23}

For less sparingly soluble compounds, the equilibrium constant, called K_a, is more rigorously expressed in terms of ionic activities or activity coefficients:

$$K_a = \frac{(a_{Al^{3+}})(a_{OH^{-1}})^3}{a_{Al(OH)_3}} = (\gamma_{Al^{3+}})(c_{Al^{3+}})(\gamma_{OH^-})^3(c_{OH^-})^3$$

In general, $\gamma \approx 1.0$ for $c < 1 \times 10^{-3}$ gmoles/L. As c rises above 1×10^{-3} gmoles/L, γ decreases, but may pass through a minimum and then increase. Mullin [1] presents activity-coefficient data at 25°C for soluble inorganic compounds over a wide range of concentration.

Although the solubility of most inorganic compounds increases with increasing temperature, a few common compounds exhibit a so-called negative or inverted solubility, in certain ranges of temperature, where solubility decreases with increasing temperature. These compounds are the so-called hard salts, which include anhydrous Na_2SO_4 and $CaSO_4$.

A considerable change in the solubility curve can occur when a phase transition from one stable hydrate to another takes place. For example, in Table 17.5, $Na_2SO_4 \cdot 10H_2O$ is the stable form from 0°C to about 32.4°C. In that temperature range, the solubility increases rapidly from 4.8 to 49.5 g (hydrate-free basis)/100 g H_2O. From 32.4°C to 100°C, the stable form is Na_2SO_4, whose solubility decreases slowly from 49.5 to 42.5 g/100 g H_2O. In the phase diagram of Figure 17.2 for the $MgSO_4$-water system, the solubility-temperature curves of each of the four hydrated forms has a distinctive slope.

The solubility characteristic of a solute in a particular solvent is, by far, the most important property for determining: (1) the best method for causing crystallization, and (2) the ease or difficulty in growing crystals. Crystallization by cooling is only attractive for compounds having a solubility that decreases rapidly with decreasing temperature above ambient temperature. Such is not the case for most of the compounds in Table 17.5. For NaCl, crystallization by cooling would be undesirable because the solubility decreases

only by about 10% when the temperature decreases from 100 to 0°C. For most soluble inorganic compounds, cooling by evaporation is the preferred technique.

Solid compounds with a very low solubility can be produced by reacting two soluble compounds. For example, in Table 17.6, solid $Al(OH)_3$ can be formed by the reaction

$$AlCl_{3(aq)} + 3NaOH_{(aq)} \Leftrightarrow Al(OH)_{3(ppt)} + 3NaCl_{(aq)}$$

However, the reaction is so fast that only very fine crystals, called a precipitate, are produced, with no simple method to cause them to grow to large crystals.

EXAMPLE 17.3

The concentrate from an evaporation system is 4,466 lb/h of 37.75 wt% $MgSO_4$ at 170°F and 20 psia. It is mixed with 9,860 lb/h of a saturated aqueous recycle filtrate of $MgSO_4$ at 85°F and 20 psia and sent to a vacuum crystallizer, operating at 85°F and 0.58 psia in the vapor space, to produce water vapor and a magma of 20.8 wt% crystals and 79.2 wt% saturated solution. The magma is sent to a filter, from which filtrate is recycled as mentioned above. Determine the lb/h of water evaporated and the maximum production rate of crystals in tons/day (dry basis for 2000 lb/ton).

SOLUTION

For the saturated filtrate at 85°F, the weight fraction of $MgSO_4$, from Figure 17.2, is 28 wt%. Therefore, $MgSO_4$ in the recycle filtrate is 9,860(0.28) = 2,760 lb/h. By material balance around the mixing step,

	lb/h		
Component	**Feed**	**Recycle Filtrate**	**Crystallizer Feed**
$MgSO_4$	1,686	2,760	4,446
H_2O	2,780	7,100	9,880
	4,466	9,860	14,326

The material balance around the crystallizer is conveniently made by a balance on $MgSO_4$. At 85°F, from Figure 17.2, the magma is 20.8 wt% $MgSO_4 \cdot 7H_2O$ crystals and 79.2 wt% of 28 wt% aqueous $MgSO_4$ liquid. Because the MW of $MgSO_4$ and $MgSO_4 \cdot 7H_2O$ are 120.4 and 246.4, respectively, the crystals are 120.4/246.4 = 0.4886 mass fraction $MgSO_4$. Therefore, by a $MgSO_4$ balance,

$$4{,}446 = 0.28\,L + 0.4886\,S \quad (1)$$

where

L = lb/h of liquid

S = lb/h of crystals

Also,

$$S = 0.208(S + L) \quad (2)$$

Solving (1) and (2) simultaneously,

$$S = 2{,}856 \text{ lb/h}$$
$$L = 10{,}876 \text{ lb/h}$$

By a total material balance around the crystallizer,

$$F = V + L + S$$

where F = total feed rate and V = evaporation rate. Therefore,

$$14{,}326 = V + 10{,}876 + 2{,}856 \quad (3)$$

Solving,

$$V = 594 \text{ lb/h}$$

The results in tabular form are:

	lb/h for crystallizer			
Component	**Feed**	**Vapor**	**Liquid**	**Crystals**
$MgSO_{4(aq)}$	4,446	0	3,045	0
$MgSO_4 \cdot 7H_2O_{(s)}$	0	0	0	2,856
H_2O	9,880	594	7,831	0
	14,326	594	10,876	2,856

The maximum production rate of crystals is

$$\frac{2{,}856}{2{,}000}(24) = 34.3 \text{ tons/day}$$

A large number of organic compounds, particularly organic acids with relatively moderate melting points (125–225°C), are also soluble in water. Some data are given in Table 17.7, where it is seen that the solubility often increases significantly with increasing temperature. For example, the solubility of o-phthalic acid increases from a very low value of 0.56 to 18.0 g/100 g H_2O when the temperature increases from 20 to 100°C.

Table 17.7 Solubility and Melting Point of Some Organic Compounds in Water

	Melting	Solubility, g/100 g H_2O at T, °C							
Compound	Point, °C	0	10	20	30	40	60	80	100
Adipic acid	153	0.8	1.0	1.9	3.0	5.0	18	70	160
Benzoic acid	122	0.17	0.20	0.29	0.40	0.56	1.16	2.72	5.88
Fumaric acid (trans)	287	0.23	0.35	0.50	0.72	1.1	2.3	5.2	9.8
Maleic acid	130	39.3	50	70	90	115	178	283	—
Oxalic acid	189	3.5	6.0	9.5	14.5	21.6	44.3	84.4	—
o-phthalic acid	208	0.23	0.36	0.56	0.8	1.2	2.8	6.3	18.0
Succinic acid	183	2.8	4.4	6.9	10.5	16.2	35.8	70.8	127
Sucrose	d	179	190	204	219	238	287	362	487
Urea	133	67	85	105	135	165	250	400	730
Uric acid	d	0.002	0.004	0.006	0.009	0.012	0.023	0.039	0.062

EXAMPLE 17.4

Oxalic acid is to be crystallized from a saturated aqueous solution initially at 100°C. To what temperature does the solution have to be cooled to crystallize 95% of the acid as the dihydrate?

SOLUTION

Assume a basis of 100 g of water. From Table 17.7, the amount of dissolved oxalic acid at 100°C is 84.4 g.

Amount to be crystallized = 0.95(84.4) = 80.2 g.

Amount of oxalic acid left in solution = 84.4 − 80.2 = 4.2 g.

MW of oxalic acid = 90.0.

MW of water = 18.0.

Water of hydration for $2H_2O = \dfrac{2(18.0)}{90.0} = 0.4\dfrac{\text{g } H_2O}{\text{g oxalic acid}}$.

Therefore water of crystallization = 0.4(80.2) = 32.1 g H_2O.

Liquid water remaining = 100 − 32.1 = 67.9 g.

Final solubility must be $\dfrac{4.2}{67.9} \times 100 = 6.19\dfrac{\text{g}}{100\text{ g } H_2O}$.

From Table 17.7, by linear interpolation, temperature = 10.6°C.

Enthalpy Balances

When an anhydrous solid compound, whose solubility increases with increasing temperature, dissolves isothermally in water or some other solvent, heat must be absorbed by the solution. This amount of heat per mole of compound in an infinite amount of solvent varies with temperature and is referred to as the *heat of solution at infinite dilution* (ΔH_{sol}^{∞}). For example, in Table 17.5, the solubility of anhydrous NaCl is seen to increase slowly with increasing temperature from 10 to 100°C. Correspondingly, the heat of solution at infinite dilution in Table 17.5 is modestly endothermic (+) at room temperature. In contrast, the solubility of anhydrous KNO_3 increases more rapidly with increasing temperature, resulting in a higher endothermic heat of solution. For compounds that form hydrates, the heat of solution at infinite dilution may be negative (exothermic) for the anhydrous form, but becomes less negative and often positive as higher hydrates are formed by the reaction:

$$A \cdot nH_2O_{(s)} \rightarrow A_{(aq)} + nH_2O$$

For example, the following heats of solution at infinite dilution in kJ/mol of compound at 18°C for four hydrates of $MgSO_4$ clearly show this effect:

$MgSO_4$	−88.3
$MgSO_4 \cdot H_2O$	−58.6
$MgSO_4 \cdot 6H_2O$	−2.3
$MgSO_4 \cdot 7H_2O$	+13.3

Heats of a solution for a number of hydrated and anhydrous compounds are listed in Table 17.5.

As a solid compound continues to dissolve in a solvent, the heat of solution, which is now referred to as the integral heat of solution, varies somewhat, as shown in Figure 17.9 for several compounds as a function of concentration. The integral heat of solution at saturation is numerically equal, but opposite in sign, to the heat of crystallization. The difference between the integral heat of solution at saturation and the heat of solution at infinite dilution is the heat of dilution:

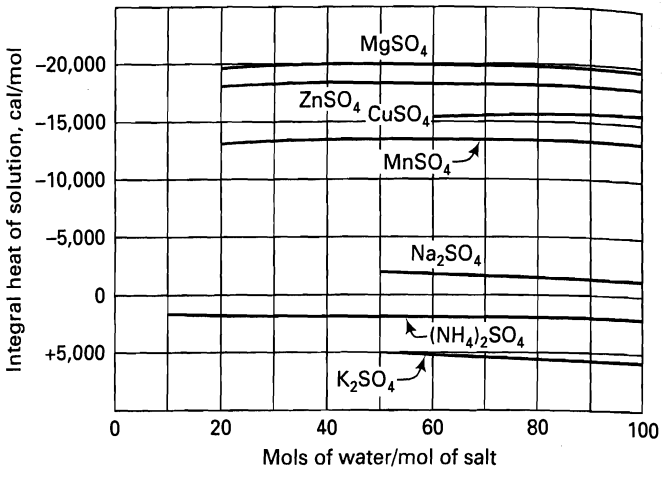

Figure 17.9 Integral heats of solution for sulfates in water at 25°C.

$$\Delta H_{sol}^{sat} - \Delta H_{sol}^{\infty} = \Delta H_{dil}$$

with

$$\Delta H_{sol}^{sat} = -\Delta H_{crys}$$

As indicated in Figure 17.9, the heat of dilution is relatively small; therefore, it is common to use:

$$\Delta H_{crys} \approx -\Delta H_{sol}^{\infty}$$

An energy-balance calculation around a crystallizer is complex because it can involve not only the integral heat of solution and/or heat of crystallization, but also the specific heats of the solute and solvent and the heat of vaporization of the solvent. The calculation is readily made if an enthalpy-mass fraction diagram is available for the system, including solubility and phase-equilibria data. Mullin [1] lists 11 aqueous binary systems for which such a diagram has been constructed. A diagram for the $MgSO_4$-H_2O system is shown in Figure 17.10. The enthalpy datum is pure liquid water at 32°F (consistent with steam tables in American Engineering Units) at Point *p* and solid $MgSO_4$ at 32°F (not shown in Figure 17.10).

Points *a* to *l*, *n*, *p*, and *q* in the enthalpy-mass fraction diagram of Figure 17.10 correspond to the same points in the phase diagram of Figure 17.2. In Figure 17.10, the isotherms in the region above Curve pabcdq pertain to enthalpies of unsaturated solutions of $MgSO_4$. The straightness of these isotherms indicates that the heat of dilution is almost negligible. In this solid-free region, a 30 wt% aqueous solution of $MgSO_4$ has a specific enthalpy at 110°F of −31 Btu/lb solution.

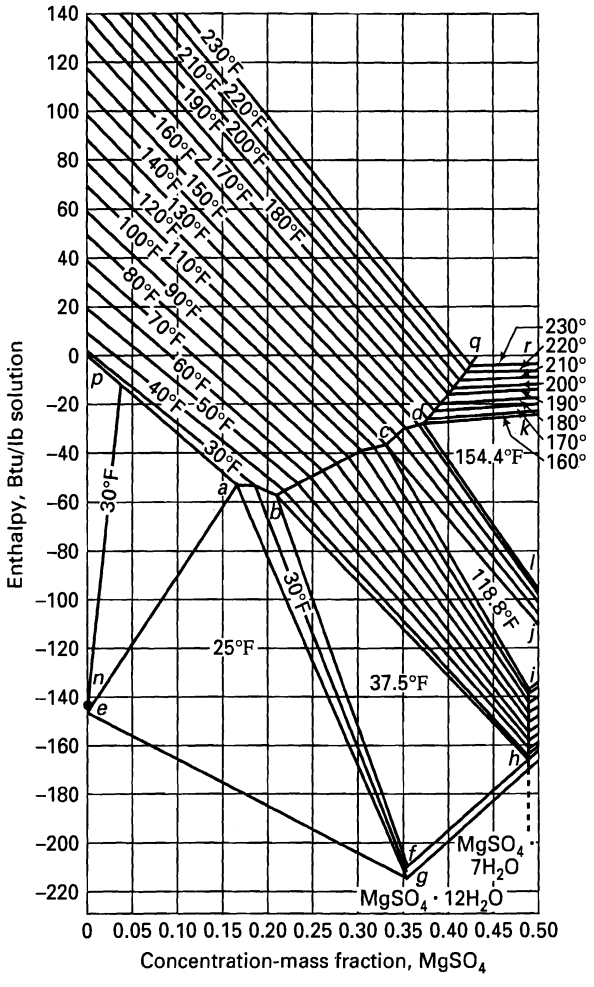

Figure 17.10 Enthalpy-concentration diagram for the $MgSO_4$-H_2O system at 1 atm.

In the region below the solubility curve *pabcdq*, in both Figures 17.2 and 17.10, the following phases exist at equilibrium:

Region	Temperature Range, °F	Phases
pae	25–32	ice and aqueous solution of $MgSO_4$
ea	25	ice and eutectic mixture
ag	25	eutectic and $MgSO_4 \cdot 12H_2O$
abfg	25–37.5	saturated solution and $MgSO_4 \cdot 12H_2O$
bcih	37.5–118.8	saturated solution and $MgSO_4 \cdot 7H_2O$
cdlj	118.8–154.4	saturated solution and $MgSO_4 \cdot 6H_2O$
dqrk	154.4–	saturated solution and $MgSO_4 \cdot H_2O$

Pure ice exists at Point *e*, where in Figure 17.10 the specific enthalpy is –147 Btu/lb, which is the heat of crystallization of water at 32°F. If a 30 wt% aqueous solution of $MgSO_4$ is cooled from 110°F to 70°F, the equilibrium magma will consist of a saturated solution of 26 wt% $MgSO_4$ and crystals of $MgSO_4 \cdot 7H_2O$ (49 wt% $MgSO_4$) as determined from the ends of the 70°F tie line that extends from solubility curve *bc* to $MgSO_4 \cdot 7H_2O$ solid line *ih*. The relative amounts of the two equilibrium phases can be computed from a $MgSO_4$ balance. For a basis of 100 lb of mixture, let S be the pounds of crystals and A be the pounds of saturated aqueous solution. Thus, the $MgSO_4$ balance is

$$0.30(100) = 0.49\,S + 0.26\,A$$

where

$$100 = S + A$$

Solving, $S = 17.4$ lb and $A = 82.6$ lb. The enthalpy of the mixture at 70°F is –65 Btu/lb, which is equivalent to enthalpies of –46 and –155 Btu/lb, respectively, for the solution and crystals.

EXAMPLE 17.5

For the conditions of Example 17.3, calculate the Btu/h of heat addition for the crystallizer.

SOLUTION

An overall energy balance around the crystallizer gives

$$m_{\text{feed}} H_{\text{feed}} + Q_{\text{in}} = m_{\text{vapor}} H_{\text{vapor}} + m_{\text{liquid}} H_{\text{liquid}} + m_{\text{crystals}} H_{\text{crystals}} \quad (1)$$

where liquid refers to the saturated-liquid portion of the magma.

From the solution to Example 17.3, the feed consists of two streams:

$$m_{\text{feed1}} = 4{,}466 \text{ lb/hr of } 37.75 \text{ wt\% } MgSO_4 \text{ at } 170°F$$

$$m_{\text{feed2}} = 9{,}860 \text{ lb/hr of } 28.0 \text{ wt\% } MgSO_4 \text{ at } 85°F$$

From Figure 17.10,

$$H_{\text{feed1}} = -20 \text{ Btu/lb}$$

$$H_{\text{feed2}} = -43 \text{ Btu/lb}$$

Therefore,

$$m_{\text{feed}} H_{\text{feed}} = 4{,}466(-20) + 9{,}860(-43) = -513{,}000 \text{ Btu/h}$$

$$m_{\text{vapor}} = 594 \text{ lb/h at } 85°F \text{ and } 0.58 \text{ psia}$$

The vapor enthalpy does not appear on Figure 17.10, but enthalpy tables for steam can be used since they are based on the same datum (i.e., liquid water at 32°F).

Therefore, $H_{\text{vapor}} = 1099$ Btu/lb from steam tables and

$$m_{\text{vapor}} H_{\text{vapor}} = 594(1099) = 653{,}000 \text{ Btu/h}$$

The liquid plus crystals can be treated together as the magma. From the solution to Example 17.3,

$$m_{\text{liquid}} + m_{\text{crystals}} = m_{\text{magma}} = 10{,}876 + 2{,}856$$
$$= 13{,}732 \text{ lb/h of } 32.4 \text{ wt\% } MgSO_4 \text{ at } 85°F$$

From Figure 17.10,

$$H_{\text{magma}} = -67 \text{ Btu/lb}$$

and

$$m_{\text{magma}} H_{\text{magma}} = 13{,}732(-67) = -920{,}000 \text{ Btu/lb}$$

From (1),

$$Q_{\text{in}} = 653{,}000 - 920{,}000 - (-513{,}000) = 246{,}000 \text{ Btu/h}$$

In the absence of an enthalpy-mass fraction diagram, a reasonably accurate energy balance can be made if data for heat of crystallization and specific heats of the solutions are available or can be estimated and the heat of dilution is neglected, as shown in the next example.

EXAMPLE 17.6

The feed to a cooling crystallizer is 1,000 lb/h of 32.5 wt% $MgSO_4$ in water at 120°F. This solution is cooled to 70°F to form crystals of the heptahydrate. Estimate the heat removal rate in Btu/h.

SOLUTION

Material balance

From Figure 17.2, the feed at 120°F contains no crystals, but the magma at 70°F consists of crystals of the heptahydrate and a mother liquor of 26 wt% $MgSO_4$. By material balance in the manner of Example 17.3, the following results are obtained:

	lb/hr		
	Feed	Mother Liquor	Crystals
H_2O	675	530	0
$MgSO_4$	325	186	0
$Mg_2SO_4 \cdot 7H_2O$	0	0	284
	1,000	716	284

Take a thermodynamic path consisting of cooling the feed from 120°F to 70°F followed by crystallization at 70°F. From Hougen, Watson, and Ragatz [3], the specific heat of the feed is approximately constant over the temperature range at 0.72 Btu/lb-°F. Therefore, the heat that must be removed to cool the feed to 70°F is

$$1{,}000(0.72)(120 - 70) = 36{,}000\,\text{Btu/h}$$

For data presented earlier in this section, the heat of crystallization can be taken as the negative of the heat of solution at infinite dilution:

$$-13.3\,\text{kJ/mole of heptahydrate}$$

or

$$-23.2\,\text{Btu/lb of heptahydrate}$$

Therefore, the heat that must be removed during crystallization of the heptahydrate is

$$284(23.2) = 6{,}600\,\text{Btu/h}$$

The total heat removal is 36,000 + 6,600 = 42,600 Btu/h.

If this example is solved with Figure 17.10, in the manner of Example 17.5, the result is 44,900 Btu/h, which is 5.4% higher.

17.3 KINETIC AND TRANSPORT CONSIDERATIONS

Crystallization is a complex phenomenon that involves three steps: *nucleation,* mass transfer of the solute to the crystal surface, and incorporation of the solute into the crystal lattice structure. Collectively, these phenomena are referred to as *crystallization kinetics.* Experimental data show that the driving force for all three steps is *supersaturation.*

Supersaturation

The solubility property discussed in the previous section refers to relatively large crystals of the size that can be seen by the naked eye, i.e., larger than 20 μm in diameter. As crystal size decreases below this diameter, solubility noticeably increases, making it possible to supersaturate a solution if it is cooled slowly without agitation. This phenomenon, based on the work of Miers and Isaac [4] in 1907, is represented in Figure 17.11, where the normal solubility curve, c_s is represented as a solid line. The solubility of very small crystals can fall in the metastable region which is shown to have a metastable limiting solubility, c_m, given by the dashed line.

Consider a solution at a temperature, T_1, given by the vertical line in Figure 17.11. If the concentration is given by Point *a*, the solution is undersaturated and crystals of all sizes dissolve. At Point *b*, equilibrium exists between a saturated solution and crystals that can be seen by the naked eye. In the metastable region at Point c, crystals can grow but cannot nucleate. If no crystals are present, none can form. For that concentration, the difference between the temperature at Point *e* on the solubility curve and Point *c* in the metastable region is the supersaturation temperature difference, which may be about 2°F. The supersaturation, $\Delta c = c - c_s$, is the difference in concentration between Points *c* and *b*.

At Point *d*, spontaneous nucleation of very small crystals, invisible to the naked eye, occurs. The difference in temperature between Points *f* and *d* is the limit of the supersaturation temperature difference. The limiting supersaturation is $\Delta c_{\text{limit}} = c_m - c_s$.

The relationship between solubility and crystal size is given quantitatively by the Kelvin equation (also known as

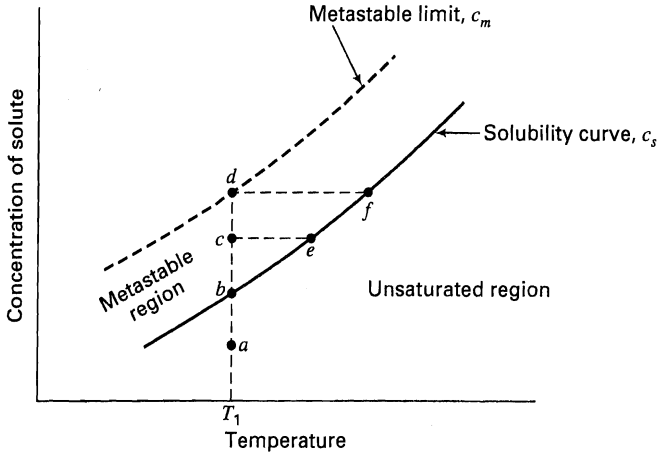

Figure 17.11 Representative solubility-supersolubility diagram.

the Gibbs–Thompson and Ostwald equations):

$$\ln\left(\frac{c}{c_s}\right) = \left(\frac{4v_s\sigma_{s,L}}{vRTD_p}\right) \qquad (17\text{-}16)$$

where

v_s = molar volume of the crystals

$\sigma_{s,L}$ = interfacial tension

v = number of ions/molecule of solute

c/c_s = supersaturation ratio = S

Measured values of interfacial tension (also called surface energy) range from as low as 0.001 J/m^2 for very soluble compounds to 0.170 for compounds of low solubility.

As might be expected, (17-16), in a more general form, applies to the effect of droplet diameter on vapor pressure and solubility in another liquid phase.

It is common to define a relative supersaturation, s, by

$$s = \frac{c - c_s}{c_s} = \frac{c}{c_s} - 1 = S - 1 \qquad (17\text{-}17)$$

In practice, s is usually less than 0.02 or 2%. For such small values, $\ln(c/c_s)$ can be approximated by s with no more than a 1% error.

EXAMPLE 17.7

Determine the effect of crystal diameter on the solubility of KCl in water at 25°C.

SOLUTION

From Table 17.5, by interpolation, $c_s = 35.5$ g/100 g H_2O.

Because KCl dissociates into K^+ and Cl^-, $v = 2$.

MW of KCl = 74.6.

Density of KCl crystals = 1980 kg/m^3.

$$v_s = \frac{74.6}{1980} = 0.0376\ \text{m}^3/\text{kmol}$$

$$T = 298\ \text{K}$$

$$R = 8314\ \text{J/kmol-K}$$

From Mullin [1], page 200,

$$\sigma_{s,L} = 0.028\ \text{J/m}^2$$

From (17-16),

$$c = c_s \exp\left(\frac{4v_s\sigma_{s,L}}{vRTD_p}\right)$$

$$= 35.5 \exp\left[\frac{4(0.0376)(0.028)}{2(8315)(298)D_p}\right] \text{ for } D_p \text{ in m, or} \qquad (1)$$

$$= 35.5 \exp(0.00085/D_p, \mu\text{m})$$

D_p, μm	c/c_s	c, g KCl/100 g H_2O
0.01	1.0887	38.65
0.10	1.0085	35.80
1.00	1.00085	35.53
10.00	1.000085	35.50
100.00	1.0000085	35.50

Nucleation

To determine the volume or residence time of the magma in a crystallizer, the rate of *nucleation* (birth) of crystals and their rate of growth must be known or estimated. The relative rates of nucleation and growth are very important because they determine crystal size and size distribution. Nucleation may be *primary* or *secondary* depending on whether the supersaturated solution is free of crystalline surfaces or contains crystals, respectively. Primary nucleation requires a high degree of supersaturation and is the principal mechanism occurring in precipitation. The theory of primary nucleation is well developed and applies as well to the condensation of liquid droplets from a supersaturated vapor and the formation of droplets of a second liquid phase from an initial liquid phase. However, secondary nucleation is the principal mechanism in commercial crystallizers, where crystalline surfaces are present and large crystals are desirable.

Primary Nucleation

Primary nucleation can be homogeneous or heterogeneous. The former occurs within the supersaturated solution in the absence of any foreign matter, such as dust. Molecules in the solution first associate to form a *cluster,* which may dissociate or grow. If a cluster gets large enough to take on the appearance of a lattice structure, it becomes an *embryo.* Further growth can result in a stable crystalline *nucleus* whose size exceeds that given by (17-16) for the prevailing degree of supersaturation.

The rate of homogeneous nucleation is given by classical chemical kinetics in conjunction with (17-16), as discussed by Nielsen [5]. The resulting expression is

$$B^o = A \exp\left[\frac{-16\pi v_s^2\sigma_{s,L}^3 N_a}{3v^2(RT)^3\left[\ln\left(\frac{c}{c_s}\right)\right]^2}\right] \qquad (17\text{-}18)$$

where

B^o = rate of homogeneous primary nucleation, number of nuclei/cm^3-s

A = frequency factor

N_a = Avogadro's number = 6.022×10^{26} molecules/kmol

Theoretically, $A = 10^{30}$ nuclei/cm^3-s; however, observed values are generally different due to the unavoidable presence of foreign matter. Thus, (17-18) can also be applied to heterogeneous primary nucleation, where A is determined experimentally and may be many orders of magnitude different from the theoretical value. A value of 10^{25} is often quoted.

The rate of primary nucleation is extremely sensitive to the supersaturation ratio, S, defined by (17-17), as illustrated in the following example.

EXAMPLE 17.8

Using the data in Example 17.7, estimate the effects of relative supersaturation on the primary homogeneous nucleation of KCl from an aqueous solution at 25°C. Use values of s corresponding to values of c/c_s of 2.0, 1.5, and 1.1.

SOLUTION

For $c/c_s = 2.0$, $\ln(c/c_s) = 0.693$. From (17-18), using data in Example 17.7,

$$B^o = 10^{30} \exp\left[\frac{-16(3.14)(0.0376)^2(0.028)^3(6.022 \times 10^{26})}{3(2)^2(8315)^3(298)^3(0.693)^2}\right]$$

$$= 2.23 \times 10^{25} \text{ nuclei/cm}^3\text{-s}$$

Calculations for the other values of c/c_s are obtained in the same manner with the following results:

c/c_s	B^o, nuclei/cm^3-s
2.0	2.23×10^{25}
1.5	2.60×10^{16}
1.1	0

Since large values of the supersaturation ratio ($c/c_s > 1.02$) are essentially impossible for crystallization of solutes of moderate to high solubility (e.g., solutes listed in Tables 17.5 and 17.7), primary nucleation for these solutes never occurs. However, for relatively insoluble solutes (e.g., solutes listed in Table 17.6), large values of c/c_s can be generated rapidly from ionic reactions causing rapid precipitation of very fine particles. If $A = 10^{25}$ is used, B^o is divided by 10^5.

Secondary Nucleation

Nucleation in industrial crystallizers occurs mainly by secondary nucleation caused by the presence of existing crystals in the supersaturated solution. Secondary nucleation can occur by: (1) fluid shear past crystal surfaces that sweeps away nuclei, (2) collisions of crystals with each other, and (3) collisions of crystals with metal surfaces such as the crystallizer vessel wall or agitator blades. The latter two mechanisms, which are referred to as *contact nucleation* are the most common types since they can occur at the low values of relative supersaturation that are typically encountered in industrial applications.

In the absence of a theory for the complex phenomena of secondary nucleation, the following empirical power-law function, which correlates much of the experimental data, is widely used:

$$B^o = k_N s^b M_T^j N^r \tag{17-19}$$

where M_T = mass of crystals per volume of magma and N = agitation rate (e.g., rpm of an impeller). The constants, k_N, b, j, and r, are determined from experimental data, on the system of interest, as discussed below in the section on a crystallizer model.

Crystal Growth

In 1897, Noyes and Whitney [6] presented a mass-transfer theory of crystal growth based on equilibrium at the crystal-solution interface. Thus, they wrote

$$dm/dt = k_c A(c - c_s) \tag{17-20}$$

where dm/dt = rate of mass deposited on the crystal surface, A = surface area of the crystal, k_c = mass-transfer coefficient, c = mass solute concentration in the bulk supersaturated solution, and c_s = mass solute concentration in the solution at saturation. Nernst [7] proposed the existence of a thin stagnant film of solution adjacent to the crystal face through which molecular diffusion of the solute took place. Thus, $k_c = \mathcal{D}/\delta$, where $\mathcal{D}$ = diffusivity and δ = film thickness, where the latter was assumed to depend on velocity of the solution past the crystal as determined by the degree of agitation.

The theory of Noyes and Whitney was challenged by Miers [8], who showed experimentally that an aqueous solution in contact with crystals of sodium chlorate was not saturated at the crystal–solution interface, but was supersaturated. This finding led to a two-step theory of crystal growth, referred to as the diffusion-reaction theory, as described by Valeton [9]. Mass transfer of solute from the bulk of the solution to the crystal–solution interface occurs in the first step, as given by a modification of (17-20):

$$dm/dt = k_c A(c - c_i) \tag{17-21}$$

where c_i is the supersaturated concentration at the interface. In the second step, a first-order reaction is assumed to occur at the crystal–solution interface, in which solute molecules are integrated into the crystal-lattice structure. Thus, for this kinetic step,

$$dm/dt = k_i A(c_i - c_s) \tag{17-22}$$

If (17-21) and (17-22) are combined to eliminate c_i, we obtain

$$dm/dt = \frac{A(c - c_s)}{1/k_c + 1/k_i} \tag{17-23a}$$

Typically, k_c will depend on the velocity of the solution as shown in Figure 17.12. At low velocities, the growth rate

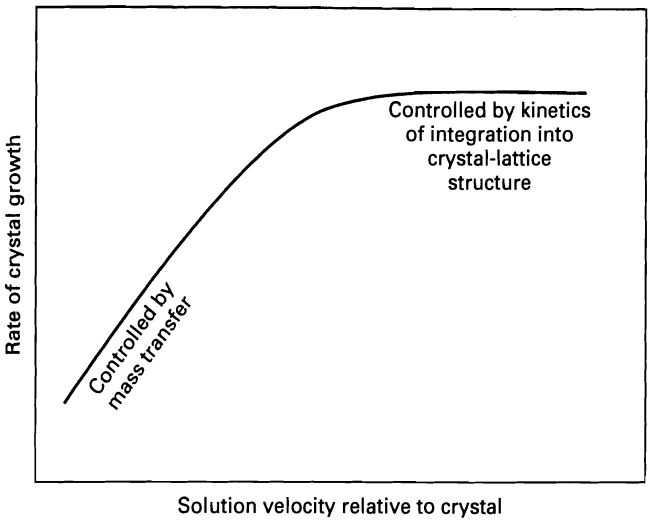

Figure 17.12 Effect of solution velocity past crystal on the rate of crystal growth.

may be controlled by the first step. The second step can be important, especially when the solution velocity past the crystal surface is high, such that k_c is large compared to k_i. In adsorption, the kinetic step is rarely important. It is also unimportant in dissolution, the reverse of crystallization.

The mass-transfer coefficient, k_c, for the first step, is independent of the crystallization process and can be estimated from general fluid-solid particle mass-transfer-coefficient correlations described in Chapters 3 and 15. The kinetic coefficient, k_i, is peculiar to the crystallization process. A number of theories have been advanced for the kinetic step, as discussed in Myerson [10]. One prominent theory is that of Burton, Cabrera, and Frank [11], which is based on a growth spiral starting from a screw dislocation, as shown in Figure 17.13 and verified in some experimental studies using scanning-electron microscopy. A dislocation is an imperfection in the crystal structure. The screw-dislocation theory predicts a growth rate proportional to: $(c_i - c_s)^2$ at low supersaturation and to $(c_i - c_s)$ at high supersaturation. Unfortunately, the theory does not provide a means to predict k_i. Accordingly, (17-23a) is generally applied with k_c estimated from available correlations and k_i back-calculated from experimental data.

Although crystals do not grow as spheres, let us develop an equation for the rate of increase of the diameter of a spherical crystal. Rewriting (17-23a) in terms of an overall coefficient,

$$dm/dt = K_c A(c - c_s) \tag{17-23b}$$

Since $A = \pi D_p^2$ and $m = \frac{\pi D_p^3}{6}\rho$

Equation (17-23b) becomes

$$\frac{dD_p}{dt} = \frac{2K_c(c - c_s)}{\rho} = \frac{2K_c(\Delta c)}{\rho} \tag{17-24}$$

If the rate of growth is controlled by k_i, which is assumed to be independent of D_p, then

$$\frac{\Delta D_p}{\Delta t} = \frac{2k_i \Delta c}{\rho} \tag{17-25}$$

and the rate of increase of crystal size is linear in time for a constant supersaturation. If the rate of growth is controlled by k_c at a low velocity, then, from (15-60),

$$K_c = k_c = 2\mathcal{D}/D_p \tag{17-26}$$

where $\mathcal{D}$ is solute diffusivity.

Substitution of (17-26) into (17-24) gives

$$\frac{dD_p}{dt} = \frac{4\mathcal{D}(\Delta c)}{D_p \rho} \tag{17-27}$$

Integration from D_{p_o} to D_p gives

$$\frac{D_p^2 - D_{p_o}^2}{2} = \frac{4\mathcal{D}(\Delta c)}{\rho} t \tag{17-28}$$

If $D_{p_o} \ll D_p$, (17-28) reduces to

$$D_p = \left(\frac{8\mathcal{D}(\Delta c)t}{\rho}\right)^{1/2} \tag{17-29}$$

In this case, the increase in crystal diameter slows with time.

At higher solution velocities where k_c still controls, the use of (15-62) results in

$$K_c = k_c = C_1/D_p^{1/2} \tag{17-30}$$

For this case, the increase in crystal diameter also slows with time, but not as rapidly as predicted by (17-29). It is

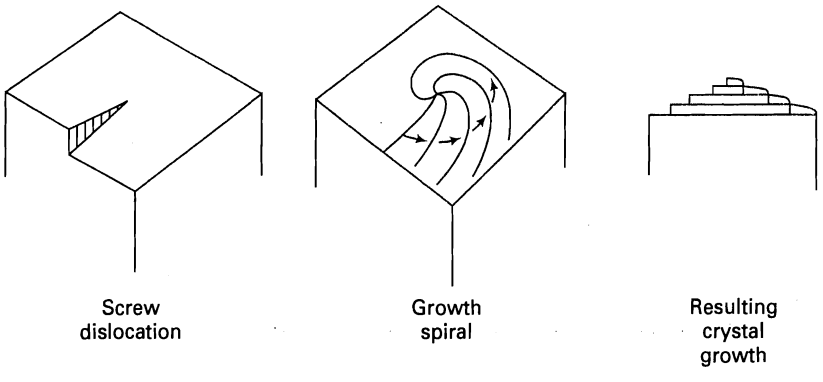

Figure 17.13 Screw-dislocation mechanism of crystal growth.

common to assume that the rate of crystal growth is controlled by k_i and, thus, is not dependent on crystal size and is, therefore, invariant with time. This assumption will be utilized in a latter section of this chapter to develop a useful crystallizer model.

EXAMPLE 17.9

The heptahydrate of $MgSO_4$ is to be crystallized batchwise from a seeded aqueous solution. A low supersaturation is to be used to avoid primary nucleation and a mild agitation is to be applied to minimize secondary nucleation. The temperature in the crystallizer will be maintained at 35°C, at which the solubility of $MgSO_4$ in water is 30 wt%. The crystallizer will be charged with 3,000 lb of a saturated solution at that temperature. To this solution will be added 2 lb of heptahydrate seed crystals of 50 μm in diameter. A supersaturation of 0.01 gm of heptahydrate per gm of solution at 35°C will be maintained during crystallization by operating the crystallizer at vacuum and using heat exchange and the heat of crystallization to gradually evaporate water from the solution. Based on the assumptions and data listed below, determine the following if the final crystal size is to be 400 μm.

(a) Yield of crystals of heptahydrate in pounds.

(b) Number of crystals.

(c) Amount of water in pounds that will have to be evaporated.

(d) Product magma density in pounds of crystals per pound of solution.

(e) Crystallizer volume in gallons if the volume occupied by the magma during operation is at the most 50% of the crystallizer volume.

(f) Crystallizer pressure in psia and the boiling-point elevation in °F.

(g) Time in minutes to grow the crystals to the final size.

(h) Amount of heat transfer in Btu.

(i) Also, determine whether crystal growth is controlled by mass transfer, by surface reaction (incorporation into the lattice), or by both.

Assumptions and Data:

1. No primary or secondary nucleation.
2. Properties of aqueous 30 wt% $MgSO_4$ at 35°C:

   density = 1.34 g/cm^3

   viscosity = 8 cP

   diffusivity of $MgSO_4 = 1.10 \times 10^{-5}$ cm^2/s
3. Density of the crystals = 1.68 g/cm^3.
4. Crystal shape can be approximated as a sphere.
5. Average crystal-face growth rate, including effects of both mass transfer and surface reaction = 0.005 mm/min.
6. Solution velocity past crystal face = 5 cm/s.

SOLUTION

Molecular weights:		
	$MgSO_4$	120.5
	$MgSO_4 \cdot 7H_2O$	246.6
	H_2O	18.02

Initial charge:

900 lb aq $MgSO_4$
2,100 lb H_2O
3,000 lb
+2 lb $MgSO_4 \cdot 7H_2O$ crystal seeds

(a) Crystals grow from 50 μm to 400 μm in diameter:

$$\text{yield} = 2\left(\frac{400}{50}\right)^3 = 1{,}024 \text{ lb} \quad MgSO_4 \cdot 7H_2O$$

(b) Number of crystals, based on the crystal seeds,

$$= \frac{\text{mass of seeds}}{\text{mass/seed}}$$

$$= \frac{2(454)}{1.68\left(\frac{3.14}{6}\right)(50 \times 10^{-4})^3}$$

$$= 8.26 \times 10^9, \text{ where mass/seed} = \rho_p V_p = \rho \frac{\pi D_p^3}{6}$$

(c) Pounds of heptahydrate crystallized = 1,024 − 2 = 1,022 lb

$$H_2O \text{ of hydration} = 1{,}022\left(\frac{246.6 - 120.5}{246.6}\right) = 523 \text{ lb}$$

$MgSO_4$ in crystals = 1,022 − 523 = 499 lb

$MgSO_4$ left in solution = 900 − 499 = 401 lb

$$H_2O \text{ left in solution} = 401\left(\frac{70}{30}\right) = 936 \text{ lb}$$

H_2O evaporated = 2,100 − 523 − 936 = 641 lb

(d) Final mother liquor = 936 + 401 = 1,337 lb

$$\text{Magma density} = \left(\frac{1{,}024}{1{,}337}\right) = 0.766\left(\frac{\text{lb crystals}}{\text{lb mother liquor}}\right)$$

(e) Initially, using the factor of 8.33 lb/gal for 1.0 g/cm^3,

$$\text{Solution volume} = \frac{3{,}000}{8.33(1.34)} = 269 \text{ gal}$$

Finally,

$$\text{Solution volume} = \frac{1{,}337}{8.33(1.34)} = 120 \text{ gal}$$

$$\text{Crystal volume} = \frac{1{,}024}{8.33(1.68)} = 73 \text{ gal}$$

$$\text{Total volume} = 193 \text{ gal}$$

Therefore, initial conditions before crystallization will control the volume.

$$\text{Make crystallizer volume} = \frac{269}{0.5} = 538 \text{ gal}$$

(f) Calculate H_2O partial pressure by Raoult's law applied to mother liquor:

$$\text{lbmol } MgSO_4 = \frac{401}{120.5} = 3.33$$

$$\text{lbmol } H_2O = \frac{936}{18.02} = 51.95$$

$$\text{Total} = 55.28 \text{ lbmol}$$

$$x_{H_2O} = \frac{51.95}{55.28} = 0.94$$

At 35°C = 95°F, $P^s_{H_2O} = 0.8153$ psia.

Therefore, $p_{H_2O} = x_{H_2O} P^s_{H_2O} = 0.94(0.8153) = 0.766$ psia.

This corresponds to a saturation temperature of 93°F.

Therefore, boiling-point elevation = 2°F.

(g) Growth rate = 0.005 mm/min.

Therefore, diameter grows at 0.01 mm/min.

Must grow from 50 μm = 0.05-mm diameter to 0.40-mm diameter.

$$\text{Time} = \frac{0.40 - 0.05}{0.01} = 35 \text{ min}$$

(h) Enthalpy balance:

$$FH_F + Q = VH_V + MH_M \tag{1}$$

Assume charge is at 35°C = 95°F; then, from Figure 17.10, $H_F = -40$ Btu/lb.

From the steam tables, $H_V = 1{,}102.2 + 0.9$ (for the boiling-point elevation) = 1,103.1 Btu/lb.

$$\text{Wt\% MgSO4 in magma} = \frac{(499 + 401 + 1)}{(3{,}000 + 2 - 641)} = \frac{901}{2{,}361}$$
$$= 0.38.$$

From Figure 17.10, $H_M = -90$ Btu/lb.

From (1),

$$Q = 641(1{,}103.1) + 2{,}361(-90) - 3{,}002(-40)$$
$$= 615{,}000 \text{ Btu} = \text{heat transferred to crystallizer}$$

(i) Assume mass-transfer controlled, using molar amount of crystals, n, and molar concentrations, c.

The molar form of (17-21) is

$$\frac{dn}{dt} = 4\pi r^2 k_c(\Delta c), \tag{2}$$

where r is the crystal radius

$n = \frac{4}{3}\pi r^3 \rho_M$, using a molar density.

Therefore,

$$\frac{dn}{dt} = 4\pi r^2 \rho_M \frac{dr}{dt} \tag{3}$$

Equating (2) and (3),

$$4\pi r^2 k_c(\Delta c) = 4\pi r^2 \rho_M \frac{dr}{dt}$$

$$\frac{dr}{dt} = \frac{k_c \Delta c}{\rho_M} \tag{4}$$

From (15-62),

$$N_{Sh} = \frac{k_c D_p}{\mathcal{D}} = \frac{2k_c r}{\mathcal{D}} = 2 + 0.6(N_{Re})^{1/2}(N_{Sc})^{1/3}$$

For $r = \frac{50}{2} = 25$ μm,

$$N_{Re} = \frac{D_p v \rho}{\mu} = \frac{(50 \times 10^{-6})(100)(5)(1.34)}{0.08} = 0.42$$

$$N_{Sc} = \frac{\mu}{\rho \mathcal{D}} = \frac{0.08}{1.34(1.10 \times 10^{-5})} = 5{,}430$$

$$N_{Sh} = 2 + 0.6(0.42)^{1/2}(5{,}430)^{1/3}$$

$$= 2 + 6.8 = 8.8 = \frac{2k_c r}{\mathcal{D}}$$

$$k_c = \frac{(8.8)(1.1 \times 10^{-5})}{2(25 \times 10^{-4})} = 0.019 \text{ cm/s}$$

For $r = \frac{400}{2} = 200$ μm,

$$N_{Re} = 0.42\left(\frac{400}{50}\right) = 3.36$$

$$N_{Sh} = 2 + 0.6(3.36)^{1/2}(5{,}430)^{1/3}$$
$$= 2 + 19.3 = 21.3$$

$$k_c = \frac{(21.3)(1.1 \times 10^{-5})}{2(200 \times 10^{-4})} = 0.006 \text{ cm/s}$$

Thus, k_c changes by a factor of 3 as crystal size changes from 25 to 200 μm.

Assume a Δc based on the given supersaturation of 0.01 g crystal per g solution.

$$\Delta c = \frac{0.01(1.34)}{246.6} = 54.3 \times 10^{-6} \frac{\text{mol}}{\text{cm}^3}$$

$$\rho_M \text{ of crystals} = \frac{1.68}{246.6} = 6.81 \times 10^{-3} \frac{\text{mol}}{\text{cm}^3}$$

From (4),

$$\frac{dr}{dt} = k_c \frac{54.3 \times 10^{-6}}{6.81 \times 10^{-3}} = 0.008\, k_c$$

for the lowest value of $k_c = 0.006$ cm/s,

$$\frac{dr}{dt} = 0.008(0.006) = 48 \times 10^{-6} \text{ cm/s}$$

or

$$480 \times 10^{-6}(60) = 0.029 \text{ mm/min.}$$

But this is six times faster than the growth rate. Therefore, crystal growth is largely controlled by surface reaction.

17.4 EQUIPMENT FOR SOLUTION CRYSTALLIZATION

Before developing a crystallizer model in Section 17.5, it is useful to describe the most widely used equipment for solution crystallization. Such equipment may be classified according to the three schemes shown in Table 17.8.

Table 17.8 Classification of Equipment for Solution Crystallization

Operation Modes	Methods for Achieving Supersaturation	Crystallizer Features for Achieving Desired Crystal Growth
Batch	Cooling	Agitated or nonagitated
Continuous	Evaporation	Baffled or unbaffled
		Circulating liquor or circulating magma
		Classifying or nonclassifying
		Controlled or uncontrolled
		Cooling jacket or cooling coils

Although industrial equipment is available for batch or continuous operation, the latter is generally preferred. The choice of method for achieving supersaturation depends strongly on the effect of temperature on solubility. From the data in Table 17.5, it is seen that for many inorganic compounds in the near-ambient temperature range, e.g., 10–40°C, the change in solubility is small and may be insufficient to utilize the cooling method. This is certainly the case for $MgCl_2$ and NaCl. For KNO_3 and Na_2SO_4, crystallization by cooling may be feasible. The majority of industrial crystallizers use the evaporation method or a combination of cooling and evaporation. Direct-contact cooling with agitation and evaporation can be achieved by bubbling air through the magma.

To produce crystals of a desired size distribution, considerable attention must be paid to the selection of features of the design of the crystallizer. The use of mechanical agitation can result in smaller and more uniformly sized crystals of a higher purity that are produced in less time. The use of vertical baffles can promote more uniform mixing. Supersaturation and uniformity can be controlled by circulation between a crystallizing zone and a supersaturation zone. In a circulating-liquor design, only the mother liquor is circulated, while in the circulating-magma design the mother liquor and crystals are circulated together. The circulation may be limited to the crystallizer vessel or may include pumping through an external heat exchanger. In a classifying crystallizer, the smaller crystals are separated from the larger and retained in the crystallizing zone for further growth or removed from the zone and redissolved. In a controlled design, one or more techniques are used to control the degree or supersaturation to avoid undesirable nucleation. Cooling crystallizers may use a vessel jacket or internal coils, with the latter preferred because of the ease of wiping the crystals off the cooling surface.

A large number of patented commercial crystallizer designs have been developed. Many of them are described in Myerson [10] and by Mullin [1]. Only four of the more common solution crystallizers are described and illustrated here. The designs suffice to illustrate most of the features found in the many other designs.

Circulating, Batch Crystallizers

Although batch crystallizers can be operated without agitation or circulation by simply charging a hot solution to an open vessel and allowing the solution to stand as it cools by natural convection, the resulting crystals may be undesirably large, interlocked, impure because of entrapment of mother liquor, and difficult to remove from the vessel. Therefore, if the desired product of the crystallization operation is the crystals, it is preferable to use a more elaborate crystallizer configuration similar to either of the two batch crystallizers shown in Figure 17.14. In the design with external circulation, a high magma velocity is used for the flow of magma through the tubes of the heat exchanger to obtain a reasonable heat-transfer rate with a small temperature-driving force and minimization of crystal formation on the heat exchanger tube surfaces. This design can also be used for continuous crystallization, when the solubility-temperature curve dictates cooling crystallization.

In Figure 17.14b, crystallization is accomplished by evaporation under a vacuum pulled by a two-stage, steam-jet-ejector system though a water-cooled condenser. The

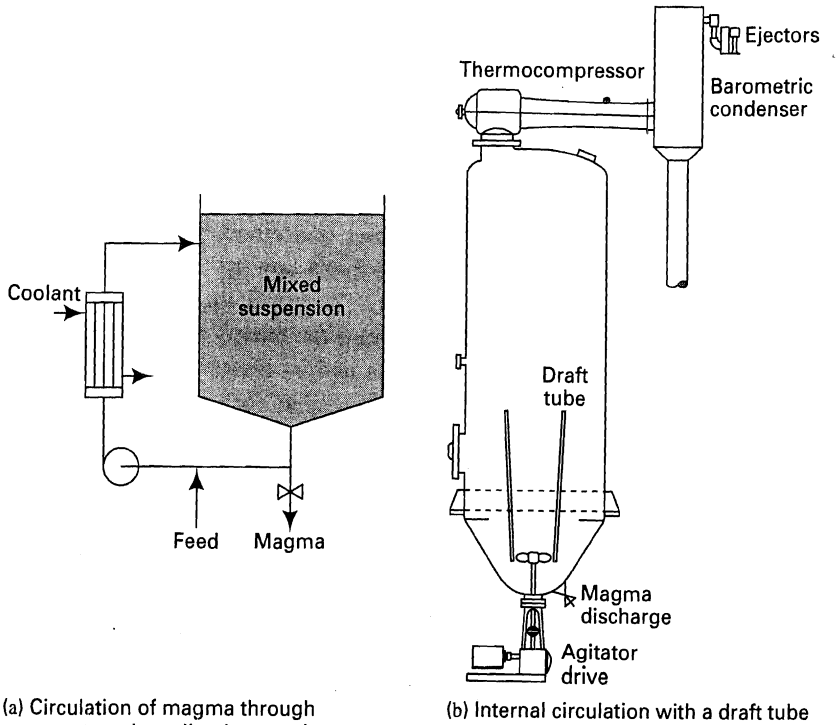

(a) Circulation of magma through an external, cooling heat exchanger

(b) Internal circulation with a draft tube

Figure 17.14 Circulating, batch cooling crystallizers.

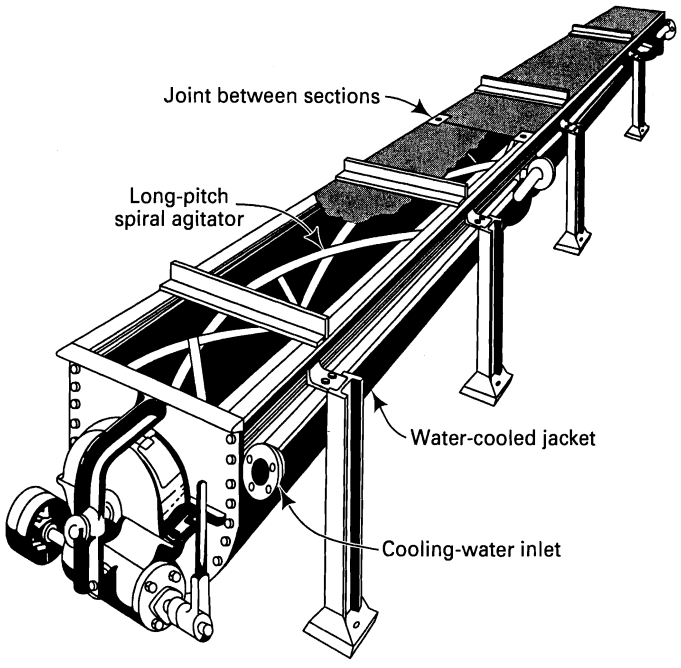

Figure 17.15 Swenson–Walker continuous, cooling crystallizer.

magma is circulated internally through a draft tube by a propeller. The energy for evaporation is supplied from the hot feed. A typical cycle, which includes charging the feed to the vessel, crystallization, and removal of the magma, may range from 2 to 8 h.

Continuous, Cooling Crystallizers

Figure 17.15 is a schematic diagram of a typical scraped-surface crystallizer known as the Swenson–Walker continuous, cooling crystallizer, described in detail by Seavoy and Caldwell [12]. The feed flows through a semicylindrical trough, typically 1 m wide × 3–12 m long. The trough has a water-cooled jacket and is provided with a low-speed (3–10 rpm) helical agitator-conveyor that scrapes the wall and prevents growth of crystals on the trough wall and promotes crystal growth by gentle agitation. Standard-size units can be linked together. The crystallization process may be controlled by the rather slow rate of heat transfer, with the major resistance due to the magma on the inside. Overall heat-transfer coefficients of only 10–25 Btu/h-ft^2-°F (57–142 W/m^2-K) are typically observed, based on a log-mean temperature difference between the magma and the coolant. Production rates of up to 20 tons per day of crystals of $Na_3PO_4 \cdot 12\ H_2O$ and $Na_2SO_4 \cdot 10\ H_2O$ of moderate size and uniformity have been achieved. Both salts show a significant decrease in solubility with decreasing temperature making the cooling crystallizer a viable choice.

EXAMPLE 17.10

The cooling crystallizer of Example 17.6 is to be a scraped-surface unit with 3 ft^2 of cooling surface per foot of running length of crystallizer. Cooling will be provided by a countercurrent flow of chilled water entering the cooling jacket at 60°F and leaving at 85°F. The overall heat-transfer coefficient, U, is expected to be 20 Btu/hr-ft^2-°F. What length of crystallizer is needed?

SOLUTION

From Example 17.6, using Figure 17.10, the required rate of heat transfer is 44,900 Btu/h. The log mean temperature driving force for heat transfer is

$$\Delta T_{LM} = \frac{(120-85)-(70-60)}{\ln\left(\frac{120-85}{70-60}\right)} = 20°F$$

The area for heat transfer is

$$A = \frac{Q}{U\Delta T_{LM}} = \frac{44{,}900}{20(20)} = 112\ \text{ft}^2$$

The crystallizer length = 112/3 = 37 ft.

Continuous, Vacuum, Evaporating Crystallizers

A large number of designs for continuous, vacuum, evaporating crystallizers have been developed. A particularly successful and widely used design of this type is the Swenson draft-tube, baffled (DTB) crystallizer, described by Newman and Bennett [13] and shown in one of several variations in Figure 17.16. In the main body of the crystallizer, evaporation occurs, under vacuum, at the boiling surface, which is located several inches above a draft tube that extends down to within several inches of the bottom of the main body of the crystallizer vessel. Near the bottom and inside of the draft tube is a low-rpm propeller that directs the magma upward through the draft tube toward the boiling surface under conditions of a small degree of supercooling and in the absence of any violent flashing action. Thus, nucleation and buildup of crystals on the walls are minimized. Surrounding the draft tube is an annular space where the magma flows back downward for re-entry into the draft tube. The outer wall of the annular space is a skirt baffle, surrounded by an annular settling zone, whose outer wall is the wall of the crystallizer. A portion (perhaps 10%) of the magma flowing downward through the first annular space turns around and flows outward and upward through the settling zone where larger crystals can settle, leaving a mother liquor containing fine crystals, which flows to a circulating pipe where it is joined by the feed and flows upward through a pump and then a heat exchanger. The circulating solution is heated several degrees to provide the energy for feed preheat and subsequent evaporation and to dissolve the finer crystals. The circulating magma re-enters the main body of the crystallizer just below the bottom of the draft tube. Further classification of crystals by size can be accomplished by providing an elutriation leg, as shown at the bottom of the main body of the crystallizer in Figure 17.16. In that case, product magma is withdrawn through a pipe from a nozzle located near the bottom of the elutriation leg where the largest crystals are present. Otherwise, the product magma may be withdrawn from the lower part of the annular region surrounding the draft tube.

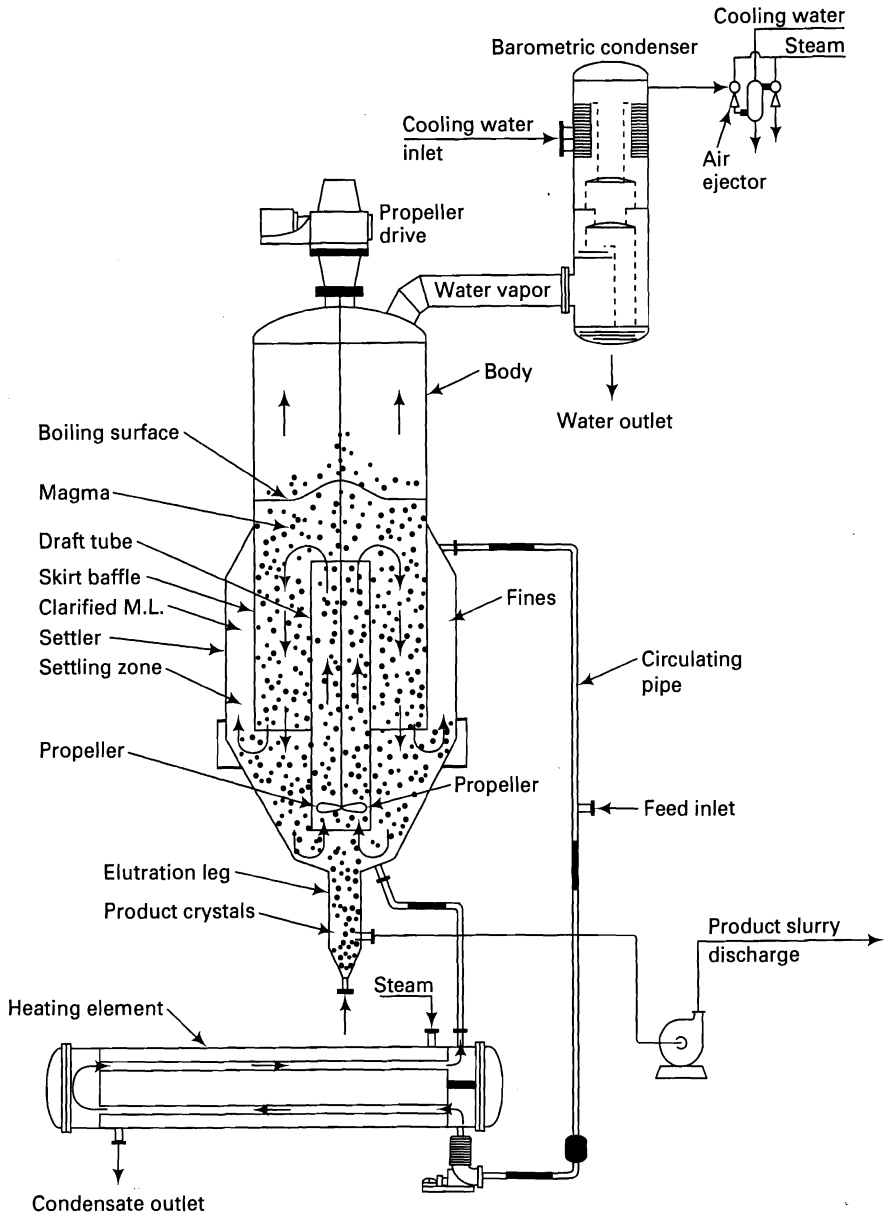

Figure 17.16 Swenson draft-tube, baffled (DTB) crystallizer.

17.5 THE MSMPR CRYSTALLIZATION MODEL

Because of the popularity of the DTB crystallizer, a mathematical model, due to Randolph [14], for its design and analysis is quite useful and is now found in the process equipment model libraries of a few continuous, steady-state, computer-aided simulation programs. This model is referred to as the *Mixed-Suspension, Mixed-Product-Removal* (*MSMPR*) model and is based on the following assumptions:

1. Continuous, steady-flow, steady-state operation.
2. Perfect mixing of the magma.
3. No classification of crystals.
4. Uniform degree of supersaturation throughout the magma.
5. Crystal growth rate independent of crystal size.
6. No crystals in the feed, but seeds are added initially.
7. No crystal breakage.
8. Uniform temperature.
9. Mother liquor in product magma in equilibrium with the crystals.
10. Nucleation rate constant and uniform and due to secondary nucleation by crystal contact.
11. Crystal-size distribution (CSD) uniform in the crystallizer and equal to that in the magma.
12. All crystals have the same shape.

Modifications to the model to account for: (1) classification of crystals due to settling, elutriation, and fines dissolving, and (2) variable growth rate are discussed by Randolph and Larson [15]. The central part of the MSMPR model is the estimation, by a crystal-population balance, of the crystal-size distribution (CSD), which is determined in practice by the rpm of the propeller in the draft tube and the external circulation rate. It is relatively easy to conduct experiments

in a small laboratory crystallizer that approximates the MSMPR model and can provide some of the necessary crystal nucleation rate and growth rate data to design a large-scale, industrial crystallizer.

Crystal-Population Balance

The crystal-population balance accounts for all crystals in the magma and, together with the mass balance, makes possible the determination of the CSD. Let L = a characteristic crystal size (e.g., from a screen analysis), N = cumulative number of crystals of size L and smaller in the magma in the crystallizer, and V_{ML} = volume of mother liquor in the magma in the crystallizer. A typical cumulative-numbers undersize plot based on these variables is shown in Figure 17.17, where the slope of the curve, n, at a given value of L is the number of crystals per unit size per unit volume, given by

$$n = \frac{d(N/V_{ML})}{dL} = \frac{1}{V_{ML}}\frac{dN}{dL} \tag{17-31}$$

The limits of n, as shown in Figure 17.17, vary from n^o at $L = 0$ to 0 at $L = L_T$, the largest crystal size. In the MSMPR model, the cumulative plot of Figure 17.17 is independent of time and location in the magma. The plot is, in fact, the numbers-cumulative CSD for the crystals in the product magma.

For a constant, crystal-size growth rate, independent of crystal size, $G = dL/dt$, or

$$\Delta L = G\Delta t \tag{17-32}$$

and

$$L = Gt_L \tag{17-33}$$

where t_L = residence time in the magma in the crystallizer for crystals of size L. Equation (17-32) is referred to as the ΔL *law of McCabe* [16], who found that the law correlated experimental data on the growth of crystals of KCl and $CuSO_4 \cdot 5H_2O$ surprisingly well. Although McCabe's experiments were conducted in a small, laboratory crystallizer under ideal conditions, his resulting ΔL law is applied to commercial crystallization even though conditions may be far from ideal.

From (17-31), $dN = nV_{ML}\,dL$ = number of crystals in the size range dL. Now withdraw ($\Delta n\,dL$) crystals per unit volume in time increment Δt. Because of the perfect mixing assumption for the magma,

$$\frac{\text{number of crystals withdrawn}}{\text{mother-liquor volume withdrawn}} = \frac{\text{number of crystals}}{\text{mother-liquor volume in the crystallizer}}$$

Therefore,

$$\frac{\text{number of crystals withdrawn}}{\text{number of crystals in crystallizer}} = \frac{\text{mother-liquor volume withdrawn}}{\text{mother-liquor volume in the crystallizer}}$$

or

$$\frac{\Delta n dL}{n dL} = -\frac{\Delta n}{n} = \frac{Q_{ML}\,\Delta t}{V_{ML}} \tag{17-34}$$

where Q_{ML} = volumetric flow rate of mother liquor in the withdrawn product magma and V_{ML} = volume of mother liquor in the crystallizer. Combining (17-32) and (17-34) and taking the limit,

$$-\frac{dn}{dL} = \frac{Q_{ML}\,n}{GV_{ML}} \tag{17-35}$$

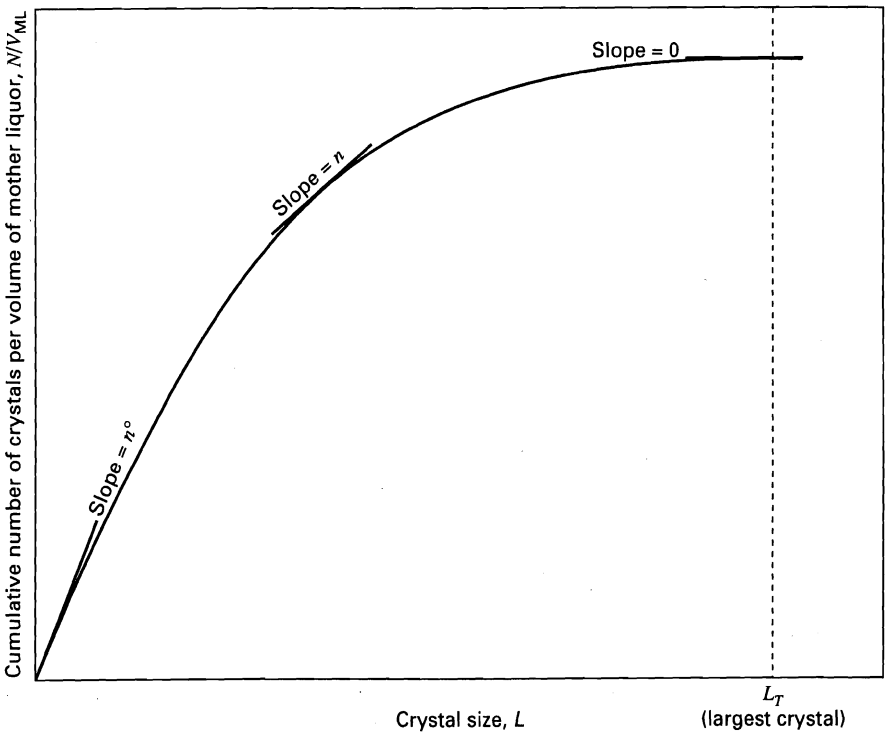

Figure 17.17 Typical cumulative-numbers-undersize distribution.

which is a simplified version of the following more-general, transient-population balance equation that allows for crystals in the feed and a nonuniform growth rate, but does assume a constant volume of mother liquor in the crystallizer:

$$\frac{\partial n}{\partial t} + \frac{\partial (nG)}{\partial L} + \frac{(Q_{ML})_{\text{out}}\, n}{V_{ML}} - \frac{(Q_{ML})_{\text{in}}\, n_{\text{in}}}{V_{ML}} = 0 \quad (17\text{-}36)$$

The retention time of mother liquor in the crystallizer is $\tau = V_{ML}/Q_{ML}$. Therefore, (17-35) can be rewritten as

$$-\frac{dn}{n} = \frac{dL}{G\tau} \quad (17\text{-}37)$$

If (17-37) is integrated for a constant growth rate and residence time, we obtain

$$n = n^{\circ} \exp(-L/G\tau) \quad (17\text{-}38)$$

This equation is the starting point for determining distribution curves for crystal population, crystal size or length, crystal surface area, and crystal volume or mass.

For example, to obtain crystal population, the number of crystals per unit volume of mother liquor below size L is

$$N/V_{ML} = \int_0^L n\,dL \quad (17\text{-}39)$$

The total number of crystals per unit volume of mother liquor is

$$N_T/V_{ML} = \int_0^{\infty} n\,dL \quad (17\text{-}40)$$

Combining (17-38) to (17-40), the cumulative number of crystals of size smaller than L, as a fraction of the total is

$$x_n = \frac{\int_0^L n^{\circ} e^{-L/G\tau}\, dL}{\int_0^{\infty} n^{\circ} e^{-L/G\tau}\, dL} = 1 - \exp(-L/G\tau) \quad (17\text{-}41)$$

Or if we define a dimensionless crystal size as

$$z = L/G\tau \quad (17\text{-}42)$$

then,

$$x_n = 1 - e^{-z} \quad (17\text{-}43)$$

A plot of (17-43), shown in Figure 17.18a, is referred to as the cumulative distribution or cumulative crystal population. For a given value of z, x_n is the fraction of crystals having a smaller value of z. Also of interest is the corresponding differential plot of dx_n/dz, shown in Figure 17.18b, where from (17-43),

$$\frac{dx_n}{dz} = e^{-z} \quad (17\text{-}44)$$

The differential plot gives the fraction of the crystals in a given interval of z. At small values of z, the fraction is seen to be large, while at large values of z, the fraction is small.

In Figures 17.18a and b, four different distribution plots are shown. From statistics, (17-41) is one of a number of *moment equations,* which for a relation $n = f(z)$, are given by

$$x_k = \frac{\int_0^z n z^k\, dz}{\int_0^{\infty} n z^k\, dz} \quad (17\text{-}45)$$

where k is the order of the moment. Thus, (17-43) is obtained by setting $k = 0$ and thus, is the zeroth moment of the distribution. Results for this moment and the corresponding first (length or size), second (area), and third (volume or mass) moments are summarized in Table 17.9. Corresponding cumulative and differential plots are included in Figure 17.18.

Of particular interest in the design and operation of a crystallizer is the predominant crystal size, L_{pd}, in terms of the volume or mass distribution. This size corresponds to the peak of the differential-mass distribution and is derived as follows: From Table 17.9,

$$dx_m/dz = (z^3/6)e^{-z} \quad (17\text{-}46)$$

At the peak,

$$\frac{d\left(\frac{dx_m}{dz}\right)}{dz} = 0 = \frac{3z^2 e^{-z}}{6} - \frac{z^3 e^{-z}}{6} \quad (17\text{-}47)$$

Solving (17-47) for z,

$$z = 3 = \frac{L}{G\tau} \quad (17\text{-}48)$$

Therefore,

$$L_{pd} = 3G\tau \quad (17\text{-}49)$$

Similar developments using the differential expressions in Table 17.9 show that the most populous sizes in terms of the number of crystals, the size of crystals, and the surface area of crystals are 0, $G\tau$, and $2G\tau$, respectively. If L_{pd} is selected, (17-41) and (17-43) can be used to estimate cumulative and differential screen analyses.

To utilize the distributions of Table 17.9, values of G and τ are needed. The growth rate depends on the supersaturation and the degree of agitation. The residence time depends on the design and operation of the crystallizer. It is also useful to know B° and n°, which are related as follows:

$$\frac{1}{V_{ML}}\frac{dN}{dt} = \frac{1}{V_{ML}}\frac{dN}{dL}\left(\frac{dL}{dt}\right) \quad (17\text{-}50)$$

$$\lim_{L\to 0} \frac{1}{V_{ML}}\frac{dN}{dt} = B^{\circ}$$

$$\frac{dL}{dt} = G$$

$$\lim_{L\to 0} \frac{1}{V_{ML}}\frac{dN}{dL} = n^{\circ}$$

Therefore,

$$B^{\circ} = Gn^{\circ} \quad (17\text{-}51)$$

Combining (17-51) with (17-38),

$$n = \frac{B^{\circ}}{G} \exp(-L/G\tau) \quad (17\text{-}52)$$

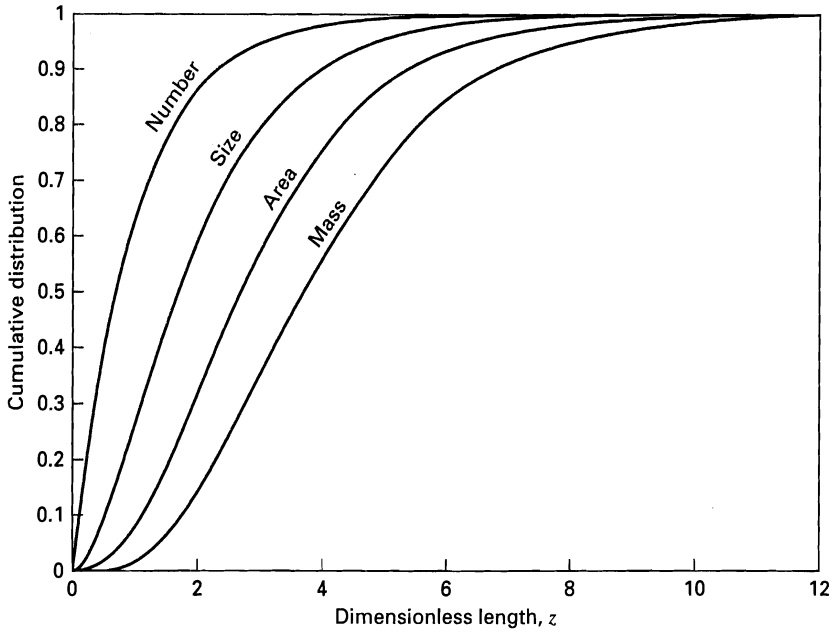

(a) Cumulative distributions

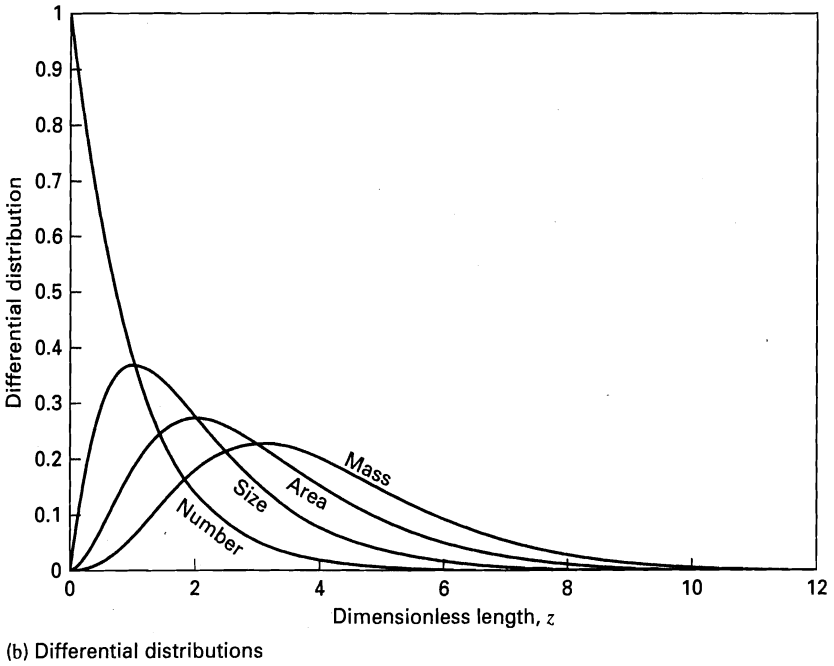

(b) Differential distributions

Figure 17.18 Crystal-size distributions predicted by the MSMPR model.

Table 17.9 Cumulative and Differential Plots for Moments of Crystal Distribution for Constant Growth Rate

Moment	Distribution Basis	Cumulative	Differential
Zeroth	Number	$x_n = 1 - e^{-z}$	$dx_n/dz = e^{-z}$
First	Size or length	$x_L = 1 - (1+z)e^{-z}$	$dx_L/dz = ze^{-z}$
Second	Area	$x_a = 1 - \left(1 + z + \frac{z^2}{2}\right)e^{-z}$	$dx_a/dz = \frac{z^2}{2}e^{-z}$
Third	Volume or mass	$x_m = 1 - \left(1 + z + \frac{z^2}{2} + \frac{z^3}{6}\right)e^{-z}$	$dx_m/dz = \frac{z^3}{6}e^{-z}$

$z = L/G\tau$.

This equation can be used with experimental data, as shown in the following example, to obtain values of nucleation and growth rates for a given set of operating conditions when the assumptions of the MSMPR model hold. The effect of operating conditions on B° can be expressed as an empirical, power-law function of the form given by (17-19). However, since the growth rate can be proportional to the relative supersaturation, s, raised to an exponent, (17-19) can be rewritten as

$$B^\circ = k'_N G^i M_T^j N^r \tag{17-53}$$

Unfortunately, k'_N can be sensitive to the size of the equipment and is, therefore, best determined from data for a commercial crystallizer as discussed by Zumstein and Rousseau [17]. The exponents i, j, and r can be determined from small-scale experiments.

The necessary nucleation rate for a crystallization operation is related to the predominant crystal size by the MSMPR model. From (17-40) and (17-38),

$$n_c = N_T/V_{ML} = \int_0^\infty n\,dL = n^\circ \tau G \int_0^\infty e^{-z}\,dz = n^\circ \tau G \tag{17-54}$$

The mass of crystals per unit volume of mother liquor is

$$m_c = \int_0^\infty m_p n dL \tag{17-55}$$

where m_p = mass of particle, given by

$$m_p = f_v L^3 \rho_p \tag{17-56}$$

where f_v is defined in (17-11).

Combining (17-55), (17-56), and (17-38), followed by integration gives

$$m_c = 6 f_v \rho_p n^\circ (G\tau)^4 \tag{17-57}$$

Combining (17-54) and (17-57), the number of crystals per unit mass of crystals is

$$\frac{n_c}{m_c} = \frac{1}{6 f_v \rho_p (G\tau)^3} \tag{17-58}$$

Combining (17-48) with (17-58),

$$\frac{n_c}{m_c} = \frac{9}{2 f_v \rho_p L_{pd}^3} \tag{17-59}$$

or the corresponding required nucleation rate is

$$B^\circ = \frac{n_c C}{m_c V_{ML}} = \frac{9C}{2 f_v \rho_p V_{ML} L_{pd}^3} \tag{17-60}$$

where C = mass rate of production of crystals.

EXAMPLE 17.11

A continuous, vacuum-evaporating crystallizer of the DTB type is to be used to produce 2,000 lb/hr of $Al_2(SO_4)_3 \cdot 18H_2O$ ($\rho_p = 105$ lb/ft^3). The magma contains 0.15 ft^3 crystals/ft^3 magma and the residence time of the magma in the crystallizer in 2 h. The desired predominant crystal size on a mass basis is 0.417 mm.

Estimate with the MSMPR model:

(a) Required crystal growth rate in ft/h

(b) Necessary nucleation rate in nuclei/h-ft^3 of mother liquor in the crystallizer

(c) Number of crystals produced per hour

(d) Tables and plots of estimated cumulative and differential screen analyses of the product crystals on a mass or volume basis

Also explain how the required growth and nucleation rates for the operating crystallizer might be achieved.

SOLUTION

(a) From (17-48),

$$G = \frac{L_{pd}}{3\tau} = \frac{(0.417/304.8)}{3(2)} = 2.28 \times 10^{-4} \text{ ft/h}$$

(b) Need volume of mother liquor in the crystallizer.

Volume of crystals produced $= \dfrac{2{,}000}{105} = 19.1$ ft^{3}h.

Volume of crystals in crystallizer $= 19.1(2) = 38.2$ ft^3.

Volume of magma in crystallizer $= \dfrac{38.2}{0.15} = 255$ ft^3.

Volume of mother liquor in crystallizer $= V_{ML}$
$= 255 - 38.2 = 217$ ft^3.

From (17-60), assuming $f_v = 0.5$,

$$B^\circ = \frac{9(2{,}000)}{2(0.5)(105)(217)(0.417/304.8)^3} = 3.1 \times 10^8 \frac{\text{nuclei}}{\text{h-ft}^3}$$

(c) Number of crystals produced $= 3.1 \times 10^8(217)$
$= 6.7 \times 10^{10}$/h.

(d) $$z = \frac{L}{G\tau} = \frac{L}{(2.28 \times 10^{-4})(2)}$$
$$= 2.2 \times 10^3 L, \text{ ft} \quad \text{or} \quad 7.19L, \text{ mm}$$

From Table 17.9,

$$x_m = 1 - \left(1 + z + \frac{z^2}{2} + \frac{z^3}{6}\right) e^{-z} \tag{1}$$

$$\frac{dx_m}{dz} = \frac{z^3}{6} e^{-z} \tag{2}$$

Using (1) and (2) with a spreadsheet for the older Tyler mesh sizes, the following results are obtained for the cumulative and differential screen analyses:

Tyler Mesh	Opening, mm	Dimensionless Length, z	Cumulative Screen Analysis, %	Differential Screen Analysis %
8	2.357	16.96	100.00	0.00
10	1.667	11.99	99.77	0.18
14	1.179	8.48	96.95	2.11
20	0.833	5.99	84.82	8.95
28	0.589	4.24	61.16	18.31
35	0.417	3.00	35.20	22.40
48	0.295	2.12	16.50	19.05
65	0.208	1.50	6.54	12.53
100	0.147	1.06	2.29	6.87
150	0.104	0.75	0.73	3.31
200	0.074	0.53	0.22	1.46

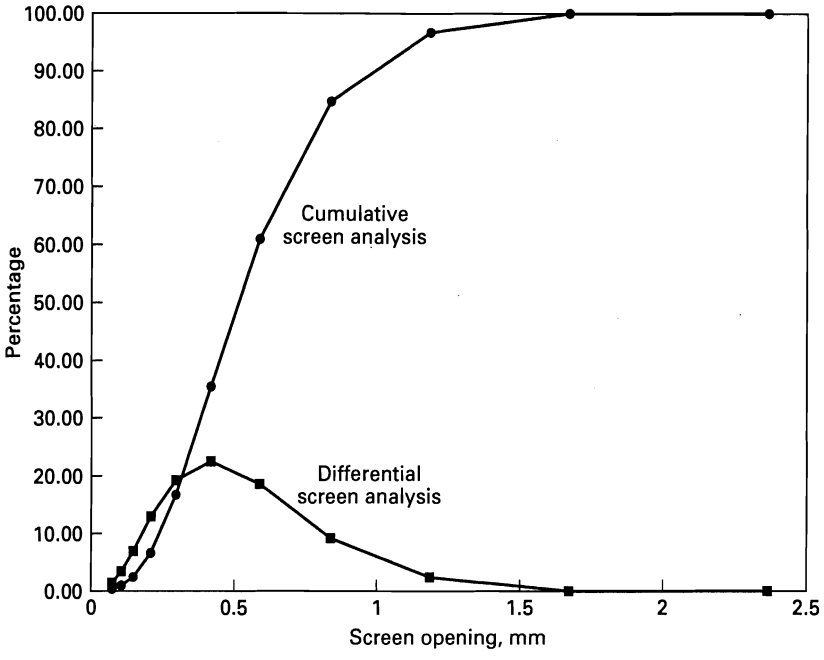

Figure 17.19 Predicted cumulative and differential screen analyses for Example 17.11.

A plot of the cumulative and differential screen analyses is shown in Figure 17.19.

Both growth and nucleation rates depend on the supersaturation. The growth may also depend on the relative velocity between the crystals and the mother liquor. The nucleation rate depends upon the degree of agitation. With a DTB crystallizer, the agitator rpm and the magma circulation rate through the external heat exchanger can be adjusted to achieve the required growth and nucleation rates.

17.6 PRECIPITATION

Solution crystallization, as discussed above, occurs when a solution containing a moderately to strongly soluble solute is cooled or partially evaporated, causing the solute to exceed its solubility sufficiently to partially crystallize. The degree of supersaturation is small, primary nucleation is avoided, and crystal growth is slow. If the process is carried out under controlled conditions, reasonably large and desirable crystals can be grown. In many respects, the process of precipitation is just the opposite of solution crystallization. Precipitation, as discussed by Nielsen [18], involves solutes that are only sparingly soluble. The precipitate is formed by changing solution pH, solvent concentration, solution temperature, or most commonly by the addition of a reagent to a solution, resulting in a reaction to produce another chemical that is almost insoluble in the resulting solution. The latter is commonly referred to as *reactive crystallization.* The degree of supersaturation produced by the reaction is very large, causing a high degree of primary nucleation. Although some growth occurs as the supersaturation is depleted, precipitates generally consist of very small particles that may be crystalline in nature and are frequently *aggregates* and *agglomerates.* Aggregates are masses of crystallites that are weakly bonded together. Agglomeration can follow, cementing aggregates together. Typical chemicals that are produced by precipitation are the sparingly soluble compounds listed in Table 17.6. Precipitation may be thought of as *fast crystallization.*

In precipitation, particle size is related to the solubility by (17-16), the Kelvin equation. However, for precipitates formed from ionic reactions in solution, the supersaturation ratio, $S = c/c_s$, is replaced by $(\pi/K_c)^{1/v}$, where π = the ionic concentration product for the reaction, K_c = (equilibrium) solubility product, and v = sum of the number of cations and anions that form the precipitated compound. Thus, for aluminum hydroxide at 15°C,

$$\pi = \left(c_{\text{Al}}^{+3}\right)\left(c_{\text{OH}}^{-}\right)^3$$

with K_c given in Table 17.6 and $v = 1 + 3 = 4$. The Kelvin relation is of great importance in precipitation because nucleation can be due to homogeneous primary nucleation.

The extent of supersaturation is a very important factor in precipitation. When a reagent is added to a solution to form a sparingly soluble compound, a very high supersaturation can be developed, depending upon the ionic concentrations in the reagent and solution before mixing. For example, consider the formation of a precipitate of $BaSO_4$ from an aqueous reagent solution containing Ba^{++} ions and an aqueous solution of, e.g., sulfuric acid.

From Table 17.6, the solubility product of $BaSO_4$ at 18°C is 0.87×10^{-10}. Figure 17.20a, taken from Nielsen [19], is a plot of sulfate ion concentration versus barium ion concentration, both in the solution just after mixing and before precipitation, with contours of constant supersaturation ratio, S. The dashed lines refer to an ideal situation where activity

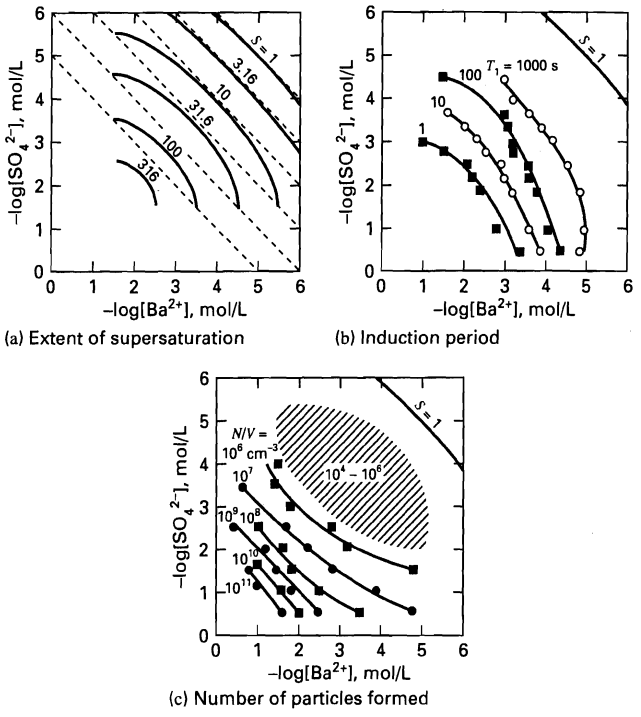

Figure 17.20 Precipitation diagrams for $BaSO_4$.

coefficients are 1.0 (concentrations = activities) and no complexes of Ba^{++} and $SO_4^{=}$, are formed. The solid, curved contours take these deviations from the ideal situation into account. Note the very large supersaturation ratios that can occur. For example, if the $SO_4^{=}$ concentration in the solution is 0.01 mol/L and the Ba^{++} concentration is 4.7×10^{-4} mol/L, the supersaturation ratio = 100.

Typically, precipitation does not take place immediately upon development of a large supersaturation because of the slow growth of very small particles. However, after a certain period of time, called the induction period, T_I visible precipitation begins. As shown in Figure 17.20b, this period is highly dependent on the initial-ion concentrations and, by superposition of Figure 17.20a, on the supersaturation ratio. For example, at a supersaturation ratio of about 300, the induction period is only one second, while at a supersaturation ratio of about 10, the induction period is more than one minute.

As shown in Figure 17.20c, the number of particles formed per unit volume of solution, N/V, also depends strongly on the initial concentrations of the anion and cation and, therefore, on the supersaturation at high ion concentrations. A minimum number of particles per unit volume or a corresponding maximum particle size is frequently observed. For $BaSO_4$, this maximum size occurs for a supersaturation ratio of about 300. The number of particles formed also depends on particle growth rate, which may be controlled by mass transfer of the ions to the particle surface and/or integration of ions into the particle crystalline structure (surface reaction). Particle growth rates during precipitation generally follow one of the following laws, which exhibit different dependencies on the relative supersaturation, $s = S - 1$:

Linear

$$G = k_1 s \tag{17-61}$$

Parabolic

$$G = k_2 s^2 \tag{17-62}$$

Exponential

$$G = k_3 f\{s\} \tag{17-63}$$

The linear rate law, which often applies for $G > 10$ nm/s, may be due to mass-transfer control or surface-adsorption control, where the latter depends more strongly on temperature. The parabolic rate law, for which G may be < 10 nm/s, applies to screw-dislocation-controlled growth. The exponential law, where $f\{s\}$ can involve a complex exponential, log, and/or power-law dependency corresponds to growth control by surface nucleation. The latter two mechanisms can occur in parallel. Rate constants for many electrolytes for the three different rate laws are given by Nielsen [20]. When growth is rapid, coprecipitation of soluble electrolytes may occur by entrapment, thus making it difficult to obtain a pure precipitate product.

Because a precipitate is formed at considerable supersaturation, the resulting particle shapes may be far from the shape corresponding to a minimum Gibbs energy, which depends on the particle surface area and interfacial tension. However, if the precipitate and mother liquor are allowed to age, then, as discussed by Nielsen, [20], the precipitate particle sizes and shapes can tend toward equilibrium values by: (1) flocculation and sintering of fine particles (2) transport of ions over the surface, and (3) ripening by dissolution and redeposition. Ripening can result in the release of coprecipitates, thus increasing precipitate purity.

The small particles produced in abundance during precipitation have a tendency to cluster together by interparticle-collision phenomena, variously referred to as agglomeration, aggregation, and flocculation. Such clusters, often called agglomerates, are common when the number of particles/cm^3 of solution exceeds 10^7. For $BaSO_4$, Figures 17.20a and c show that agglomeration may require a very large initial supersaturation ratio. Agglomeration is important mainly when particles sizes are between 1 μm and 50 μm.

EXAMPLE 17.12

Fitchett and Tarbell [21] studied the effect of impeller rpm on the crystal-size distribution obtained for the continuous precipitation of barium sulfate when mixing solutions of sodium sulfate and barium chloride. The contents of the 1.8-L crystallizer were assumed to be perfectly mixed. In their Run 15, they used feeds with dissolved salts in stoichiometric ratio to give a sodium-chloride concentration of 0.15 mol/L and an average residence time of 38 s.

Results for two different impeller speeds were as follows:

Size, μm	ln n, Number Density of Crystals, ln ($\mu m^{-1}\, L^{-1}$) 950 rpm, 0.361 J/s · kg Feeds	400 rpm, 0.028 J/s · kg Feeds
7	22.07	23.45
9	21.66	22.75
11	21.35	22.08
13	20.97	21.36
15	20.77	20.75
17	20.41	20.14
19	20.04	19.57
21	19.77	18.94
23	19.48	18.43
25	19.09	17.75
27	18.85	
29	18.49	
31	18.11	
33	17.87	

Using the MSMPR model, determine from the two sets of data:

(a) n^o, number density of nuclei, nuclei/μm-L

(b) G, linear growth rate, μm/s

(c) B^o, nucleation rate, nuclei/L-s

(d) mean crystal length, μm

(e) n_c, number of crystals/volume of mother liquor, crystals/m^3

SOLUTION

(a) From (17-38), if each set of data is fitted to

$$\ln n = \ln n^o - L/G\tau \qquad (1)$$

the best straight line yields an intercept of ln n^o and a slope of $-1/G\tau$, from which n^o and G can be determined for $\tau = 38$ s.

Using a spreadsheet, the results for 950 rpm are

intercept = 23.13, slope = −0.1601

Therefore, $n^o = \exp(23.13) = 1.11 \times 10^{10}$ crystals/μm · L

(b) $G = 1/[(38)(0.1601)] = 0.164$ μm/s

(c) The nucleation rate is given by (17-51):

$B^o = Gn^o = 0.164(1.11 \times 10^{10}) = 1.82 \times 10^9$ nuclei/L · s

(d) The mean particle length is determined from the value of z for the maximum value of dx_L/dz, which, from Table 17.9 is ze^{-z}.

$$d\frac{(ze^{-z})}{dz} = e^{-z} - ze^{-z} = 0$$

Therefore, $z = 1 = L_{mean}/G\tau$ from (17-42)

$$L_{mean} = G\tau = 0.164(38) = 6.23\ \mu m$$

(e) The number of crystals per unit volume of mother liquor is given by (17-54).

$$n_c = n^o \tau G = B^o \tau = 1.82 \times 10^9(38)$$
$$= 6.92 \times 10^{10} \text{ crystals/L} = 6.92 \times 10^7 \text{ crystals/m}^3$$

(f) In a similar manner, the following results are obtained for 400 rpm:

Intercept = 25.53, slope = −0.313

$n^o = 1.22 \times 10^{11}$ crystals/μm · L

$G = 0.0841$ μm/s

$B^o = 1.03 \times 10^{10}$ nuclei/L · s

$L_{mean} = 3.20$ μm

$n_c = 3.91 \times 10^8$ crystals/m^3

Comparing the two sets of results, we see that a higher agitator speed gives a larger mean crystal size, a larger growth rate, and a lower nucleation rate.

17.7 MELT CRYSTALLIZATION

Solution crystallization refers to crystallization of a solute from a solvent. It is most commonly conducted with aqueous solutions of dissolved inorganic salts. The phase equilibrium diagram for a water-salt system, e.g., Figure 17.2, typically includes temperatures ranging from the eutectic temperature (below 0°C) to a temperature exceeding the melting point of ice, but not greater than 200°C. Since the melting points of inorganic salts greatly exceed 200°C, the pure-salt melting point is, accordingly, not included on the diagram.

For mixtures of organic compounds, the situation is quite different. An analysis by Matsuoka et al. [22] found that more than 70% of the common organic compounds had melting points between 0 and 200°C. For binary mixtures of such compounds, the phase-equilibrium diagrams will typically include the melting points of both compounds. Typical diagrams are shown in Figure 17.1. In (b), crystals of orthochloronitrobenzene can be formed if the feed composition is less than the eutectic composition based on para-chloronitrobenzene; otherwise, pure para-chloronitrobenzene can be formed. The exception is the eutectic composition. *Eutectic-forming* systems consist of compounds that can not substitute for each other in the crystal lattice. Thus, the eutectic mixture consists of two different solid phases. The two solubility curves separating the liquid-phase region from the two solid–liquid regions are sometimes referred to as freezing-point curves, and mixtures at conditions in the liquid-phase region are referred to as *melts*.

Much less common are *solid-solution-forming* systems of the type shown in Figure 17.1c for the phenanthrene-anthracene system. These systems consist of compounds so nearly alike in structure that they can substitute for each other in the lattice structure to form a single solid phase of the two compounds over a wide range of composition. With this type of system, a mixture is crystallized. The liquid–solid phase diagram resembles that for vapor–liquid equilibrium, where the freezing-point and melting-point curves replace the dew-point and bubble-point curves, respectively. Mixtures in the liquid-phase region above the freezing-point curve are also referred to as melts. A mixture in the region

between the two curves separates into a liquid phase and a solid phase, neither of which is pure.

Crystallization of melts from either eutectic-forming or solid-solution-forming mixtures is called melt crystallization. Although theoretically, melt crystallization of eutectic-forming systems, like solution crystallization of such systems, can produce pure crystals, the crystalline product from commercial single-stage crystallizers may not meet purity specifications for reasons discussed in detail by Wilcox [23]. In that case, repeated stages of melting and crystallization may be necessary. With eutectic-forming systems, multiple stages are mandatory to produce crystals of high purity.

The separation of organic mixtures is most commonly achieved by distillation. However, if distillation: (1) requires more than 100 theoretical stages, (2) cannot produce products that meet specifications (e.g., purity and color), (3) causes decomposition of feed components, or (4) requires extreme conditions of temperature or pressure (e.g., vacuum), other separation methods should be considered. According to Wynn [24], if the compounds to be separated are: (1) disubstituted benzenes, diphenyl alkyls, phenones, secondary or tertiary aromatic or aliphatic amines, isocyanates, fused-ring compounds, heterocyclic compounds, and carboxylic acids of MW < 150; (2) have a melting-temperature range from 0 to 160°C; (3) required to be very high-purity products; or if (4) a laboratory test produces a clearly defined solid phase from which the liquid phase drains freely, then melt crystallization should be considered as an alternative or supplement, as in a hybrid process, to distillation.

Equipment for Melt Crystallization

As with solution crystallization, a large number of crystallizer designs have been proposed for melt crystallization. Only some of the more widely used commercial units are discussed here. Myerson [10] gives a detailed discussion. In all cases, crystallization is caused by cooling the mixture.

The two major methods used in melt crystallizers are *suspension crystallization* and *layer crystallization* by progressive freezing. In the former, crystals of a desired size distribution are grown slowly in a suspension by subcooling a seeded-feed melt. In the latter, crystals of uncontrolled size are grown rapidly on a cooled surface, wherein subcooling is supplied through the crystallized layer. In suspension crystallization, the remaining melt must be separated from the crystals by centrifugation, filtration, and/or settling. In layer crystallization, the remaining melt or residual liquid is drained from the solid layer, followed by melting of that layer.

Figure 17.21 shows a two-stage, scraped-wall-crystallizer system used for suspension crystallization. A cooling medium is used to control the surface temperatures of the two scraped-wall units, causing crystals to grow, which are subsequently scraped off by screws. The melt-crystal mixture is circulated through a ripening vessel. The two scraped-wall units of a typical system are 3.6 m long with 3.85 m^2 of total heat-transfer surface area. The screws are driven by a 10-kW motor.

Of more importance in commercial applications of melt crystallization is the falling-film crystallizer developed by Sulzer Brothers Limited and shown in Figure 17.22. This equipment is particularly useful for producing high-purity crystals (>99.9%) at high capacity (>10,000 tons/y). A large pair of units, each 4 m in diameter and containing 1,100 12-m-high tubes can produce 100,000 tons/yr of very pure crystals, with typical layer growth rates of 1 in./h. The feed melt flows as a film down the inside of the tubes, over a crystal layer that forms and grows by progressive freezing because the wall of the tube is cooled from the outside by a coolant. When a predetermined crystal layer thickness, typically 5–20 mm, is

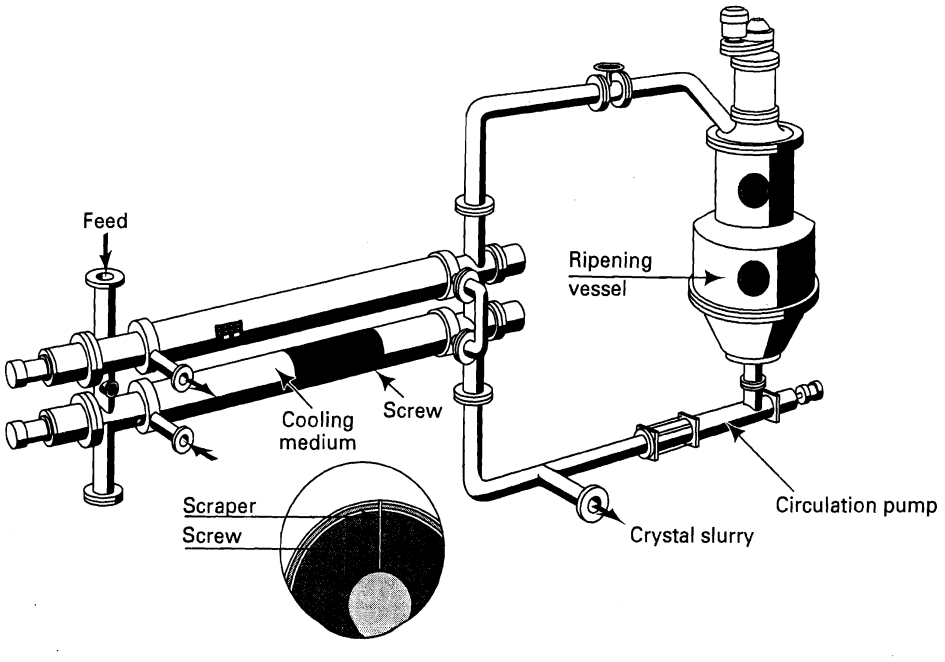

Figure 17.21 Two-stage, scraped-wall, melt crystallizer.

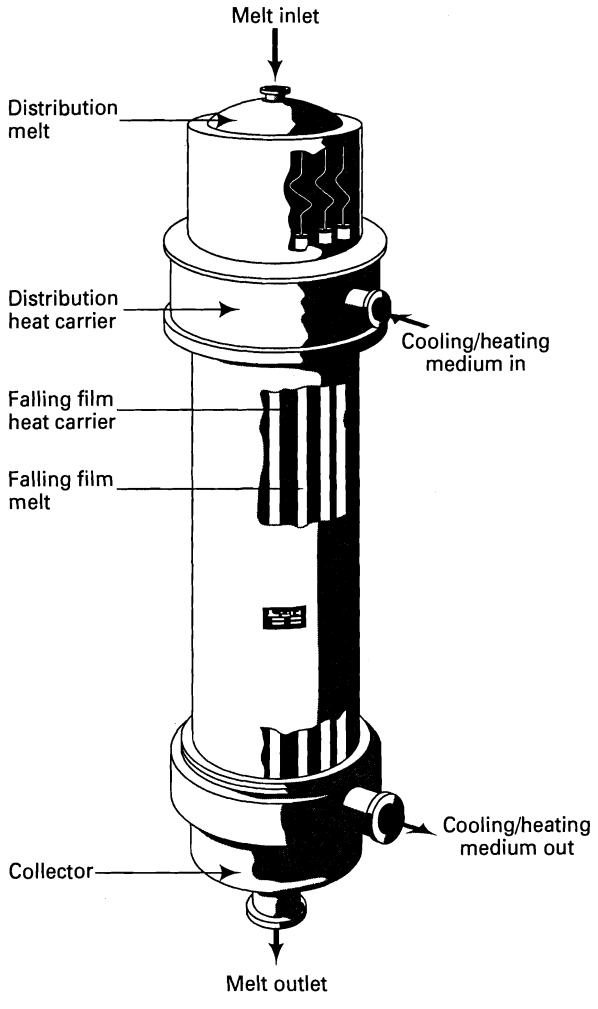

Figure 17.22 Sulzer falling-film melt crystallizer.

reached, the feed melt flow rate is stopped. The tubes are now slightly warmed to cause partial melting, called sweating, to remove impurities that may be stuck or bonded to the crystal layer. This is followed by complete melting of the remaining layer, which is of high purity. During the initial crystallization phase, melt is circulated at a high rate compared to the crystallization rate so that a uniform temperature and melt composition is approached down the length of the tube. The coolant also flows as a film down along the outside surface of the tubes.

Consider the freezing step in a falling-film crystallizer. A typical temperature profile is shown in Figure 17.23. The melt enters at the top of the tube and flows as a film down the inside wall. A coolant, at a temperature below the freezing point of the melt, also enters at the top of the tube and flows as a film down the outside wall. Heat is transferred from the melt to the coolant, causing the melt to form a crystal layer at the inside wall of the tube. As the melt and coolant flow down the tube, their temperatures decrease and increase, respectively. The thickness of the crystal layer increases with time, with the latent heat of fusion transferred from the crystal-melt interface to the coolant.

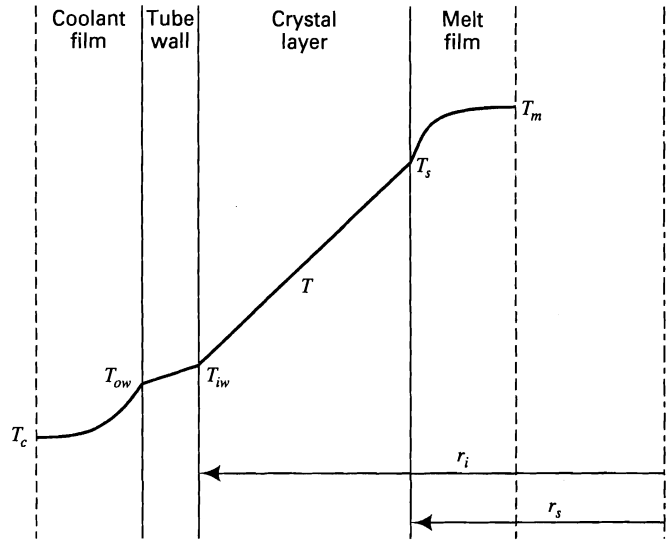

Figure 17.23 Temperature profile for melt crystallization from a falling film at a vertical location along the tube.

For a eutectic-forming, binary melt, only one component will crystallize, although small amounts of the other component may be trapped in the crystal layer, particularly if the rate of crystal formation is too fast. The temperature at the interface of the crystal layer and the melt can be assumed to be the equilibrium temperature corresponding to the saturated melt composition on the solubility curve. If mass transfer of the crystallizing component from the melt film to the phase interface is rapid, the interface temperature will correspond to the melt-film composition at that vertical location. Furthermore, if the thermal resistances of the coolant film, tube wall, and melt film are negligible compared to that of the crystal layer, and if the heat capacity of the crystal layer and metal wall are negligible, then the following simple model for the rate of increase of thickness of the crystal layer with time can be constructed.

At a particular vertical location, $T_s \approx T_m$, the melting point, and $T_{iw} \approx T_c$, the coolant bulk temperature. The rate of heat released by freezing, ΔH_f, is equal to the rate of heat conduction through the crystal layer. Thus, for a planar wall, referring to Figure 17.23, the heat evolved from fusion is equated to the rate of heat conduction through the crystal layer to give

$$\Delta H_f \frac{dm}{dt} = -A\rho_c(\Delta H_f)\frac{dr_s}{dt} = \frac{k_c A(T_m - T_c)}{r_i - r_s} \qquad (17\text{-}64)$$

with an initial condition $r_s = r_i$ at $t = 0$. Integration of (17-64) gives

$$\frac{(r_i - r_s)^2}{2} = \frac{k_c(T_m - T_c)t}{\rho_c \Delta H_f} \qquad (17\text{-}65)$$

or crystal layer thickness is

$$(r_i - r_s) = \sqrt{\frac{2k_c(T_m - T_c)t}{\rho_c \Delta H_f}} \qquad (17\text{-}66)$$

A similar derivation for a cylindrical tube wall, where r_i = inside radius of the tube, gives

$$\frac{1}{4}(r_i^2 - r_s^2) - \frac{r_s^2}{2}\ln\left(\frac{r_i}{r_s}\right) = \frac{k_c(T_m - T_c)t}{\rho_c \Delta H_f} \qquad (17\text{-}67)$$

As would be expected, the value of the left-hand side of (17-67) approaches the value of the left-hand side of (17-65) as the value of r_s approaches the value of r_i. For the planar wall, (17-66) shows that the crystal layer grows as the square root of time. Thus, for a given period of time, the growth during the first half of the time period is $(1/\sqrt{2}) = 70.7\%$ of the total growth. For the cylindrical-tube wall, if the growth is from the wall to half of the radius, 67.9% of that growth occurs during the first half of the time period to produce 75.2% of the crystal layer. The time required for this thickness of growth for the cylindrical tube is only 80% of the time for the planar wall. Thus, a conservative result is obtained by using the much simpler planar wall case of (17-66).

During operation of the falling-film crystallizer, the temperature of the melt film decreases as it flows down the tube because of heat transfer from the melt to the colder crystal layer. Based on the earlier assumptions, the melt temperature at any elevation will be the temperature corresponding to the solubility curve for the melt composition at that elevation. If we: (1) assume that the sensible heat from the cooling of the melt layer is negligible compared to the latent heat of fusion, (2) neglect any sensible-heat storage in the crystal layer and tube wall, (3) neglect vertical conduction in the tube wall, crystal layer, and melt layer, and (4) assume a constant coolant temperature, we can couple (17-66) with a material balance for the depletion of the crystallizing component as it flows down the inside tube wall. The result, which is left as an exercise, gives the crystal-layer thickness as a function of time and vertical location.

EXAMPLE 17.13

A melt of 80 wt% naphthalene and 20 wt% benzene at the saturation temperature is fed to a falling-film crystallizer, where coolant enters at 15°C. Estimate the time required for the crystal-layer thickness near the top of the 8-cm i.d. tubes to reach 2 cm.

SOLUTION

From Figure 17.24, by extrapolation the saturation temperature of the melt is 62°C. Therefore, naphthalene will crystallize, with

$$T_m - T_c = (62 - 15)1.8 = 84.6°\text{F}$$
$$r_i = 8/2 = 4\,\text{cm} = 0.131\,\text{ft}$$
$$r_s = 4 - 2 = 2\,\text{cm} = 0.0655\,\text{ft}$$

The estimate can be made with (17-67), based on the following properties for naphthalene:

$$\rho_c = 71.4\,\text{lb/ft}^3$$
$$k_c = 0.17\,\text{Btu/h-ft-°F}$$
$$\Delta H_f = 63.9\,\text{Btu/lb}$$

From (17-67), solving for time, t,

$$t = \frac{(71.4)(63.9)}{(0.17)(84.6)} \times \left[\frac{1}{4}(0.131^2 - 0.0655^2) - \frac{0.0655^2}{2}\ln\left(\frac{0.131}{0.0655}\right)\right] = 0.549\,\text{h}$$

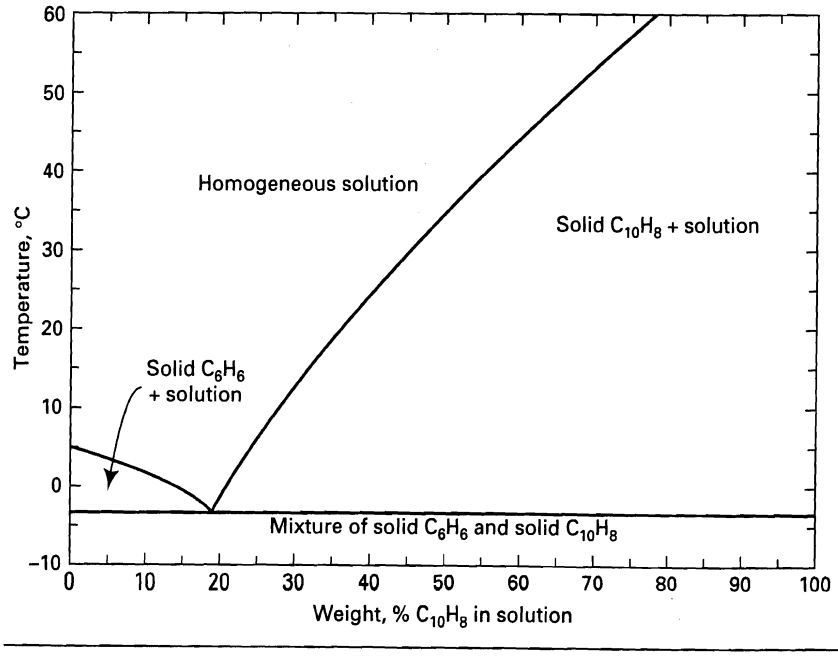

Figure 17.24 Solid–liquid phase diagram for the naphthalene-benzene system.

17.8 ZONE MELTING

When the melt consists of two components that form a solid solution, such as shown in Figure 17.1c, the liquid and solid phases at equilibrium contain amounts of both components, similar to the behavior previously discussed for vapor-liquid equilibrium. Accordingly, multiple stages of crystallization are required to obtain products of high purity. A particularly useful technique for doing this, especially when impurities are to be removed to achieve a very high-purity product, is zone melting, as developed by Pfann [25, 26] and discussed further by Zief and Wilcox [27].

The zone-melting technique, when carried out batchwise, is illustrated in Figure 17.25. Starting with an impure crystal slab, a melt zone, which is thin compared to the length of the slab, is passed slowly (typically at 1 cm/h for organic mixtures) through the slab from one end to the other by fixing the slab and using a moving heat source or, less commonly, by moving the slab through a fixed heat source. Radiofrequency (RF) induction heating is particularly convenient and causes mixing in the melt. The slab can be arranged horizontally or vertically, with the latter orientation preferred because it can take advantage of any density difference between the crystals and the melt. Zone melting can be applied to the composition region near either end of the phase-equilibrium diagram. For example, for the binary mixture of phenanthrene (P) and anthracene (A) in Figure 17.1c, zone melting could be used to remove small amounts of A from P or small amounts of P from A.

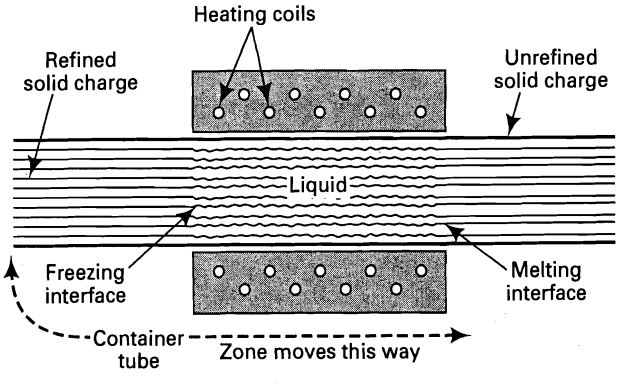

Figure 17.25 Zone melting.

[From *Perry's Chemical Engineers' Handbook,* 6th ed., R.H. Perry, D.W. Green, and J.O. Maloney, eds., McGraw-Hill, New York (1984) with permission.]

A solid–liquid equilibrium distribution coefficient, K, can be defined in a manner analogous to that for liquid–liquid equilibrium. Thus,

$$K_i = \frac{\text{concentration of impurity, } i, \text{ in the solid phase}}{\text{concentration of impurity, } i, \text{ in the melt phase}} \tag{17-68}$$

For example, if the concentration is expressed in mole fractions and the impurity is anthracene in the system of Figure 17.1c, then at 120°C, $K_i = 0.30/0.12 = 2.50$. At 200°C, with phenanthrene as the impurity $K_i = 0.11/0.28 = 0.393$. Thus, K_i can be greater than or less than one. When greater than one, the impurity raises the melting point and the impurity concentrates in the solid phase; when less than one, the impurity lowers the melting point and concentrates in the melt phase. However, when K_i approaches a value of 1, purification by zone melting becomes very difficult.

Near either end of the composition range, the equilibrium curves for the solid and liquid phases approach straight lines, and therefore, the values of K_i become constants. In these composition ranges, an equation is readily developed to predict concentration of the impurity in the solid phase upstream of the moving melt zone as a function of distance down the crystal layer in the direction of movement of the melt zone. Figure 17.26 shows the position of the melt zone during zone melting. The melt zone is shown to move a distance dz. Assume that: (1) the melt zone of width, ℓ, is perfectly mixed with impurity concentration, w_L, in weight fraction; (2) no diffusion of impurity in the solid phases occurs; (3) the initial concentration of the impurity is uniform at w_o; and (4) the concentration of the impurity in the melt zone is in equilibrium with that in the solid phase upstream of the melt zone. A mass balance on the impurity for a dz movement of the melt

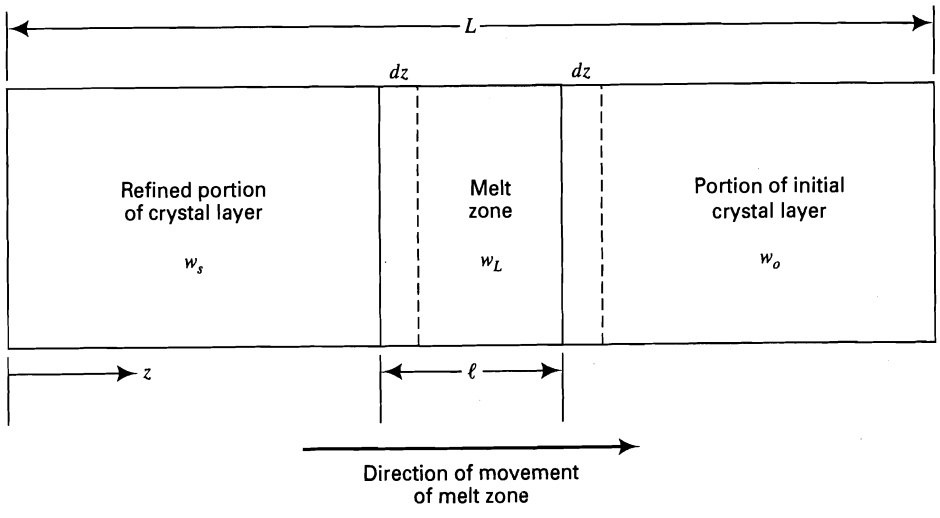

Figure 17.26 Ideal, zone-melting model.

zone is given by

(Mass of impurity added to melt zone)
− (mass of impurity removed from melt zone)
= (increase in the mass of impurity in the melt zone)

Thus,

$$w_o \rho_c A_c\, dz - w_s \rho_c A_c\, dz = \rho_L A_c \ell\, dw_L \quad (17\text{-}69)$$

From (17-68), let

$$K = w_s/w_L \quad (17\text{-}70)$$

Therefore,

$$dw_L = dw_s/K \quad (17\text{-}71)$$

Combining (17-69) to (17-71) to eliminate w_L and assuming $\rho_L = \rho_c$, we obtain

$$\frac{K}{\ell}\int_o^z dz = \int_{Kw_o}^{w_s} \frac{dw_s}{w_o - w_s} \quad (17\text{-}72)$$

Integration gives

$$\frac{w_s}{w_o} = 1 - (1 - K)\exp(-Kz/\ell) \quad (17\text{-}73)$$

for

$$z/\ell = 0 \quad \text{to} \quad z/\ell = \frac{L}{\ell} - 1$$

EXAMPLE 17.14

A crystal layer of 1 wt% phenanthrene and 99 wt% anthracene is subjected to zone melting with a melt-zone width equal to 0.1 of the length of the crystal layer ($\ell/L = 0.1$). The distribution coefficient for phenanthrene in the dilute composition region is 0.36. Determine the phenanthrene concentration profile in weight fractions at the conclusion of zone melting when the melt reaches the last 10% of the crystal layer length.

SOLUTION

From Figure 17.1c and the value of K, the phenanthrene favors distribution to the melt phase. Therefore, as the melt zone moves down the crystal layer, the phenanthrene will migrate from the upstream portion of the crystal layer into the melt zone. When the leading edge of the melt zone reaches the end of the crystal layer, all of the phenanthrene that has migrated will be in the melt layer at a uniform concentration equal to $w_s\{z/\ell = 0.9\}/K$. Assume instant freezing of this melt zone so as to maintain the uniform composition. From (17-73), with $K = 0.36$ and $w_o = 0.01$,

$$w_s = 0.01[1 - 0.64\exp(-0.36z/\ell)] \quad (1)$$

Solving (1) for values of $z/\ell = 0$ to 9 gives

z/ℓ	w_s
0	0.0036
1	0.0055
2	0.0069
3	0.0078
4	0.0085
5	0.0089
6	0.0093
7	0.0095
8	0.0096
9	0.0097

In the melt zone, $w_L = w_s/K = 0.0097/0.36 = 0.0269$. A plot of the predicted profile is shown in Figure 17.27. To further refine the anthracene, additional passes of zone melting can be made to move more of the impurity into the melt zone. However, for each pass after the first, (17-73) is not valid because at the beginning of each of the additional passes, w_o is not uniform. For example, at the beginning of the second pass, w_o becomes w_s in Figure 17.27. For the additional passes, it is necessary to numerically solve the following differential-equation form of (17-72).

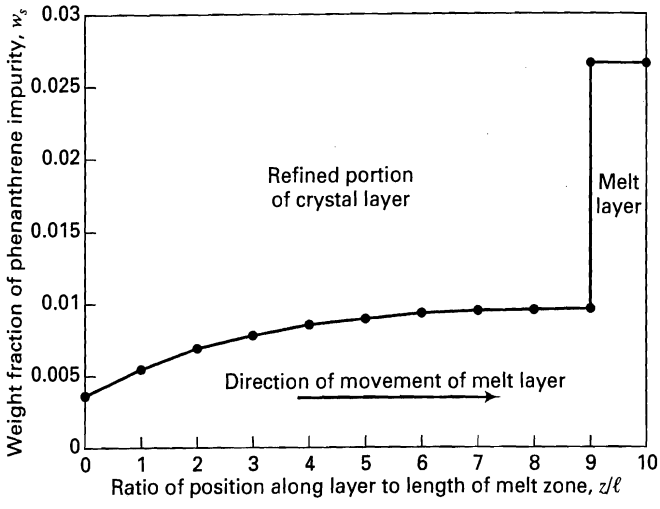

Figure 17.27 Predicted impurity profile for Example 17.14.

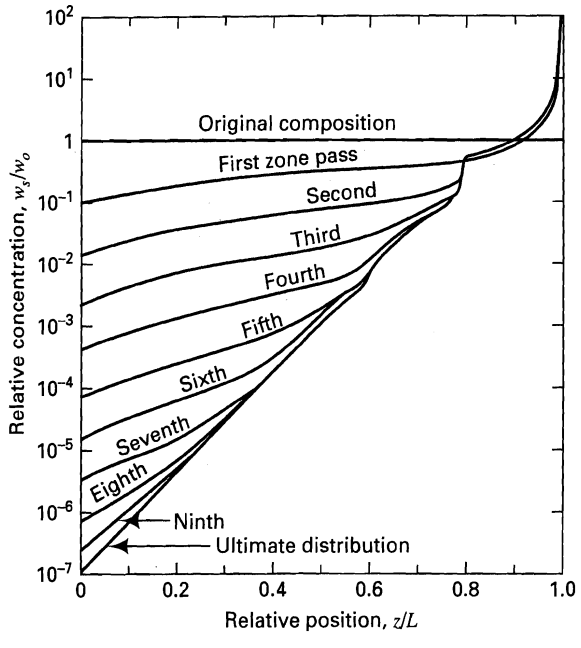

Figure 17.28 Concentration profiles for multiple zone-melting passes.

$$\frac{dw_s}{dz} = \frac{K}{\ell}(w_o - w_s) \tag{17-74}$$

where $w_o = w_o\{z = z\}$ from the results for w_s for the results from the previous pass, and $w_s\{z = 0\} = Kw_o\{z = 0\}$.

Typical impurity-concentration profiles for multiple melt-zone passes are shown in Figure 17.28 from calculations by Burris, Stockman, and Dillon [28] for the case of $K = 0.1$ and a melt-zone width of 20% of the crystal-layer length ($\ell/L = 0.2$). However, in their calculations, the melt zone was allowed to diminish to zero as the heater moved away from the crystal layer, resulting in a steep gradient from $z/L = 0.8$ to 1.0. It is seen that an ultimate distribution of the impurity is approached after 9 passes. The number of passes required to approach the ultimate distribution is given approximately by $2(L/\ell) + 1$, as observed by Herington [29]. In this example, a highly pure crystalline product can be achieved if a portion of the more pure end of the final crystal layer is taken.

17.9 DESUBLIMATION

When crystallization occurs from a vapor phase, rather than from a liquid solution or melt, the operation is referred to as *desublimation.* The reverse operation, i.e., the vaporization of a solid directly to a vapor, is *sublimation.* To understand how such a phase change can occur without going through the liquid phase, consider the phase diagram for naphthalene shown in Figure 17.29. As with most chemicals that have a vapor pressure of much less than 1 atm at the melting temperature, that temperature coincides, within a fraction of a degree Celsius, with the triple point. Below the triple-point temperature of 80.2°C, corresponding to a vapor pressure of 7.8 torr, naphthalene cannot exist as a liquid, regardless of the pressure. Below 80.2°C, naphthalene exists as a solid provided that the pressure is greater than the vapor pressure of naphthalene at the prevailing temperature. However, if the pressure falls below the vapor pressure, solid naphthalene will sublime directly to a vapor.

If naphthalene is present in an ideal gas mixture with a noncondensible inert gas, sometimes called an entrainer, at a temperature below the triple point of 80.2°C, desublimation of the naphthalene to a crystalline solid will occur if the partial pressure of naphthalene in the gas is increased to a value that exceeds its vapor pressure. For example, consider a vapor mixture of 5 mol% naphthalene in nitrogen at 70°C and a total pressure of 40 torr. The partial pressure of naphthalene is 0.05(40) = 2 torr. From Figure 17.29, this partial pressure is less than the vapor pressure of 3.8 torr. If the total pressure is increased, desublimation will begin when the total pressure is increased to 3.8/0.05 = 76 torr. Alternatively, if the pressure is maintained at 40 torr, but the temperature is reduced, desublimation will begin to take place at 61°C, where the vapor pressure of naphthalene is 2 torr. Unless nitrogen is trapped, the naphthalene crystals will be pure.

The most common occurrence of desublimation is the formation of snow crystals by condensation of water vapor from air at temperatures below 0°C. At temperatures above −40°C, the snow crystals form by heterogeneous nucleation on fine mineral particles of perhaps 10^{-5}–10^{-2} mm in diameter. At temperatures below −40°C, homogeneous nucleation can take place. As the snow crystals fall through the atmosphere, they cluster together into snowflakes. The difference between the melting point of ice and the triple point of water is less than 0.01°C, with a corresponding vapor pressure of only 4.6 torr.

As discussed by Nord [30] and Kudela and Sampson [31], a number of chemicals are amenable to purification by desublimation, preceded perhaps by sublimation. In general, they are chemicals that are solids at ambient temperature and pressure and have solid vapor pressures greater than 5 μm Hg at moderate operating temperatures. These chemicals are listed in Table 17.10. Major applications of desublimation, to obtain near-pure solid chemicals or pure-chemical solid films on substrates, include crystallization of water-insoluble

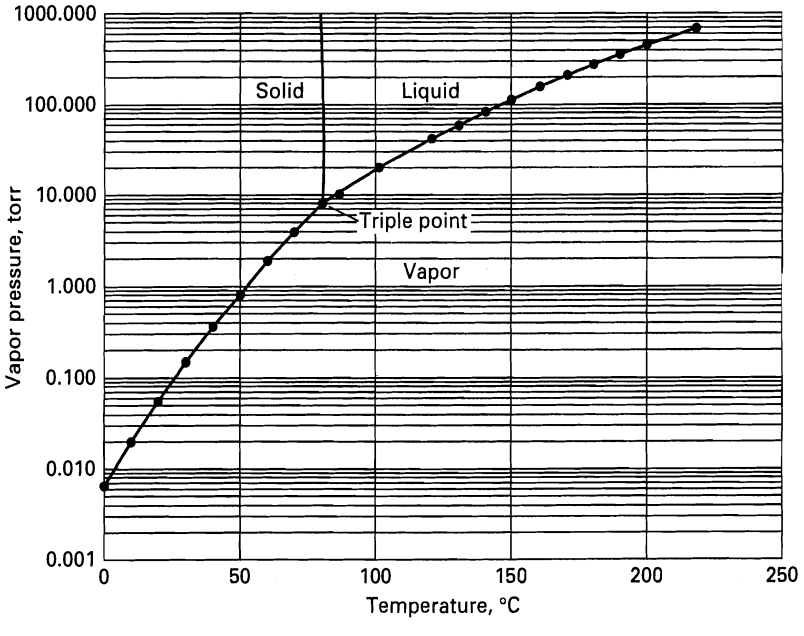

Figure 17.29 Vapor pressure of naphthalene.

Table 17.10 Chemicals Amenable to Purification by Desublimation

Aluminum chloride	Molybdenum Trioxide
Anthracene	Naphthalene
Anthranilic acid	β-Naphthol
Anthraquinone	Phthalic anhydride
Benzanthrone	o-Phthalimide
Benzoic acid	Pyrogallol
Calcium	Salicylic acid
Camphor	Sulfur
Chromium chloride	Terephthalic acid
Cyanuric chloride	Titanium tetrachloride
Ferric chloride	Thymol
Hafnium tetrachloride	Uranium hexafluoride
Iodine	Zirconium tetrachloride
Magnesium	

organic chemicals from mixtures with inert, nonvolatile gases and vapor-deposition of metals.

Desublimation is almost always effected by cooling the gas mixture at nearly constant pressure. As discussed by Holden and Bryant [32], cooling may be achieved by any of the following techniques:

1. Heat transfer from the gas through a solid surface, on which the crystals form.
2. Quenching by addition of a vaporizable liquid.
3. Quenching by addition of a cold, noncondensable gas.
4. Expansion of the gas mixture through a nozzle.

The first technique, which is widely used, has the disadvantage that the crystals must be removed by scraping of or by melting from the heat-transfer surface. The second technique, which is less common, must use a liquid in which the sublimate is not soluble. If excess water is used, this technique will produce a slurry of the crystals and nonvaporized liquid. The third technique, which is also common, produces dry crystals, sometimes called a snow. The fourth technique is much less common, because the degree of cooling necessary may require either a high pressure upstream of the nozzle or a vacuum downstream.

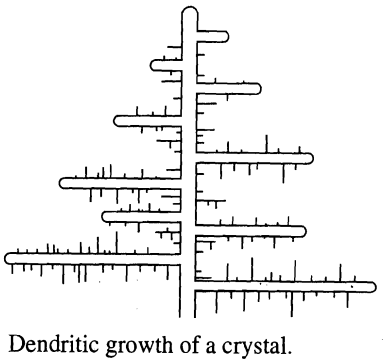

Figure 17.30 Dendritic growth of a crystal.

The number, size, and shape of the crystals produced in the snow of the third technique depend on the relative rates of nucleation, crystal growth, and crystal agglomeration. Frequently, as commonly observed with snow crystals, dendritic growth occurs, producing undesirable crystals of the shape shown in Figure 17.30. The main stem grows rapidly, followed by slower rates of growth of primary branches, and much slower growth of secondary branches. If the dendritic crystals can be suspended in the vapor long enough, the spaces between the branches can fill in to produce a more-desirable dense shape.

Desublimation in a Heat Exchanger

This technique is used in industry to recover, from a gas mixture, a number of organic chemicals, including anthracene, maleic anhydride, naphthalene, phthalic anhydride, and salicylic acid. The crystals are deposited on the outside of the tubes while a coolant flows through the inside of the tubes. If the rate of desublimation is controlled by the rate of conduction of heat through the deposited crystal layer, then a relationship for the time to deposit a crystal layer of given thickness is derived in a manner similar to that for the falling-film melt crystallizer in Section 17.8. The result, which is similar to (17-67), except that the crystal layer grows outward from the outside radius of the cylindrical tube, r_o, instead of inward from radius, r_i in (17-67), is

$$t = \frac{\rho_c \Delta H_s}{k_c(T_g - T_c)} \left[\frac{r_s^2}{2} \ln\left(\frac{r_s}{r_o}\right) - \frac{1}{4}\left(r_s^2 - r_a^2\right) \right] \quad (17\text{-}75)$$

where r_s is the radius to the crystal layer-gas interface. Equation (17-75) ignores any sensible heat associated with cooling of the gas. If the sensible heat is not negligible, then it must be added in (17-75) to the heat of sublimation, ΔH_s. If the heat-transfer resistance in the gas phase is negligible, the temperature, T_g, in (17-75) corresponds to the temperature where the partial pressure of the desubliming solute equals its vapor pressure. The derivation of (17-75) including the sensible-heat correction is given in detail by Singh and Tawney [33].

EXAMPLE 17.15

A desublimation unit of the heat-exchanger type is to be sized for the recovery of 100 kg/h of naphthalene (N) from a gas stream, where the other components are noncondensable under the conditions of operation. The heat-exchanger tubes are 1 m long with an outside diameter of 2.5 cm. Tube spacing is such that N can build up to a maximum thickness of 1.25 cm. The gas enters the unit at 800 torr and 80°C with a mole fraction for N of 0.0095. The coolant is cooling water, which flows through the inside of the tubes, countercurrently to the flow of gas. The inlet and outlet temperatures of the cooling water are 25°C and 45°C, respectively. Determine the number of tubes needed and the time required to reach the maximum thickness, if the gas leaves at 60°C.

SOLUTION

Assume the properties

C_P of gas = 0.26 cal/g-°C

MW of naphthalene = 128.2

k_c of solid naphthalene = 1.5 cal/h-cm-°C

ΔH_s of naphthalene = 115 cal/g

ρ_c of solid naphthalene = 1.025 g/cm^3

When the maximum thickness of N is achieved, the amount of sublimate per tube, if uniform, is

$$\begin{aligned} m &= \pi(r_s^2 - r_o^2)L\rho_c \\ &= 3.14[(1.25 + 1.25)^2 - 1.25^2]100(1.025) \\ &= 1{,}510 \text{ g} = 1.51 \text{ kg} \end{aligned}$$

The entering gas has a partial pressure for N of 0.0095(800) = 7.6 torr. From Figure 17.29, the saturation temperature for this partial pressure is 79.7°C. This is just slightly below the entering-gas temperature of 80°C, which is less than the triple-point temperature. Therefore, N will condense as a solid. At the exit temperature of the gas, 60°C, the vapor pressure of N is 1.8 torr. Assuming saturation at the exit and no pressure drop, the mole fraction of N in the exit gas will be 1.8/800 = 0.00225. Thus, per mole of entering gas, 0.0073 moles of N will be condensed. If the gas is assumed to be nitrogen and N, then M_r, the ratio of the mass of gas mixture to the mass of N condensed, will be

$$M_r = \frac{28(0.9905) + 128.2(0.0095)}{(128.2)(0.0073)} = 30.94$$

The sensible heat plus the heat of fusion is

$$\begin{aligned} M_r C_{P_g}(T_{\text{in}} - T_{\text{out}})_g + \Delta H_s &= 30.94(0.26)(80 - 60) + 115 \\ &= 276 \text{ cal/g} \end{aligned}$$

Thus, for this example, with a very low mole fraction of the chemical undergoing desublimation, the sensible heat effect is large. From (17-75), the time to reach the maximum thickness of N, using the temperature driving force across the solid N of 35°C, is

$$\begin{aligned} t &= \frac{(1.025)(276)}{(1.5)(35)}\left[\frac{(2.5)^2}{2}\ln\left(\frac{2.5}{1.25}\right) - \frac{1}{4}(2.5^2 - 1.25^2)\right] \\ &= 5.37 \text{ h} \end{aligned}$$

The number of tubes required is

$$\frac{(100)(5.37)}{1.51} = 356$$

17.10 EVAPORATION

Before crystallization of a solute from an aqueous solution takes place, it is customary to bring the concentration of the solute close to the solubility curve. This is accomplished by evaporation of the solvent in an evaporator. Such a device is also used to concentrate solutions even when the solute is not subsequently crystallized, e.g., solutions of sodium hydroxide. When the vapor formed is essentially pure, there is no mass-transfer resistance in the vapor phase. When the liquid phase is agitated, mass-transfer in the liquid phase is sufficiently rapid that the rate of evaporation of solvent can be determined by the rate of heat transfer from the heating medium, usually condensing steam, to the solution.

Evaporators differ in configuration and the degree of agitation of the liquid phase. The five most widely used continuous-flow evaporators are shown schematically in Figure 17.31. Their main characteristics are as follows:

(a) ***Horizontal-tube evaporator***. This unit consists of a horizontal cylindrical vessel, equipped in the lower section with a horizontal bundle of tubes, inside of which steam condenses and outside of which the solution to be concentrated boils. The vapor produced leaves the surface of the liquid solution. Agitation is provided only by the movement of the bubbles formed. Therefore, this type of unit is only suitable for low-viscosity solutions that do not deposit scale on the heat-transfer surfaces.

(b) ***Short-vertical-tube evaporator***. This unit differs significantly from the horizontal-tube evaporator. The tube bundle is arranged vertically, with the solution

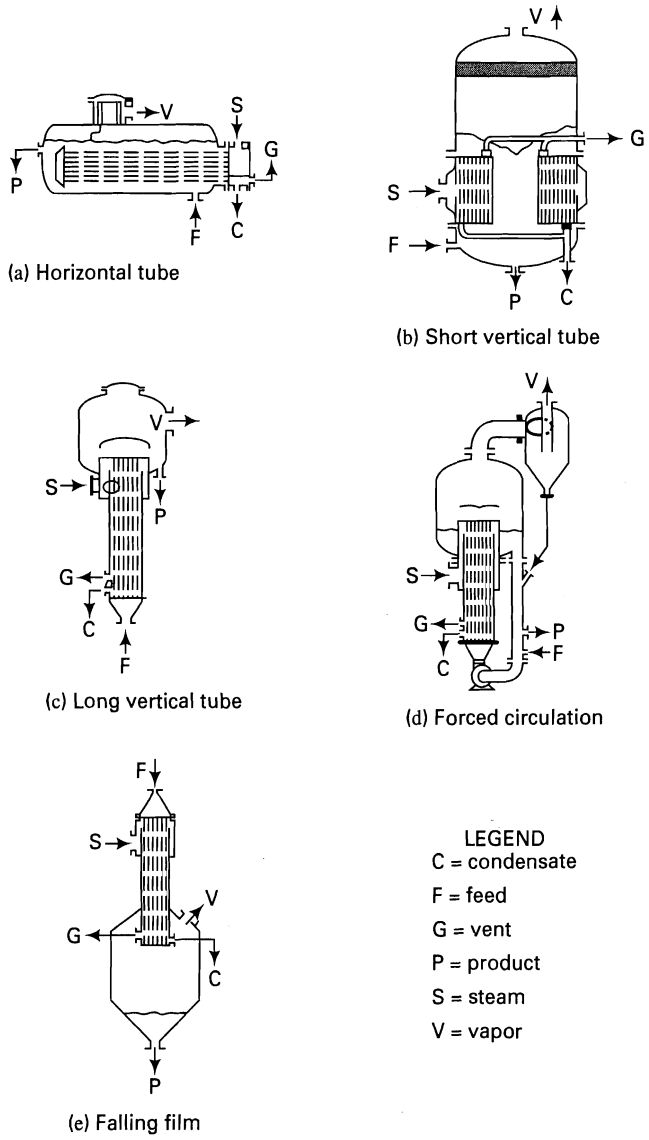

Figure 17.31 Common types of evaporators.

[From *Perry's Chemical Engineers' Handbook*, 6th edition, R.H. Perry, D.W. Green, and J.O. Maloney, eds., McGraw-Hill, New York (1984) with permission.]

inside the tubes and steam condensing outside. Boiling inside the tube causes the solution to circulate, thus providing additional agitation and, therefore, higher heat-transfer coefficients. Nevertheless, this type of evaporator is not suitable for very viscous solutions.

(c) ***Long-vertical-tube evaporator***. By lengthening the vertical tubes and providing a separate vapor-liquid disengagement chamber, as shown in Figure 17.31c, a higher tube-entering liquid velocity can be achieved and, thus, an even higher heat-transfer coefficient.

(d) ***Forced-circulation evaporator***. To handle very viscous solutions, a pump is used to force the solution upward through relatively short tubes.

(e) ***Falling-film evaporator***. This unit is widely used to concentrate heat-sensitive solutions such as fruit juices. The solution enters at the top and flows as a film down the inside walls of the tubes. The concentrate and the vapor produced are separated at the bottom.

For a given pressure in the vapor space of an evaporator, the boiling temperature of an aqueous solution will be equal to that of pure water if the solute is not dissolved in the water, but rather consists of small, insoluble, colloidal material. If the solute is soluble, the boiling temperature will be greater than that of pure water by an amount known as the

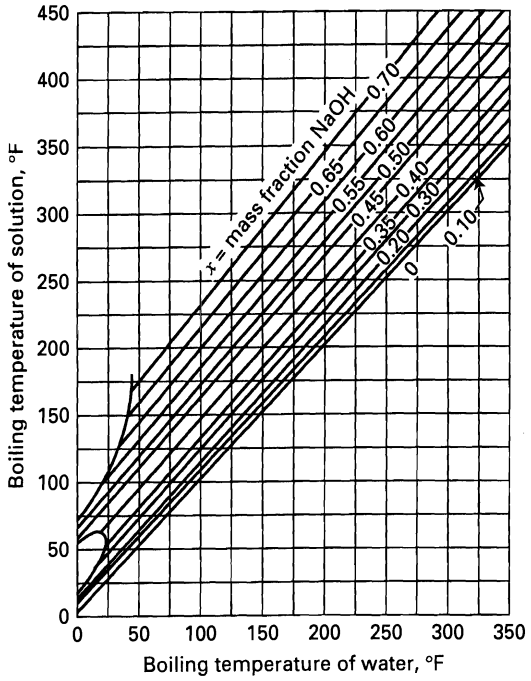

Figure 17.32 Dühring chart for aqueous solutions of sodium hydroxide.

[From W.L. McCabe, J.C. Smith, and P. Harriott, *Unit Operations of Chemical Engineering*, 5th ed., McGraw-Hill, New York (1993) with permission.]

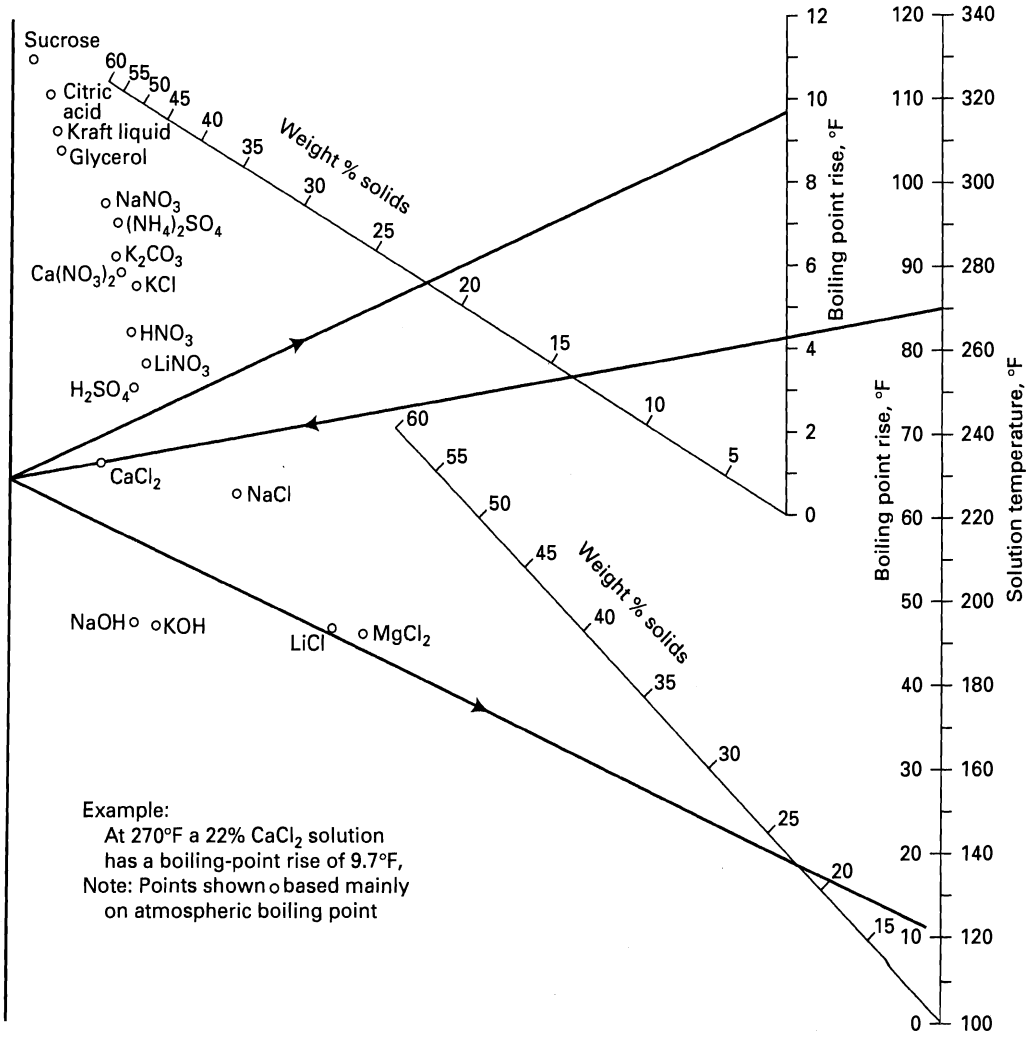

Figure 17.33 Nomograph for boiling-point elevation of aqueous solutions.

[From *Perry's Chemical Engineers' Handbook*, 6th ed., R.H. Perry, D.W. Green, and J.O. Maloney, eds., McGraw-Hill, New York (1984) with permission.]

boiling-point elevation of the solution. If, as is usually the case, the solute has little or no vapor pressure, the evaporator pressure is equal to the partial pressure of the water in the solution. Then, by a modified Raoult's law,

$$P = p_{H_2O} = \gamma_{H_2O} x_{H_2O} P^s_{H_2O} \qquad (17\text{-}76)$$

Thus, for a given P and x_{H_2O}, a temperature can be determined to give the required $P^s_{H_2O}$ provided that γ_{H_2O} can be estimated. For solutions dilute in the solute, γ_{H_2O} approaches a value of 1.0. For concentrated solutions, the value of γ_{H_2O} can be estimated from correlations for electrolyte solutions as discussed by Reid, Prausnitz, and Poling [34].

Alternatively, the boiling temperature of the solution can be estimated by using a *Dühring-line chart* if it is available for the particular solute. Such a chart is shown in Figure 17.32 for the sodium hydroxide-water solution. The straight lines on this chart for different mass fractions of NaOH obey *Dühring's rule,* which states that as the pressure is increased, the boiling temperature of the solution increases linearly with the boiling temperature of the pure solvent. A nomograph for other solutes in water is given in Figure 17.33. The use of Figures 17.32 and 17.33, and (17-76) is illustrated in the following example.

EXAMPLE 17.16

An aqueous, NaOH solution is being evaporated at 6 psia. If the solution is 35-wt% NaOH, determine:

(a) The boiling temperature of the solution.

(b) The boiling-point elevation.

(c) The activity coefficient for water from (17-76).

SOLUTION

From steam tables, pure water has a vapor pressure of 6 psia at 170°F.

(a) From the Dühring-line chart of Figure 17.32, the boiling temperature of the solution is 207°F.

(b) The boiling-point elevation is:

$$207 - 170 = 37°\text{F}$$

Alternatively, the nomograph of Figure 17.33 may be used by drawing a straight line through the point for NaOH and a solution (boiling-point) temperature of 207°F. That line is extended to the left to the intersection with the leftmost vertical line. A straight line is then drawn from that intersection point through the lower, inclined line labeled weight percent solids at 35 (wt% NaOH). This second line is extended so as to intersect the right, vertical line. The value of the boiling-point elevation at this point of interaction is read as 36°F, which is close to the value of 37°F from the Dühring chart.

(c) The mole fraction of water in the solution is, for complete ionization of NaOH:

$$x_{H_2O} = \frac{0.65/18}{0.65/18 + 2(0.35)/40} = 0.674$$

Vapor pressure of pure water at 207°F = 13.3 psia. From (17-76),

$$\gamma_{H_2O} = \frac{6}{0.674(13.3)} = 0.67$$

Evaporator Model

The following mathematical model is widely used to make material balance, energy balance, and heat-transfer rate calculations to size evaporators operating under continuous-flow, steady-state conditions. The model is based on the schematic diagram in Figure 17.34. A so-called thin liquor at temperature, T_f, with weight-fraction solute, w_f, is fed to the evaporator at mass flow rate, m_f. A heating medium, e.g., saturated steam, is fed to the heat-exchanger tubes at temperature and pressure, T_s and P_s, and mass flow rate, m_s. Saturated condensate leaves the heat exchanger at the same temperature and pressure. Heat-transfer rate, Q, to the solution in the evaporator causes the solution in the evaporator at temperature, T_e, to partially evaporate to produce a vapor at temperature, T_v, with flow rate, m_v. The so-called thick-liquor concentrate leaves at temperature, T_p, with weight-fraction solute, w_p, at mass flow rate, m_p. The heat exchanger has a heat-transfer area, A, and overall heat-transfer coefficient, U, based on that area.

Key assumptions in formulating the mathematical model are:

1. The thin-liquor feed has only one volatile component, e.g., water.
2. Only the latent heat of the heating steam at T_s is available for heating and vaporizing the solution in the evaporator.

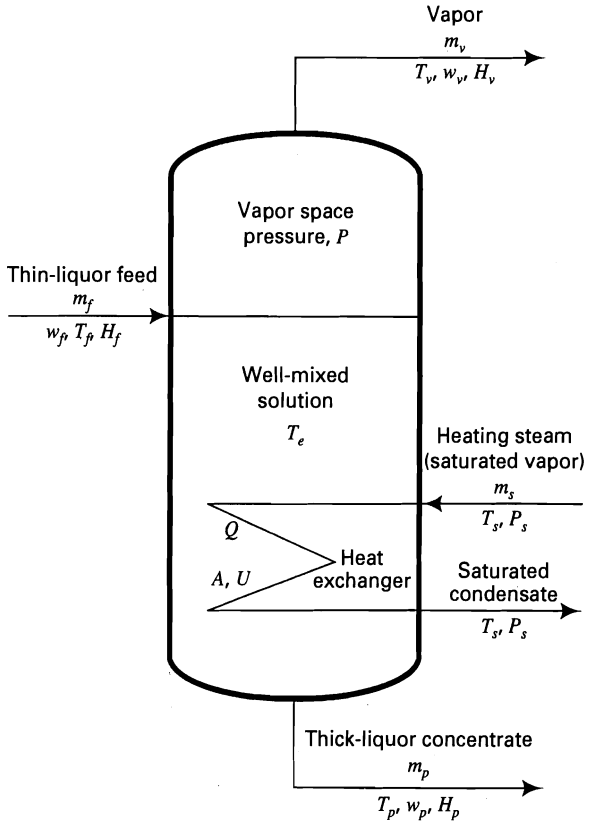

Figure 17.34 Continuous-flow, steady-state model for an evaporator.

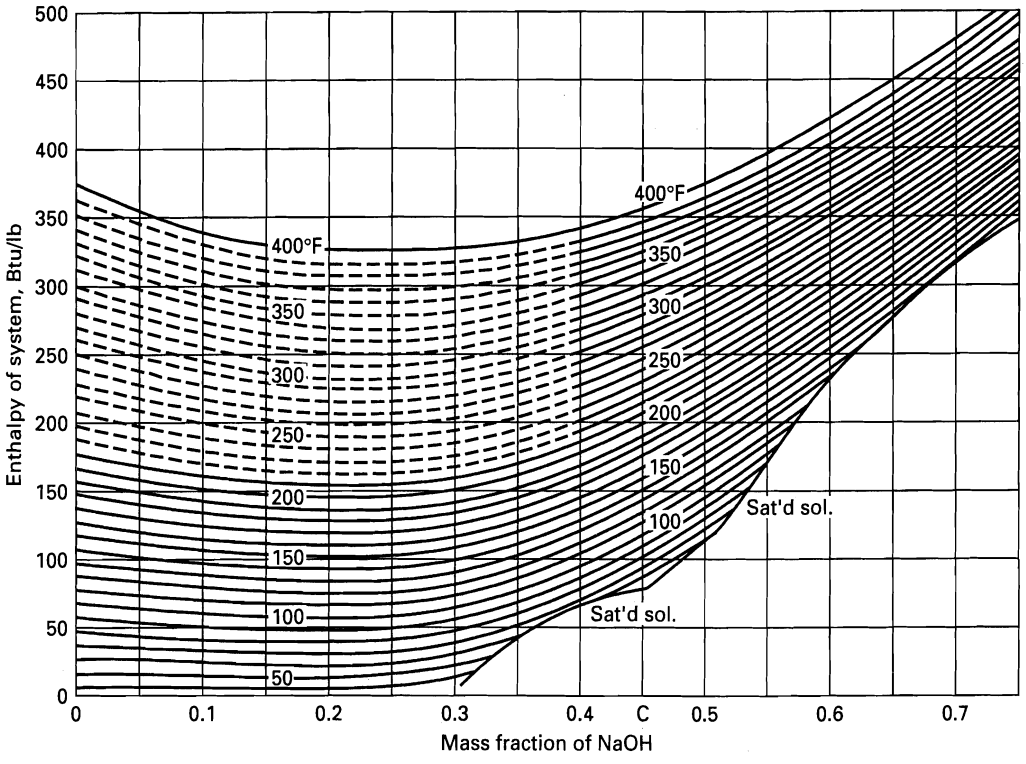

Figure 17.35 Enthalpy-concentration diagram for sodium hydroxide–water system.
[From W.L. McCabe, J.C. Smith, and P. Harriott, *Unit Operations of Chemical Engineering*, 5th ed., McGraw-Hill, New York (1993) with permission.]

3. The boiling action on the heat-exchanger surfaces agitates the solution, in the evaporator, sufficiently to achieve perfect mixing. Therefore, the temperature of the solution in the evaporator equals the exiting temperature of the thick-liquor concentrate. Thus, $T_e = T_p$. Also, $T_v = T_p$.
4. Because of Assumptions 2 and 3, the overall temperature driving force for heat transfer $= \Delta T = T_s - T_p$.
5. The ΔT is high enough to achieve nucleate boiling and not so high as to cause film boiling.
6. The exiting vapor temperature, $T_v = T_p = T_e$, corresponds to evaporator vapor-space pressure, P, taking into account the boiling-point elevation of the solution unless the solute is small, insoluble particles, such as colloidal matter.
7. No heat loss from the evaporator.

Based on the above assumptions, the mathematical model is as follows:

Total mass balance:

$$m_f = m_p + m_v \tag{17-77}$$

Mass balance on the solute:

$$w_f m_f = w_p m_p \tag{17-78}$$

Energy (enthalpy) balance on the solution:

$$Q = m_v H_v + m_p H_p - m_f H_f \tag{17-79}$$

where H = enthalpy per unit mass

Energy (enthalpy) balance on the heating steam:

$$Q = m_s \Delta H^{\text{vap}} \tag{17-80}$$

Heat-transfer rate:

$$Q = UA(T_s - T_p) \tag{17-81}$$

The procedure used to solve these five equations depends upon the specifications of the problem. The following example is just one illustration. The solution of the energy-balance equations is greatly facilitated if an enthalpy-concentration diagram is available for the solute–solvent system. A diagram of this type for the NaOH–water system is given in Figure 17.35. In this diagram, the enthalpy datum for water is the pure liquid at 32°F, so that the diagram has the same datum as the steam tables. For NaOH, the datum is NaOH at infinite dilution in water at 20°C (68°F). Figure 17.35, together with the Dühring chart of Figure 17.32, were first prepared by McCabe [35].

EXAMPLE 17.17

An existing forced-circulation evaporator is to be used to concentrate 44 wt% NaOH to 65 wt% NaOH using steam at 3 atm gage (barometer reads 1 atm). The feed temperature will be 40°C and the pressure in the vapor space of the evaporator will be 2.0 psia. The evaporator has a heat-transfer area of 232 m^2. The overall heat-transfer coefficient for the given conditions is estimated to be 2,000 W/m^2-°C. The density of the feed solution is 1,450 kg/m^3. Neglect heat losses from the evaporator. Determine:

(a) The temperature of the solution in the evaporator in °C.

(b) The heating steam requirement in kg/h.

(c) The m^3/h of feed solution that can be sent to the evaporator.

(d) The kg/h of concentrated NaOH solution leaving the evaporator.

(e) The rate of evaporation in kg/h.

SOLUTION

(a) At 2.0 psia, the boiling temperature of pure water is 126°F. From Figure 17.32, for 65 wt% NaOH, the solution boiling point is 240°F or 116°C. This is a considerable boiling-point elevation of 114°F.

(b) In American engineering units,

$$A = 232/0.0929 = 2{,}497 \text{ ft}^2$$

$$U = 2{,}000/5.674 = 352.5 \text{ Btu/h-ft}^2\text{-°F}$$

$$T_s = 291°\text{F for 4 atm saturated steam}$$

The driving force for heat transfer is

$$\Delta T = T_s - T_p = 291 - 240 = 51°\text{F}$$

From (17-81),

$$Q = UA\,\Delta T = 352.5(2{,}497)(51) = 44{,}900{,}000 \text{ Btu/h}$$

The heat of vaporization of steam at 291°F is 917 Btu/lb.

From (17-80),

$$m_s = Q/\Delta H^{\text{vap}} = 44{,}900{,}000/917 = 48{,}950 \text{ lb/h}$$

or

$$Q = 48{,}950(0.4536) = 22{,}200 \text{ kg/h}$$

It should be noted that the heat flux is 44,900,000/2,497 = 18,000 Btu/h-ft^2. This heat flux is safely in the nucleate-boiling region.

(c) From (17-79), using Figure 17.35 for NaOH solutions and the steam tables for water vapor, the energy balance on the solution is as follows, where the evaporated water is superheated steam at 240°F and 2.0 psia., and $m_v = m_f - m_p$:

$$44{,}900{,}000 = (m_f - m_p)(1168) + m_p(340) - m_f(115) \quad (1)$$

From (17-78),

$$0.44m_f = 0.65m_p \quad (2)$$

Substituting (2) into (1) to eliminate m_p, we obtain

$$m_f = \frac{44{,}900{,}000}{\left(1 - \dfrac{0.44}{0.65}\right)(1{,}168) + \left[\dfrac{0.44}{0.65}(340) - 115\right]}$$

$$= 91{,}170 \text{ lb/h}$$

or

$$m_f = (91{,}170)(0.4536) = 41{,}350 \text{ kg/h}$$

(d) From (2),

$$m_p = \frac{0.44}{0.65}(41{,}350) = 27{,}990 \text{ kg/h}$$

(e) $$m_v = m_f - m_p = 41{,}350 - 27{,}990 = 13{,}360 \text{ kg/h}$$

Multiple-Effect Evaporator Systems

When condensing steam is used to evaporate water from an aqueous solution, the heat of condensation of the higher-temperature condensing steam is less than the heat of vaporization of the lower-temperature boiling water. Consequently, less than 1 kilogram of vapor is produced per kilogram condensation of heating steam. This ratio is called the *economy*. In Example 17.17, the economy is 13,360/22,200 = 0.602 or 60.2%. To reduce the amount of steam required and, thereby, increase the economy, a series of evaporators, called *effects*, can be used as shown in Figure 17.36. The increased economy is achieved by operating the effects

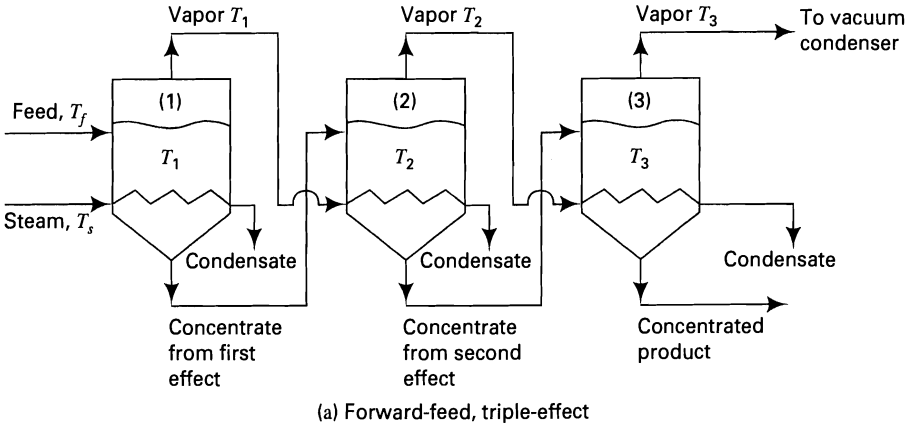

(a) Forward-feed, triple-effect

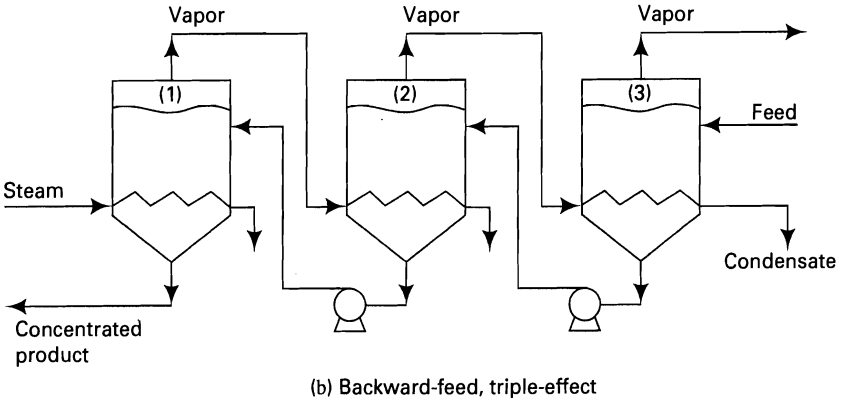

(b) Backward-feed, triple-effect

Figure 17.36 Multiple-effect evaporator systems.

at different pressures, and thus at different boiling temperatures, so that vapor produced in one effect can be condensed to supply the heat in another effect.

In Figure 17.36a, referred to as a *forward-feed, triple-effect-evaporator* system, approximately one-third of the total evaporation occurs in each effect. The fresh feed solution and steam both enter the first effect, which operates at pressure P_1. The concentrate from the first effect is sent to the second effect. The vapor produced in the first effect is also sent to the second effect where it condenses, giving up its heat of condensation to cause additional evaporation of the solution. To achieve a temperature-driving force for heat transfer in the second effect, the pressure of the second effect, P_2, is lower than that of the first effect. This procedure is repeated in the third effect. For three effects, the flow rate of steam entering the first is only about one-third of the amount of steam that would be required if only one effect were used. However, the temperature-driving force in each of the three effects is only about one-third of that in a single effect. Therefore, the heat transfer area of each of the three evaporators in a triple-effect system is approximately the same as for the one evaporator in a single-effect unit. Therefore, the savings in annual heating-steam cost must offset the additional capital investment for equipment.

When the temperature of the fresh feed is significantly below its saturation temperature corresponding to the pressure in the first effect, *backward-feed* operation is desirable, as shown in Figure 17.36b. The cold fresh feed is sent to the third effect, which operates at the lowest pressure and, therefore, the lowest temperature. Unlike the forward-feed system, pumps are required to move the concentrate from one effect to the next because $P_1 > P_2 > P_3$. However, unlike gas compressors, liquid pumps are not high-cost items.

Calculations for multieffect evaporator systems involve the same types of mass-balance, energy-balance, and heat-transfer equations as for a single-effect system. These equations are usually solved by an iterative method, especially when boiling-point elevations occur. The particular iterative procedure depends on the problem specifications. The following example illustrates a typical procedure.

EXAMPLE 17.18

A feed of 44,090 lb/h of an aqueous solution containing 8 wt% colloids is to be concentrated to 45 wt% colloids in a triple-effect-evaporator system using forward feed. The feed enters the first effect at 125°F, and the third effect operates at 1.94 psia in the vapor space. Fresh saturated steam at 29.3 psia is used for heating in the first effect. The specific heat of the colloids can be assumed constant at 0.48 Btu/lb-°F. Overall heat-transfer coefficients are estimated to be:

Effect	U, Btu/h-ft^2-°F
1	350
2	420
3	490

If the heat-transfer areas of each of the three effects are to be equal, determine:

Evaporation temperatures, T_1 and T_2, in the first two effects.

Heating steam flow rate, m_s.

Solution flow rates, m_1, m_2, and m_3 leaving the three effects.

SOLUTION

The unknowns, which number seven, are $A(= A_1 = A_2 = A_3)$, T_1, T_2, m_s, m_1, m_2, and m_3. Therefore, seven independent equations are needed. Because the solute is colloids (insolubles), boiling-point elevations do not occur.

It is convenient to add three additional unknowns and, therefore, three additional equations, making a total of 10 equations. The added unknowns are the heat-transfer rates, Q_1, Q_2, and Q_3 in the three effects. The 10 equations, which are similar to (17-78) to (17-81), are

Overall colloid mass balance

$$w_f m_f = w_3 m_3 \tag{1}$$

Energy balances on the solutions

$$Q_1 = (m_f - m_1)H_{v_1} + m_1 H_1 - m_f H_f \tag{2}$$

$$Q_2 = (m_1 - m_2)H_{v_2} + m_2 H_2 - m_1 H_1 \tag{3}$$

$$Q_3 = (m_2 - m_3)H_{v_3} + m_3 H_3 - m_2 H_2 \tag{4}$$

Energy balances on steam and water vapors

$$Q_1 = m_s \Delta H_s^{\text{vap}} \tag{5}$$

$$Q_2 = (m_f - m_1)\Delta H_2^{\text{vap}} \tag{6}$$

$$Q_3 = (m_1 - m_2)\Delta H_3^{\text{vap}} \tag{7}$$

Heat-transfer rates

$$Q_1 = U_1 A_1 (T_s - T_1) = U_1 A_1 \Delta T_1 \tag{8}$$

$$Q_2 = U_2 A_2 (T_1 - T_2) = U_2 A_2 \Delta T_2 \tag{9}$$

$$Q_3 = U_3 A_3 (T_2 - T_3) = U_3 A_3 \Delta T_3 \tag{10}$$

From (1),

$$m_3 = (w_f / w_3) m_f = (0.08/0.45)(44{,}090) = 7{,}838 \text{ lb/h}$$

Also, the flow rate of colloids in the feed is (0.08)(44,090) = 3,527 lb/h.

Initial estimates of solution temperature in each effect:

With no boiling-point elevation, the temperature of the solution in the third effect is the saturation temperature of water at the specified pressure of 1.94 psia or 125°F. The temperature of the heating steam entering the first effect is the saturation temperature of 249°F at 29.3 psia. Thus, if only one effect were used, the temperature driving force for heat transfer, ΔT, would be 249 − 125 = 124°F. With no boiling-point elevations, the ΔTs for the three effects must sum to the value for one effect. Thus,

$$\Delta T_1 + \Delta T_2 + \Delta T_3 = 124°\text{F} \tag{11}$$

As a first approximation, assume that the ΔTs for the three effects are, using (8)–(10), inversely proportional to the given values of U_1, U_2, and U_3. Thus,

$$\Delta T_1 = \frac{U_3}{U_1} \Delta T_3 \tag{12}$$

$$\Delta T_2 = \frac{U_3}{U_2} \Delta T_3 \tag{13}$$

Solving (11), (12), and (13), we obtain

$$\Delta T_1 = 48.6°\text{F}$$
$$\Delta T_2 = 40.6°\text{F}$$
$$\Delta T_3 = 34.8°\text{F}$$

$$T_1 = T_s - \Delta T_1 = 249 - 48.6 = 200.4°\text{F}$$
$$T_2 = T_1 - \Delta T_2 = 200.4 - 40.6 = 159.8°\text{F}$$
$$T_3 = T_2 - \Delta T_3 = 159.8 - 34.8 = 125°\text{F}$$

Initial Estimates of m_1 and m_2:

The total evaporation rate for the three effects is $m_f - m_3 = 44{,}090 - 7{,}838 = 36{,}252$ lb/h. Assume, as a first approximation, equal amounts of vapor produced in each effect. Then,

$$m_f - m_1 = 36{,}252/3 = 12{,}084 \text{ lb/h}$$
$$m_1 = 44{,}090 - 12{,}084 = 32{,}006 \text{ lb/h}$$
$$m_2 = 32{,}006 - 12{,}084 = 19{,}922 \text{ lb/h}$$
$$m_3 = 19{,}922 - 12{,}084 = 7{,}838 \text{ lb/h}$$

Corresponding estimates of the mass fractions of colloids are

$$w_1 = 3{,}527/32{,}006 = 0.110$$
$$w_2 = 3{,}527/19{,}922 = 0.177$$
$$w_3 = 3{,}527/7{,}838 = 0.450 \text{ (given)}$$

The remaining calculations are iterative in nature to obtain corrected values of T_1, T_2, m_1, and m_2, as well as values of A, m_s, Q_1, Q_2, and Q_3. These calculations are best carried out on a spreadsheet. Each iteration consists of the following steps:

Step 1

Combine (2) through (7) to eliminate Q_1, Q_2, and Q_3. Using the approximations for T_1, T_2, T_3, w_1, and w_2, the specific enthalpies for the resulting equations are calculated and the equations are solved for new approximations of m_s, m_1, and m_2. Corresponding approximations for w_1 and w_2 are computed.

For the first iteration, the enthalpy values are

$$\Delta H_s^{\text{vap}} = 946.2 \text{ Btu/lb}$$
$$\Delta H_2^{\text{vap}} = 977.6 \text{ Btu/lb}$$
$$\Delta H_3^{\text{vap}} = 1{,}002.6 \text{ Btu/lb}$$
$$H_{v_1} = 1{,}146 \text{ Btu/lb}$$
$$H_{v_2} = 1{,}130 \text{ Btu/lb}$$
$$H_{v_3} = 1{,}116 \text{ Btu/lb}$$
$$H_f = 0.92(92.9) + 0.08(0.48)(125 - 32) = 89.0 \text{ Btu/lb}$$
$$H_1 = 0.89(168.4) + 0.110(0.48)(200.4 - 32) = 158.8 \text{ Btu/lb}$$
$$H_2 = 0.823(127.7) + 0.177(0.48)(159.8 - 32) = 116.0 \text{ Btu/lb}$$
$$H_3 = 0.55(92.9) + 0.45(0.48)(125 - 32) = 71.2 \text{ Btu/lb}$$

When these enthalpy values are substituted into the combined energy balances, the following equations are obtained:

$$m_s = 49{,}250 - 1.043\, m_1 \tag{14}$$
$$44{,}090 = 1.994\, m_1 - 1.037\, m_2 \tag{15}$$
$$8{,}168 = 1.997\, m_2 - m_1 \tag{16}$$

Solving (14), (15), and (16),

$$m_s = 15{,}070 \text{ lb/h}$$
$$m_1 = 32{,}770 \text{ lb/h}$$
$$m_2 = 20{,}500 \text{ lb/h}$$

Corresponding values of colloid mass fractions are

$$w_1 = 0.108$$
$$w_2 = 0.172$$

It may be noted that these values of m_1, m_2, w_1, and w_2 are close to the first approximations. This is often the case.

Step 2

Using the values computed in Step 1, values of Q are determined from (5), (6), and (7); and values of A are determined from (8), (9), and (10).

$$Q_1 = 15{,}070(946.2) = 14{,}260{,}000 \text{ Btu/h}$$
$$Q_2 = (44{,}090 - 32{,}770)(977.6) = 11{,}070{,}000 \text{ Btu/h}$$
$$Q_3 = (32{,}770 - 20{,}500)(1{,}002.6) = 12{,}400{,}000 \text{ Btu/h}$$

$$A_1 = \frac{14{,}260{,}000}{(350)(48.6)} = 838 \text{ ft}^2$$

$$A_2 = \frac{11{,}070{,}000}{(420)(40.6)} = 649 \text{ ft}^2$$

$$A_3 = \frac{12{,}400{,}000}{(490)(34.8)} = 727 \text{ ft}^2$$

Step 3

Because the three areas are not equal, calculate the arithmetic-average, heat-transfer area and a new set of ΔT driving forces from (8), (9), and (10). Normalize these values so they sum to the overall ΔT (124°F in this example). From the ΔT values, compute T_1 and T_2.

$$A_{\text{avg}} = \frac{838 + 649 + 727}{3} = 738 \text{ ft}^2$$

$$\Delta T_1 = \frac{14{,}260{,}000}{(350)(738)} = 55.2°\text{F}$$

$$\Delta T_2 = \frac{11{,}070{,}000}{(420)(738)} = 35.7°\text{F}$$

$$\Delta T_3 = \frac{12{,}400{,}000}{(490)(738)} = 34.3°\text{F}$$

These values sum to 125.2°F. Therefore, they are normalized to

$$\Delta T_1 = 55.2(124/125.2) = 54.7°\text{F}$$
$$\Delta T_2 = 35.7(124/125.2) = 35.3°\text{F}$$
$$\Delta T_3 = 34.3(124/125.2) = 34.0°\text{F}$$
$$T_1 = 249 - 54.7 = 194.3°\text{F}$$
$$T_2 = 194.3 - 35.3 = 159.0°\text{F}$$

Steps 1 through 3 are now repeated using the new values of T_1 and T_2 from Step 3 and the new values of w_1 and w_2 from Step 1. The iterations are continued until the values of the unknowns no longer change significantly and $A_1 = A_2 = A_3$. The subsequent iterations for this example are left as an exercise. Based on the results of the first iteration, the economy of the three-effect system is

$$\frac{44{,}090 - 7{,}838}{15{,}070} = 2.41 \quad \text{or} \quad 241\%$$

Overall Heat-Transfer Coefficients in Evaporators

In an evaporator, the overall heat-transfer coefficient, U, depends mainly on the steamside, condensening coefficient, the solution-side coefficient, and a scale or fouling resistance on the solution side. The conduction resistance of the metal wall of the heat-exchanger tubes is usually negligible. Steam condensation is generally of the film, rather than dropwise, type. When boiling occurs on the surfaces of the heat-exchanger tubes, it is of the nucleate-boiling, rather than film-boiling, regime. In the absence of boiling on the tube surfaces, heat transfer is by forced convection to the solution. Local coefficients for film condensation, nucleate boiling, and forced convection of aqueous solutions are all relatively large, of the order of 1,000 Btu/h-ft^2-°F (5,700 W/m^2-K). Thus, the overall coefficient would be about one-half of this. However, when fouling occurs, the overall coefficient can be substantially less. Table 17.11, taken from Geankoplis [36], lists ranges of overall heat-transfer coefficients for different types of evaporators. The higher coefficients in forced-circulation evaporators are mainly a consequence of the greatly reduced fouling due to the high liquid velocity in the tubes.

Table 17.11 Typical Heat-Transfer Coefficients in Evaporators

	U	
Type Evaporator	Btu/h-ft^2-°F	W/m^2-K
Horizontal-tube	200–500	1,100–2,800
Short-tube vertical	200–500	1,100–2,800
Long-tube vertical	200–700	1,100–3,900
Forced circulation	400–2,000	2,300–11,300

SUMMARY

1. Crystallization involves the formation of solid crystalline particles from a homogeneous fluid phase. However, if the fluid is a gas, the process is usually referred to as desublimation.

2. In crystalline solids, as opposed to amorphous solids, the molecules, atoms, and/or ions are arranged in a regular lattice pattern. When crystals grow unhindered, they form polyhedrons with flat sides and sharp corners. Although the faces of a crystal may grow at different rates, referred to as crystal habit, the Law of Constant Interfacial Angles restricts the angles between corresponding faces to be constant. Crystals can form only seven different crystal systems, which include 14 different space lattices. Because of crystal habit, a given crystal system can take on different shapes, e.g., plates, needles, and prisms, but not spheres.

3. Crystal-size distributions can be determined or formulated in terms of differential or cumulative analyses, which are convertible, one from the other. A number of different, mean-particle sizes can be derived from crystal-size distribution data.

4. The most important thermodynamic properties for crystallization calculations are melting point, solubility, heat of fusion, heat of crystallization, heat of solution, heat of transition, and supersaturation. Solubilities of inorganic salts in water can vary widely from a negligible value to a concentration of greater than 50 wt%. Many salts crystallize in hydrated forms, with the number of waters of crystallization of the stable hydrate depending upon temperature. The solubility of sparingly soluble compounds is usually expressed in terms of a solubility product. When available, phase diagrams and enthalpy-concentration diagrams are extremely useful for making material- and energy-balance calculations.

5. Crystals smaller in size than can be seen by the naked eye (<20 mm) are more soluble than the normally listed solubility. Supersaturation ratio for a given crystal size is the ratio of the actual solubility of a small-size crystal to the solubility of larger crystals that can be seen by the naked eye. The driving force for nucleation and growth of crystals is supersaturation.

6. Primary nucleation, which requires a high degree of supersaturation, occurs in systems free of crystalline surfaces, and can be homogeneous or heterogeneous. Secondary nucleation occurs when crystalline surfaces are present. Crystal growth involves the mass transfer of the solute up to the crystal surface followed by incorporation of the solute into the crystal-lattice structure.

7. Equipment for solution crystallization can be classified according to operation mode (batch or continuous), method for achieving supersaturation (cooling or evaporation), and features for achieving desired crystal growth (e.g., agitation, baffles, circulation, and classification). Of primary importance is the effect of temperature on solubility. Three of the most widely used types of equipment for solution crystallization are: (1) batch crystallizer with external or internal circulation, (2) continuous, cooling crystallizer, and (3) continuous, vacuum, evaporating crystallizer.

8. The MSMPR crystallization model is widely used to simulate the often used continuous, vacuum, evaporating draft-tube, baffled crystallizer. Some of the assumptions of this model are perfect mixing of the magma, no classification of crystals, uniform degree of supersaturation throughout the magma, crystal growth rate independent of crystal size, no crystals in the feed, no crystal breakage, uniform temperature, equilibrium in product magma between mother liquor and crystals, constant and uniform nucleation rate due to secondary nucleation by crystal contact; uniform crystal-size distribution, and all crystals with the same shape.

9. For a specified crystallizer feed, magma density, magma residence time, and predominant crystal size, the MSMPR model can predict the required nucleation rate and crystal-growth rate, number of crystals produced per unit time, and crystal-size distribution.

10. Precipitation, leading to very small crystals, occurs with solutes that are only sparingly soluble. The precipitate is often produced by reactive crystallization from the addition of two soluble salt solutions, producing one soluble and one insoluble salt. Unlike solution crystallization, which takes place at a low degree of supersaturation, precipitation occurs at a very high supersaturation that results in very small crystals.

11. When both components of a mixture can be melted at reasonable temperatures (e.g., certain mixtures of organic compounds), melt crystallization can be used to separate the components. If the

components form a eutectic mixture, pure crystals of one of the components can be formed. If the components form a solid solution, repeated stages of melting and crystallization are required to achieve high purity.

12. A large number of crystallizer designs have been proposed for melt crystallization. The two major methods are suspension crystallization and layer crystallization. Of particular importance is the falling-film crystallizer, which can be designed and operated for high production rates when the components form eutectic mixtures. For components that form solid solutions, the zone-melting technique developed by Pfann can be employed to produce nearly pure compounds.

13. A number of chemicals are amenable to purification by desublimation, preceded perhaps by sublimation. Desublimation is almost always achieved by cooling the gas mixture at constant pressure. The cooling can be accomplished by heat transfer, quenching with a vaporizable liquid, or quenching with a cold, noncondensible gas.

14. Evaporation can be used to concentrate a solute prior to solution crystallization. Common evaporators include the horizontal-tube unit, short-vertical-tube unit, long-vertical-tube unit, forced-circulation unit, and the falling-film unit. For a given evaporation pressure, the presence of the solution can cause a boiling-point elevation.

15. The most widely used evaporator model assumes that the liquor being evaporated is well-mixed such that the temperature and solute concentration are uniform and at exiting conditions.

16. The economy of an evaporator is defined as the mass ratio of water evaporated to heating steam required. The economy can be increased by using multiple evaporator effects that operate at different pressures such that vapor produced in one effect can be used as heating steam in a subsequent effect. The solution being evaporated can progress through the effects in forward, backward, or mixed directions.

17. Evaporators typically operate so that solutions are in the nucleate-boiling regime. Overall, heat-transfer coefficients are generally high because boiling occurs on one side and condensation on the other side.

REFERENCES

1. MULLIN, J.W., *Crystallization,* 3rd ed., Butterworth-Heinemann, Boston (1993).

2. GRABER, S., T.A., and M.E., TABOADA, M., *Chem. Eng. Ed.,* **25,** 102–105 (1991).

3. HOUGEN, O.A., K.M. WATSON, and R.H., RAGATZ, *Chemical Process Principles, Part I, Material and Energy Balances,* 2nd ed., John Wiley & Sons (1954).

4. MIERS, H.A., and F. ISAAC, *Proc. Roy. Soc.,* **A79,** 322–351 (1907).

5. NIELSEN, A.E., *Kinetics of Precipitation,* Pergamon Press, New York (1964).

6. NOYES, A.A., and W.R. WHITNEY, *J. Am. Chem. Soc.,* **19,** 930–934 (1897).

7. NERNST, W., *Zeit. für Physik. Chem.,* **47,** 52–55 (1904).

8. MIERS, H.A., *Phil. Trans.,* **A202,** 492–515 (1904).

9. VALETON, J.J.P., *Zeit. für Kristallographie,* **59,** 483 (1924).

10. MYERSON, A.S., Ed., *Handbook of Industrial Crystallization,* Butterworth-Heinemann, Boston (1993).

11. BURTON, W.K., N. CABRERA, and F.C. FRANK, *Phil. Trans.,* **A243,** 299–358 (1951).

12. SEAVOY, G.E., and H.B. CALDWELL, *Ind. Eng. Chem.,* **32,** 627–636 (1940).

13. NEWMAN, H.H., and R.C. BENNETT, *Chem. Eng. Prog.,* **55** (3), 65–70 (1959).

14. RANDOLPH, A.D., *AIChE Journal,* **11,** 424–430 (1965).

15. RANDOLPH, A.D., and M.A. LARSON, *Theory of Particulate Processes,* 2nd ed., Academic Press, New York (1988).

16. MCCABE, W.L., *Ind. Eng. Chem.* **21,** 30–33 and 112–19 (1929).

17. ZUMSTEIN, R.C., and R.W. ROUSSEAU, *AIChE Symp. Ser.,* **83** (253), 130 (1987).

18. NIELSEN, A.E., *Kinetics of Precipitation,* Pergamon Press, Oxford, England (1964).

19. NIELSEN, A.E., Chapter 27 in *Treatise on Analytical Chemistry, Part 1,* Volume 3, 2nd ed., Editors I.M. Kolthoff and P.J. Elving, John Wiley & Sons, New York (1983).

20. NIELSEN, A.E., *J. Crys. Gr.,* **67,** 289–310 (1984).

21. FITCHETT, D.E., and J.M. TARBELL, *AIChE J.,* **36,** 511–522 (1990).

22. MATSUOKA, M., M. OHISHI, A. SUMITANI, and K. OHORI, World Congress III of Chemical Engineers, Tokyo, Sept. 21-325, 1986, pp. 980–983.

23. WILCOX, W.R., *Ind. Eng. Chem.,* **60** (3), 13–23 (1968).

24. WYNN, N., *Chemical Engineering,* **98** (7) 149–154 (1991).

25. PFANN, W.G., *Trans. AIME.,* **194,** 747 (1952).

26. PFANN, W.G., *Zone Melting,* 2nd ed., John Wiley and Sons, New York (1966).

27. ZIEF, M., and W.R. WILCOX, *Fractional Solidification,* Marcel Dekker, New York (1967).

28. BURRIS, JR., L., C.H. STOCKMAN, and I.G. DILLON, *Trans. AIME,* **203,** 1017 (1955).

29. HERINGTON, E.F.G., *Zone Melting of Organic Compounds,* John Wiley & Sons, New York (1963).

30. NORD, M., *Chem. Eng.,* **58** (9), 157–166 (1951).

31. KUDELA, L., and M.J. SAMPSON, *Chem. Eng.,* **93** (12), 93–98 (1986).

32. HOLDEN, C.A., and H.S. BRYANT, *Sep. Sci.,* **4** (1), 1–13 (1969).

33. SINGH, N.M., and R.K. TAWNEY, *Ind. J. Tech.,* **9,** 445–447 (1971).

34. POLING, B.E., J.M. PRAUSNITZ, and J.P. O'CONNELL, *The Properties of Gases and Liquids,* 5th ed., McGraw-Hill Book Co., New York (2001), p. 8.191.

35. MCCABE, W.L., *Trans. AIChE,* **31,** 129–164 (1935).

36. GEANKOPLIS, C.J., *Transport Processes and Unit Operations,* 3rd ed., Prentice Hall, Englewood Cliffs, NJ (1993).

EXERCISES

Section 17.1

17.1 Estimate the sphericities of the following simple particle shapes:

(a) a cylindrical needle with a height, H, equal to 5 times the diameter, D

(b) a rectangular prism of sides a, $2a$, and $3a$

17.2 A certain circular plate of diameter, D, and thickness, t, has a sphericity of 0.594. What is the ratio of t to D?

17.3 A laboratory screen analysis for a batch of crystals of hypo (sodium thiosulfate) is as follows. Prepare both differential and cumulative-undersize plots of the data, using a spreadsheet.

U.S. Screen	Mass Retained, gm
6	0.0
8	8.8
12	21.3
16	138.2
20	211.6
30	161.7
40	81.6
50	44.1
70	28.7
100	13.2
140	9.6
170	8.8
230	7.4
	735.0

In preparing your plots, determine whether arithmetic, semilog, or log-log plots are preferred.

17.4 Derive expressions for the surface-mean and mass-mean diameter from a particle-size analysis based on counting, rather than weighing, particles in given size ranges, letting N_i be the number of particles in a given size range of average diameter, $\bar{D}_{p_i}$.

17.5 Using the screen analysis of Exercise 17.3, calculate, with a spreadsheet, the surface-mean, mass-mean, arithmetic-mean, and volume-mean crystal diameters, assuming that all particles have the same sphericity and volume shape factor.

17.6 A precipitation process for producing perfect spheres of silica has been developed. The individual particles are so small that most cannot be discerned by the naked eye. Using optical microscopy, the particle size distribution has been measured, with results given in the table below. Using these data on a spreadsheet program:

(a) Produce plots of the differential and cumulative particle-size analyses

(b) Determine:

(1) surface-mean diameter

(2) arithmetic-mean diameter

(3) mass-mean diameter

(4) volume-mean diameter

PSD of Silica Spheres

Particle-Size Interval, μm	Number of Particles
1.0–1.4	2
1.4–2.0	5
2.0–2.8	14
2.8–4.0	60
4.0–5.6	100
5.6–8.0	190
8.0–12.0	250
12.0–16.0	160
16.0–22.0	110
22.0–30.0	70
30.0–42.0	28
42.0–60.0	10
60.0–84.0	1
Total	1,000

17.7 A screen analysis for a sample of glauber's salt from a commercial crystallizer is as follows, where the crystals can be assumed to have a uniform sphericity and volume shape factor.

U.S. Screen	Mass Retained, gm
14	0.0
16	0.9
18	25.4
20	111.2
25	113.9
30	225.9
35	171.7
40	116.5
45	55.1
50	31.5
60	8.7
70	10.5
80	4.4
	875.7

Use a spreadsheet to determine in microns:

(a) a plot of the differential analysis

(b) a plot of the cumulative oversize analysis

(c) a plot of the cumulative undersize analysis

(d) the surface-mean diameter

(e) the mass-mean diameter

(f) the arithmetic-mean diameter

(g) the volume-mean diameter

Section 17.2

17.8 1,000 grams of water is mixed with 50 grams of Ag_2CO_3 and 100 grams of AgCl. At equilibrium at 25°C, calculate the concentrations in moles/liter of Ag^+, Cl^-, and CO_3^- ions and the grams of Ag_2CO_3 and AgCl in the solid phases.

17.9 5,000 lb/h of a saturated aqueous solution of $(NH_4)_2SO_4$ at 80°C is cooled to 30°C. At equilibrium, what is the amount of crystals formed in lb/h. If during the cooling process, 50% of the water is evaporated, what is the amount of crystals formed in lb/h?

17.10 7,500 lb/h of a 50 wt% aqueous solution of $FeCl_3$ at 100°C is cooled to 20°C. At 100°C, the solubility of the $FeCl_3$ is 540 g/100 g of water. At 20°C, the solubility is 91.8 g/100 g water and crystals of $FeCl_3$ are the hexahydrate. At equilibrium at 20°C, determine the lb/h of crystals formed.

17.11 The concentrate from an evaporation system is 5,870 lb/h of 35 wt% $MgSO_4$ at 180°F and 25 psia. It is mixed with 10,500 lb/h of saturated aqueous recycle filtrate of $MgSO_4$ at 80°F and 25 psia. The mixture is sent to a vacuum crystallizer, operating at 85°F and 0.58 psia in the vapor space, to produce steam and a magma of 25 wt% crystals and 75 wt% saturated solution. Determine the lb/h of water evaporated and the maximum production rate of crystals in tons/day (dry basis for 2000 lb/ton).

17.12 Urea is to be crystallized from an aqueous solution that is 90% saturated at 100°C. If 90% of the urea is to be crystallized in the anhydrous form and the final solution temperature is to be 30°C, what fraction of the water must be evaporated?

17.13 In Examples 17.3 and 17.5, heat addition to the crystallizer is by an external heat exchanger through which magma is circulated, as shown in Figure 17.16. If instead the heat is added to the feed, determine the new feed temperature. Which is the preferable way to add the heat?

17.14 For the conditions of Exercise 17.11, determine the rate at which heat must be added to the system.

17.15 For the conditions of Example 17.4, calculate the amount of heat in calories/100 grams of water that must be removed to cool the solution from 100 to 10.6°C.

Section 17.3

17.16 Based on the following data, compare the effect of crystal size on solubility in water at 25°C for (1) KCl (see Example 17.7), a soluble inorganic salt, with that for (2) $BaSO_4$, an almost insoluble inorganic salt, and (3) sucrose, a very soluble organic compound.

$$\sigma_{s,L} \text{ for barium sulfate} = 0.13 \text{ J/m}^2$$

$$\sigma_{s,L} \text{ for sucrose} = 0.01 \text{ J/m}^2$$

What conclusions can you draw from the results?

17.17 Determine the supersaturation ratio, S, required to permit 0.5-μm-diameter crystals of sucrose (MW = 342 and $\rho_c = 1{,}590$ kg/m^3) to grow if $\sigma_{s,L} = 0.01$ J/m^2.

17.18 The Kelvin equation, (17-16), predicts that solubility increases to infinity as the crystal diameter decreases to zero. However, measurements by L. Harbury [*J. Phys. Chem.*, **50,** 190–199 (1946)] for several inorganic salts in water show a maximum in the solubility curve and a solubility that approaches zero as crystal size is reduced to zero. Harbury's explanation is that the surface energy of the crystals depends not only on interfacial tension, but also on surface electrical charge, given by

$$2q^2 v_s / \pi \kappa R T D_p^4$$

where

q = electrical charge on the crystal

κ = dielectric constant

Modify (17-16) to take into account electrical charge. Make sure your equation predicts a maximum.

17.19 Using the following data, compare the effect of supersaturation ratio over the range of 1.005 to 1.02 on the primary homogeneous nucleation of $AgNO_3$, $NaNO_3$, and KNO_3 from aqueous solutions at 25°C:

	$AgNO_3$	$NaNO_3$	KNO_3
Crystal density, g/cm^3	4.35	2.26	2.11
Interfacial tension, J/m^2	0.0025	0.0015	0.0030

17.20 Estimate the effect of relative supersaturation on the primary, homogeneous nucleation of $BaSO_4$ from an aqueous solution at 25°C, if

$$\text{Crystal density} = 4.50 \text{ g/cm}^3$$

$$\text{Interfacial tension} = 0.12 \text{ J/m}^2$$

17.21 Repeat parts (g) and (i) of Example 17.9 if the solution velocity past the crystal face is reduced from 5 cm/s to 1 cm/s.

Section 17.4

17.22 The feed to a cooling crystallizer is 2,000 kg/h of 30 wt% Na_2SO_4 in water at 40°C. This solution is to be cooled to a temperature at which 50% of the solute will be crystallized as the decahydrate. Estimate the required heat-transfer area in m^2 if an overall heat-transfer coefficient of 15 Btu/h-ft^2-°F can be achieved. Assume a constant specific heat for the aqueous solution of 0.80 cal/g-°C. Chilled cooling water will flow countercurrently to the crystallizing solution, entering the crystallizer at 10°C, and exiting at a temperature sufficient to give a log-mean driving force of at least 10°C.

17.23 Two tons per hour of the dodecahydrate of sodium phosphate ($Na_3PO_4 \cdot 12H_2O$) is to be crystallized by cooling, in a cooling crystallizer, an aqueous solution that enters saturated at 40°C and leaves at 20°C. Chilled cooling water flows countercurrently, entering at 10°C and exiting at 25°C. The expected overall heat-transfer coefficient is 20 Btu/h-ft^2-°F. The average specific heat of the solution is 0.80 cal/g-°C. Estimate:

(a) The tons (2,000 lb) per hour of feed solution.

(b) The heat-transfer area in ft^2.

(c) The number of crystallizer units required if each 10-ft-long unit contains 30 ft^2 of heat-transfer surface.

Section 17.5

17.24 An aqueous feed of 10,000 kg/h, saturated with $BaCl_2$ at 100°C, enters a crystallizer that can be simulated with the MSMPR model. However, crystallization is achieved with negligible evaporation. The magma leaves the crystallizer at 20°C with crystals of the dihydrate. The crystallizer has a volume (vapor-space free basis) of 2.0 m^3. From laboratory experiments, the crystal growth rate is essentially constant at 4.0×10^{-7} m/s. Using the data below, determine:

(a) The kg/h of crystals in the magma product.

(b) The predominant crystal size in mm.

(c) The mass fraction of crystals in the size range from U.S. Standard 20 mesh to 25 mesh.

Data:

Density of the dihydrate crystals = 3.097 g/cm^3

Density of an aqueous, saturated solution of barium chloride at 20°C = 1.29 g/cm^3

17.25 The feed to a continuous crystallizer that can be simulated with the MSMPR model is 5,000 kg/h of 40 wt% sodium acetate in water. Monoclinic crystals of the trihydrate will be formed. The pressure in the crystallizer and the heat-transfer rate in the associated heat exchanger are such that 20% of the water in the feed will be evaporated at a crystallizer temperature of 40°C. The crystal growth rate, G, is 0.0002 m/h and a predominant crystal size, L_{pd}, of 20 mesh is desired.

Determine:

(a) The kg/h of crystals in the exiting magma.

(b) The kg/h of mother liquor in the exiting magma.

(c) The volume in m^3 of magma in the crystallizer if

density of the crystals = 1.45 g/cm^3

density of the mother liquor = 1.20 g/cm^3

Solubility data:

T, °C	Solubility, g sodium acetate/100 g H_2O
30	54.5
40	65.5
60	139

17.26 An MSMPR-type crystallizer is to be designed to produce 2,000 lb/h of crystals of the heptahydrate of magnesium sulfate with a predominant crystal size of 35 mesh. The magma will be 15 vol% crystals. The temperature in the crystallizer will be 50°C and the residence time will be 2 h. The densities of the crystals and mother liquor are 1.68 and 1.32 g/cm^3, respectively. Determine:

(a) The exiting flow rates in cubic feet per hour of

Crystals

Mother liquor

Magma

(b) The crystallizer volume in gallons, if the vapor space equals the magma space.

(c) The approximate dimensions in feet of the crystallizer, if the body is cylindrical with a height equal to twice the diameter.

(d) The required crystal growth rate in feet per hour.

(e) The necessary nucleation rate in nuclei per hour per cubic feet of mother liquor in the crystallizer.

(f) The number of crystals produced per hour.

(g) A screen analysis table covering a U.S. mesh range of 3-1/2 to 200, giving the predicted % cumulative and % differential screen analyses of the product crystals.

(h) Plots of the screen analyses predicted in part (g).

Section 17.6

17.27 Refer to Example 17.12. In Run 15, Fitchett and Tarbell also made measurements of number density of crystals at 200 rpm, for which the data can be fitted well by the equation

$$\ln n = 26.3 - 0.407\,L \qquad (1)$$

where

n = number density of crystals

L = crystal size, μm

Using the MSMPR model, determine in the same units as for Example 17.12:

(a) n^o

(b) G

(c) B^o

(d) mean crystal length

(e) n_c

(f) Are your results consistent with the trends found in Example 17.12?

(g) Using your results and those in Example 17.12, predict the growth rate and mean-crystal length if no agitation is used.

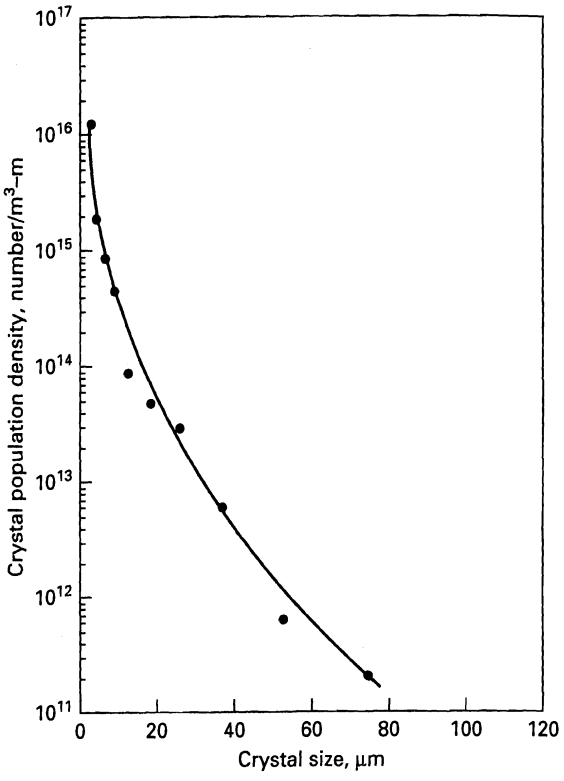

Figure 17.37 Population density of $CaCO_3$ for Exercise 17.28.

17.28 Tai and Chen [*AIChE J.*, **41,** 68–77 (1995)] studied the precipitation of calcium carbonate by mixing aqueous solutions of sodium carbonate and calcium chloride in an MSMPR crystallizer with pH control, such that the form of $CaCO_3$ was calcite rather than aragonite or vaterite. In Run S-2, which was conducted at 30°C, a pH of 8.65, and 800 rpm, with a residence time of 100 min, the crystal population density data were as shown in Figure 17.37.

Because the data do not plot as a straight line, they do not fit (17-38).

(a) Develop an empirical equation that will fit the data and determine, by regression, the constants.

(b) Can nucleation rate and growth rate be determined from the data? If so, how?

17.29 Tsuge and Matsuo ["Crystallization as a Separation Process," *ACS Symposium Series 438,* edited by Myerson and Toyokura, ACS, Washington, DC (1990), pp. 344–354] studied the precipitation of $Mg(OH)_2$ by reacting aqueous solutions of $MgCl_2$

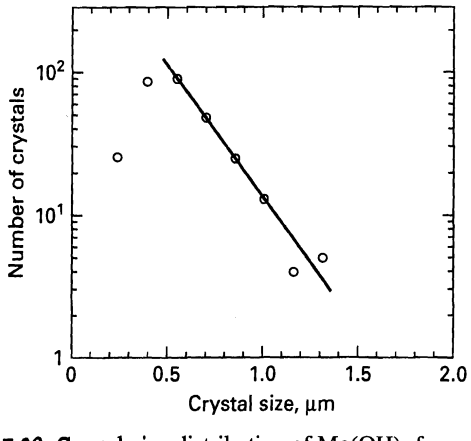

Figure 17.38 Crystal-size distribution of $Mg(OH)_2$ for Exercise 17.29.

and $Ca(OH)_2$ in a 1-liter MSMPR crystallizer operating at 450 rpm and 25°C. Crystal sizes were measured by a scanning electron microscope (SEM) and analyzed by a digitizer. Crystal size was taken to be the maximum length. A typical plot of the crystal-size distribution is given in Figure 17.38 for an assumed residence time of 5 min. Assuming that the number of crystals is proportional to $\exp(-L/G\tau)$, as in (17-38), determine:

(a) Growth rate

(b) Nucleation rate

(c) Predominant crystal size

Section 17.7

17.30 The feed to the top of a falling-film crystallizer is a melt of 60 wt% naphthalene and 40 wt% benzene at saturation conditions. If the coolant enters at the top at 10°C, determine the crystal-layer thickness for up to 2 cm, as a function of time. Necessary physical-property data are given in Example 17.13.

17.31 Paradichlorobenzene melts at 53°C, while orthodichlorobenzene melts at −17.6°C. They form a eutectic of 87.5 wt% of the ortho isomer at −23°C. The normal boiling points of these two isomers differ by about 5°C. A mixture of 80 wt% of the para isomer at the saturation temperature of 43°C is fed to the top of a falling-film crystallizer, where coolant enters at 15°C. If 8-cm i.d. tubes are used, determine the time for the crystal-layer thickness at the top of the tube to reach 2 cm. Which isomer will crystallize? Necessary physical properties are given in Perry's Chemical Engineers' Handbook, except for crystal thermal conductivity, for which we assume a value of 0.15 Btu/h-ft-°F for either isomer.

17.32 Derive (17-67).

Section 17.8

17.33 Derive the following expression for the average impurity concentration over a particular length of crystal layer, $z_2 - z_1$, after one pass or partial pass of zone melting.

$$w_{avg} = w_o \left\{ \frac{\ell(1-K)}{K(z_2 - z_1)} [\exp(-z_2 K/\ell) - \exp(-z_1 K/\ell)] + 1 \right\} \tag{1}$$

Using the results of Example 17.14, calculate w_{avg} for $z_1 = 0$ and $z_2/\ell = 9$.

17.34 In Example 17.14, let the last 20% of the crystal layer be removed, following the first pass, to $z/\ell = 9$. Calculate from (1), in Exercise 17.33, the average impurity concentration in the remaining crystal layer.

17.35 A bar of 98 wt% Al with 2 wt% of Fe impurity is to be subjected to one pass of zone refining. The solid–liquid equilibrium distribution coefficient for the impurity is 0.29. If $z/\ell = 10$ and the resulting bar is cut off at $z_2 = 0.75z$, calculate the concentration profile for Fe and the average concentration from (1) in Exercise 17.33.

Section 17.9

17.36 A desublimation unit of the heat-exchanger type is to be sized for the recovery of 200 kg/h of benzoic acid (BA) from a gas stream containing 0.8 mol% BA and 99.2 mol% N_2. The gas enters the unit at 780 torr at 130°C and leaves without pressure drop at 80°C. The coolant is pressurized cooling water that enters at 40°C and leaves at 90°C, in countercurrent flow to the gas. The heat-exchanger tubes are of the type in Example 17.15.

Some properties of benzoic acid are given in Exercise 17.37. In addition,

k_c of solid benzoic acid = 1.4 cal/h-cm-°C

ρ_c of solid benzoic acid = 1.316 g/cm^3

Determine the number of tubes needed and the time required to reach the maximum thickness of benzoic acid of 1.25 cm.

17.37 Benzoic acid is to be crystallized by bulk-phase desublimation from N_2 using a novel method described by Vitovec, Smolik, and Kugler [*Coll. Czech. Chem. Commun.*, **42**, 1108–1117 (1977)]. The gas, containing 6.4 mol% benzoic acid and the balance N_2, flows at 3 m^3/h at 1 atm and a temperature of 10°C above the dew point. The gas is directly cooled by the vaporization of 150 cm^3/h of a water spray at 25°C. The gas is further cooled in two steps by nitrogen quench gas at 1 atm as follows:

Step	Quench Gas Flow Rate, m^3/h	Quench Gas Temp., °C
1	1.5	105
2	2.0	25

The quench gases enter through porous walls of the vessel so as to prevent crystallization on the vessel wall. Based on the following data for benzoic acid, determine the final gas temperature and the fractional yield of benzoic-acid crystals, assuming equilibrium in the exiting gas.

Melting point = 122.4°C

Specific heat of solid and vapor = 0.32 cal/g-°C

Heat of sublimation = 134 cal/g

Vapor pressure:

T, °C	Vapor Pressure, torr
96	1
105	1.7
119.5	5
132.1	10
146.7	20
162.6	40
172.8	60

The vapor pressure data can be extrapolated to lower temperatures by the Antoine equation.

17.38 Derive (17-75).

Section 17.10

17.39 Fifty-thousand pounds per hour of a 20 wt% aqueous solution of NaOH at 120°F is to be fed to an evaporator operating at 3.7 psia, where the solution is concentrated to 40 wt% NaOH. The heating medium is saturated steam at a temperature 40°F higher than the exiting temperature of the caustic solution. Determine:

(a) Boiling-point elevation of the solution

(b) Saturated-heating-steam temperature and pressure

(c) Evaporation rate

(d) Heat-transfer rate

(e) Heating-steam flow rate

(f) Economy

(g) Heat-transfer area if $U = 300$ Btu/h-ft^2-°F

17.40 A 10 wt% aqueous solution of NaOH at 100°F and a flow rate of 30,000 lb/h is to be concentrated to 50 wt% by evaporation using saturated steam at 115 psia.

(a) If a single-effect evaporator is used with $U = 400$ Btu/h-ft^2-°F and a vapor-space pressure of 4 in. Hg, determine the heat-transfer area and the economy.

(b) If a double-effect evaporator system is used with forward feed and $U_1 = 450$ Btu/h-ft^2-°F and $U_2 = 350$ Btu/h-ft^2-°F, and a vapor-space pressure of 4 in. Hg in the second effect, determine the heat-transfer area of each effect, assuming equal areas, and the overall economy.

17.41 A 10 wt% aqueous solution of $MgSO_4$ at 14.7 psia and 70°F is sent to a double-effect evaporator system with forward feed at a flow rate of 16,860 lb/h, to be concentrated to 30 wt% $MgSO_4$. The pressure in the second effect is 2.20 psia. The heating medium is saturated steam at 230°F. Estimated heat-transfer coefficients in Btu/h-ft^2-°F are 400 for the first effect and 350 for the second effect. If the heat-transfer areas of the two effects are to be the same, and boiling-point elevations are neglected, determine:

(a) The pressure in the first effect

(b) The percent of the total evaporation occurring in the first effect.

(c) The heat-transfer area of each effect.

(d) The economy.